SENSORY SUBSTITUTION AND AUGMENTATION OF FORCES AND TORQUES USING TACTILE SKIN DEFORMATION FEEDBACK

A DISSERTATION
SUBMITTED TO THE DEPARTMENT OF MECHANICAL ENGINEERING
AND THE COMMITTEE ON GRADUATE STUDIES
OF STANFORD UNIVERSITY
IN PARTIAL FULFILLMENT OF THE REQUIREMENTS
FOR THE DEGREE OF
DOCTOR OF PHILOSOPHY

Zhan Fan Quek
August 2015

This dissertation is online at: http://purl.stanford.edu/hr907sz7375

I certify that I have read this dissertation and that, in my opinion, it is fully adequate in scope and quality as a dissertation for the degree of Doctor of Philosophy.

Allison Okamura, Primary Adviser

I certify that I have read this dissertation and that, in my opinion, it is fully adequate in scope and quality as a dissertation for the degree of Doctor of Philosophy.

Mark Cutkosky, Co-Adviser

I certify that I have read this dissertation and that, in my opinion, it is fully adequate in scope and quality as a dissertation for the degree of Doctor of Philosophy.

Oussama Khatib

I certify that I have read this dissertation and that, in my opinion, it is fully adequate in scope and quality as a dissertation for the degree of Doctor of Philosophy.

William Provancher

Approved for the Stanford University Committee on Graduate Studies.

Patricia J. Gumport, Vice Provost for Graduate Education

This signature page was generated electronically upon submission of this dissertation in electronic format. An original signed hard copy of the signature page is on file in University Archives.

Abstract

Haptic devices aim to render a realistic sense of touch using kinesthetic and tactile feedback. Kinesthetic feedback provides forces and torques that affect the motion of the user's hand or arm. Tactile feedback stimulates cutaneous receptors in the user's skin. Currently, most commercial haptic devices aim to provide kinesthetic feedback. Although kinesthetic feedback can convey multiple degree-of-freedom information intuitively to the user, this type of feedback can potentially be destabilizing. In contrast, tactile feedback can be used to create the perception of forces and torques without physically imparting these forces and torques to the user, and is not destabilizing. However, conveying multi-degree-of-freedom force and torque information via the tactile channel, in a manner that is intuitive to a human user, can be challenging.

This thesis focuses on the design, development, and experimental validation of a class of tactile feedback devices that provide feedback using local fingerpad skin deformation. Fingerpad skin deformation occurs in our daily interaction with objects, feels natural, and can intuitively express many degrees-of-freedom. Skin deformation tactile feedback can provide force and torque information through skin deformation cues on multiple fingers in a manner that is consistent with our interaction with external objects.

This thesis describes several novel skin deformation feedback devices and shows in human participant studies that skin deformation feedback influences perception of stiffness. Skin deformation feedback can be used in conjunction with force feedback to improve the perception of stiffness of virtual surfaces, and can also be employed for

sensory substitution and augmentation of force and/or torque information during manipulation of objects in virtual environment or teleoperation scenarios. When skin deformation feedback was used as a form of sensory substitution to convey force/torque information, study participants improved task performance compared to when no feedback was given. When skin deformation feedback was used to augment kinesthetic feedback to provide additional force/torque information, subject participants showed improvements in task performance compared to only kinesthetic feedback.

The results of this thesis show that skin deformation tactile feedback is intuitive, and can be used to convey force and torque information to substitute, or augment, kinesthetic feedback. Skin deformation tactile feedback is potentially useful in scenarios where the provision of kinesthetic force and/or torque feedback is difficult, notably in teleoperated robot-assisted surgery, space and underwater teleoperation, where kinesthetic feedback may cause system instability.

Acknowledgements

First and foremost I would like to thank my advisor, Dr. Allison Okamura, for her guidance and support during the four years of my PhD career in Stanford. She allowed me to freely explore my ideas, while consistently providing the necessary nudge to keep me on track. I have also learned various other non-academic things from you, such as the way you handle the lab, your interactions with students, your parenting stylus, and the professional manner that you conduct yourself on a daily basis.

I would also like to thank my thesis committee, Dr. Mark Cutkosky, Dr. Oussama Khatib, and Dr. William Provancher, for taking the time to assess and give feedback on my progress and on my thesis. I would especially like to thank Dr. William Provancher, who served kind of as my unofficial thesis co-advisor, and who provided valuable advice on many of the technical issues that I faced throughout my thesis journey.

I would also like to thank my funding agency: The Agency for Science, Technology and Research (ASTAR), in Singapore, for providing me with the opportunity to come over to the United States to pursue both my undergraduate study in the University of Illinois, Urbana-Champaign, and my graduate study in Stanford.

I would also like to thank past and present members of the CHARM lab: Sam Schorr, Nick Colonnese, Troy Adebar, Kirk Nichols, Andrew Stanley, Tania Morimoto, Sean Sketch, Melissa Orta, Darrel Deo, Lizmarie, Yuhang Che, Ilana Nisky, and Ryder Winck. All of you had provided a wonderful grad school experience for me, be the cute pokemon drawings by Nick, the motor bike and watch lessons by Sam, the constant punching on the stomach (and other parts of the upper body) by Troy, the talks on achieving the 1000 pound club, and the various lunch talks in which almost everything

under the world was brought up and discussed.

The Singaporean group in Stanford has provided numerous social support for me during this time. I would like to thank my Singaporean friends in Stanford for all the fond memories that you had brought into my life over here.

Finally, I would like to thank my family members - my mum, my brother, and my sister-in-law, for their support and understanding through these four to five years of overseas study. To my mum, especially, for tolerating through the hardship of being away from your son throughout these few years.

Contents

List of Tables

List of Figures

Chapter 1

Introduction

Humans perceive information using the sense of touch through integration of kinesthetic and cutaneous tactile sensory information, as shown in Fig. 1.1. Haptic devices aim to render a realistic sense of touch by replicating these kinesthetic and tactile sensations. Kinesthetic feedback provides forces and torques that affect the motion and orientation of the user's hand or arm. This type of feedback is able to convey multi-degree-of-freedom information to the user intuitively. However, systems that employ kinesthetic feedback are plagued by the problem of system stability. Issues such as time delay or inaccuracies in robot modeling might potentially destabilizes system that utilizes kinesthetic feedback. In addition, the device required to provide kinesthetic force and torque feedback is often large and mechanically complex.

To avoid some of the limitations of kinesthetic force and torque feedback, tactile feedback can be used. Tactile feedback stimulates cutaneous receptors in the user's skin. Tactile feedback can be used to create the perception of forces and torques without physically imparting these forces and torques to the user, and therefore does not affect system stability. Without the requirement to produce forces and torques, tactile feedback devices can also be designed to be compact, portable, and wearable. However, conveying multi-degree-of-freedom force and torque information via tactile feedback, in a manner that is intuitive to a human user, can be challenging.

This thesis focuses on the design, development, and experimental validation of a class of tactile feedback devices that provide feedback using local fingerpad skin

deformation. Fingerpad skin deformation occurs in our daily interaction with objects, feels natural, and can intuitively express many degrees of freedom. Skin deformation tactile feedback can provide force and torque information through skin deformation cues on multiple fingers in a manner that is consistent with our interaction with external objects.

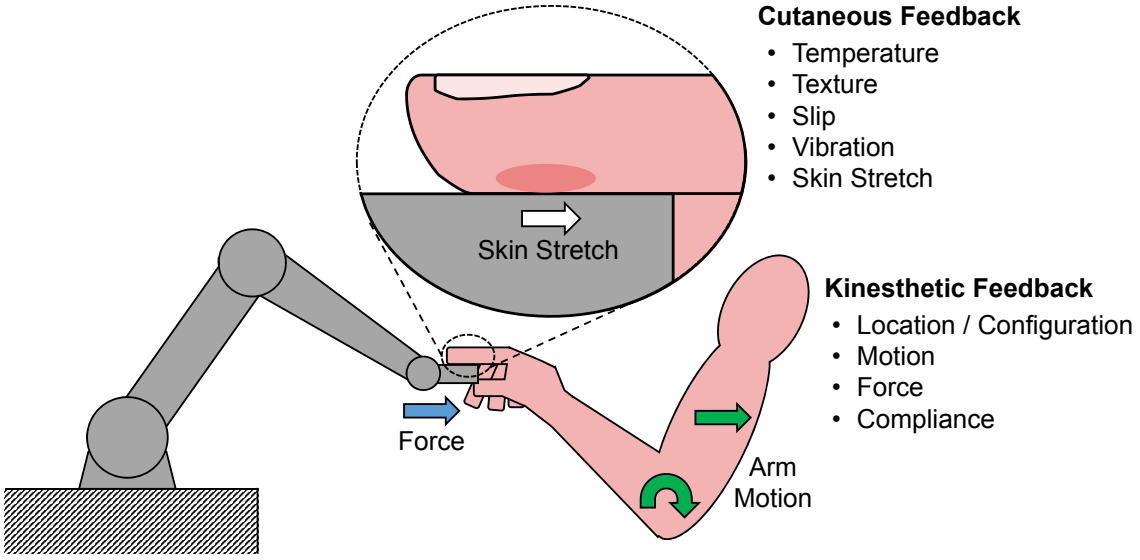

Figure 1.1: Human perceive information using the sense of touch through integration of kinesthetic and cutaneous tactile sensory information.

1.1 Motivation

The primary motivation for this work is providing haptic feedback for conveying force and torque information in teleoperation applications where it is difficult to implement traditional kinesthetic force and torque feedback. An example of such an application is robot-assisted minimally invasive surgery. Robot-assisted minimally invasive surgery involves the use of a teleoperation system in which the surgeons sits on the master console and operates the master manipulator to control the patient side robot, as shown in Fig. 1.2(a). In robot-assisted minimally invasive surgery, due to the strict safety requirements of surgical procedures, it is not desirable to incorporate large amounts of kinesthetic force and torque feedback, which may cause instability in the

teleoperation system. In addition, due to the scaling of motion between the master manipulator and the patient side manipulator, the display of forces on the master manipulator has to be scaled down in order to maintain the passivity and safety of the teleoperation system. Therefore, the feedback is severely degraded, which lowers the performance benefits that force feedback provides.

Other example applications where kinesthetic force and torque feedback faces difficulty are in space (Fig. 1.2(b)) and underwater teleoperation (Fig. 1.2(c)). In space teleoperation, due to the distance between the ground station (which houses the master manipulator) and the satellite (which houses the slave manipulator), there exist communication delays in the transmission of information between the two manipulators [73]. This time delay will results in instability in the teleoperation system when kinesthetic force feedback is used. Similar problems occur in underwater teleoperation, in which the speed of sound in water limits the communication bandwidth and latency between the master and slave devices.

Figure 1.2: Examples of teleoperation scenarios: (a) Surgeons operating the da Vinci surgical teleoperation system (b) NASA Robonaut teleoperated by an operator (c) Underwater teleoperation system. Images derived from images provided by Intuitive Surgical, NASA, and Ritsumeikan University, Japan.

The above issues can be resolved through sensory substitution and/or augmentation of force and torque feedback. This can be done using visual, audio, or tactile feedback. While visual and audio feedback are viable candidates, these types of feedback modality may not be feasible in scenarios where the vision and hearing senses are already saturated with other information. Tactile sensory substitution and augmentation is promising as it uses the same sense of touch as kinesthetic force and torque feedback. In this dissertation, we proposed to use a form of tactile feedback

called skin deformation feedback. We seek to design, implement, and experimentally validate skin deformation tactile haptic devices that provides force and torque information through skin deformation feedback.

1.2 Contributions

We briefly summarize the major contributions of this dissertation as follows:

- We investigated the effect on the perception of stiffness of virtual surfaces when augmenting force feedback with skin stretch feedback, and proposed a model to explain this effect.

- We developed a 3-Degree-of-Freedom (DoF) fingerpad skin deformation tactile device. Through human user studies, we demonstrated the feasibility of using this device for sensory substitution and augmentation of forces in 3-DoF.

- We developed a 6-Degree-of-Freedom (DoF) fingerpad skin deformation tactile device. Through human user studies, we demonstrated the feasibility of using this device for sensory substitution and augmentation of forces and torques in 6-DoF.

- We developed a novel control algorithm for the rendering of skin deformation feedback based on force and torque information.

- We integrated the skin deformation tactile devices with a surgical robotic system with skin deformation tactile feedback. We evaluated the combined system through human user studies, in which participants used the combined system to perform simulated and teleoperated surgical tasks.

1.3 Prior Work

1.3.1 Tactile Sensory Substitution

Sensory substitution is the transformation of the characteristics of one sensory modality into another sensory modality. In force-feedback sensory substitution, the force is replaced by other sensory modalities that are used to convey force magnitude and/or direction information to the user. Tactile feedback can be used for force-feedback sensory substitution, with the main forms of tactile feedback being vibrotactile, skin stretch, and normal skin deformation. Vibrotactile feedback has been used for sensory substitution in a wide variety of applications, e.g. providing grip force information for prosthetic applications [84], interaction force information in teleoperated assembly [13], and tissue interaction force information in robot-assisted surgery [68]. The main drawback of vibrotactile feedback is the difficulty of conveying force direction and magnitude information together. Tappeiner et al. [77] showed that directional cues can be conveyed using asymmetric vibration. However, their work is currently limited to in-plane direction rendering, and it is not known whether similar concepts can be used to convey 3-DoF directional cues to the user. With traditional vibrating actuators such as eccentric rotating mass motor or linear resonant actuator, multiple actuators can be placed side-by-side to convey direction information through sensory saltation [86]. Using this method, however, the actuators have to be spaced some distance apart to allow for participants to discriminate between the different vibrating actuators. Such temporal-based direction display is also not practical for use scenarios where the interaction force direction can change rapidly. Another drawback of vibrotactile feedback is that the sensitivity of the skin to ongoing vibration stimuli decreases over time [3]. Vibrotactile feedback can also be distracting and uncomfortable over long periods of usage [54].

Compared to vibrotactile feedback, skin stretch tactile feedback has the advantage of being able to convey both magnitude and directional information at the same time. Gleeson et al.[20] and Guinan et al.[22] used servo motors to move high friction surfaces across users' fingerpads to convey translation and rotation navigation information. They also designed a device that stretches the skin of the palm of the

user to convey rotational inertia [23]. These devices are shown in Fig. 1.3(a) and (b). In addition to translational skin stretch, Bark et al. [2] designed a rotational skin stretch device, shown in Fig. 1.3(c), to convey proprioceptive information to users for gait rehabilitation.

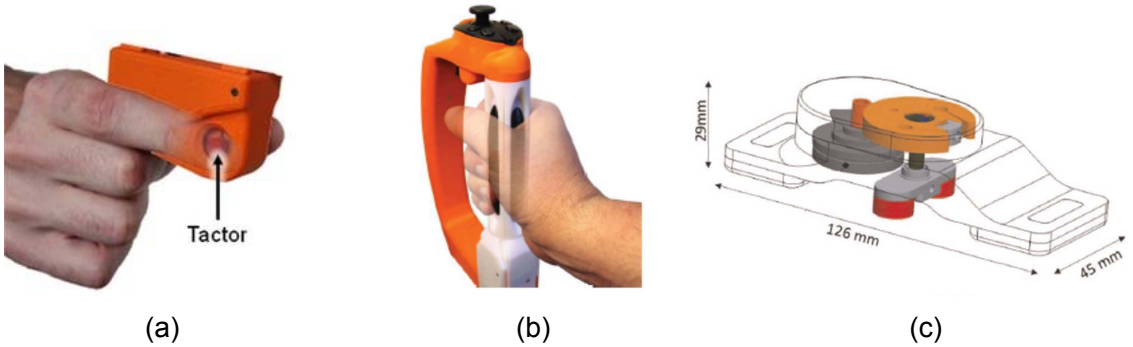

Figure 1.3: Skin stretch feedback devices: (a) Fingerpad skin stretch device (b) Device that stretches the palm of user's hand (c) Rotational skin stretch device. Photos adapted from [22], [23], and [2] respectively.

Force information can also be conveyed to the user by application of cutaneous normal force to the users' fingerpads. Minamizawa et al. [52] developed a device, shown in Fig. 1.4(a), that used dual motors to apply normal forces to the users' fingerpad. Prattichizzo et al. [61] extended the idea with a device that applies 3-DoF cutaneous forces to the fingerpad, shown in Fig. 1.4(b). Using a feedback method termed "sensory subtraction", kinesthetic forces are subtracted from the combination of kinesthetic and cutaneous sensations present during normal interaction, leaving only the cutaneous sensations that are fed back to the user using a tactile feedback device. They used the device to perform a needle insertion task, and showed that superior performance is achieved using cutaneous normal force feedback compared to visual feedback.

1.3.2 Tactile Sensory Augmentation

The same tactile modality used for sensory substitution can be used for sensory augmentation. Researchers have looked at the effect of such tactile augmentation of

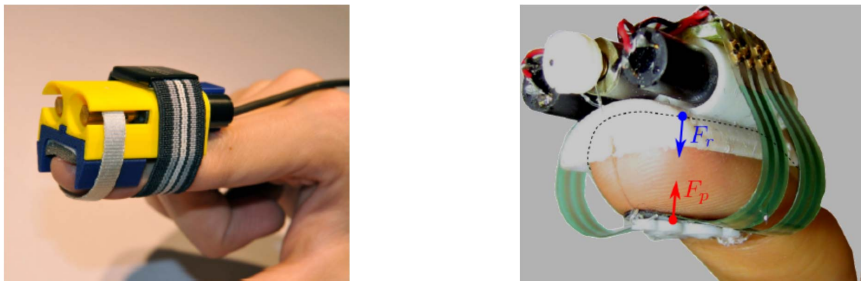

(a) (b)

Figure 1.4: Wearable cutaneous normal force feedback device: (a) 1-DoF device (b) 3-DoF device. Photos adapted from [52] and [80], respectively.

force feedback on user perception. Okamoto et al. [54] used vibration on the fingerpad to bias the perceived viscous and inertia properties of an object. In addition, Okamura et al. [55] and Kuchenbecker et al. [39] rendered vibration in conjunction with forces using a force-feedback device to increase the perception of hardness of an object. A similar concept, termed "Rate Hardness", has also been discovered as an important factor affecting perceived rigidity [41]. Several studies use this principle by rendering constant impulses or braking impulses [10][60] with magnitude proportional to the contact velocity [67] to increase the rate hardness and hence the perceived rigidity of a surface. Besides vibration and force impulses, skin stretch feedback has also been used in conjunction with force feedback to bias the perception of friction [62] of a haptically rendered virtual surface.

Several works have also looked into the effect of sensory augmentation on task performance. In many cases, adding tactile feedback to force feedback achieved performance better than the case when either tactile or force feedback is used alone. Augmenting force feedback with vibration feedback decreases the contact force error in a path-tracing task [12] and reduces reaction time to tissue puncture in a teleoperated needle insertion task [37], while augmenting force feedback with skin deformation feedback (normal skin deformation or tangential skin stretch) decreases the penetration into a forbidden region in a needle insertion task [58][80] and improves accuracy in a direction identification task [25].

In this dissertation, we combined the idea of providing tangential skin stretch and normal forces to the user's fingerpad to develop tactile devices that can provide skin

deformation cues to the fingerpad. This skin deformation cues are used to provide force and torque information to substitute or augment kinesthetic force and torque feedback.

1.3.3 Other Forms of Tactile Feedback

Other forms of tactile feedback had been developed, not for tactile sensory substitution or augmentation of force/torque feedback, but for research into human perception, or to provide tactile feedback to systems where such types of feedback are absent. Hayward and Cruz-Hernandez [28] constructed an array of piezoelectric actuators closely packed within a membrane to create lateral skin stretch. Their device generates a programmable stress field within the fingerpad. Drewing et al. [15] also constructed a multiple-contact shear display using mechanical linkages and servo motors, as shown in Fig. 1.5(a). Using this device, they performed perceptual experiments to determine the human sensitivity for tactile movement perception, and found that the direction perception Just Noticeable Difference (JND) is no better than 14 degrees for all subjects.

Winfield et al. [92] designed a device, called the T-pad, which can rapidly alter the friction property of a surface through out-of-plane vibration. By generating in-plane vibration, and by rapidly changing the property of the surface between low and high friction through out-of-plane vibration, the device can modulate the amount of shear force applied to the subject. Such an approach can be used to render tactile feedback in devices such as tablets and smartphones. Chubb et al. [9] improved on the design of the original T-pad to increase the in-plane vibration frequency, and they found that this helped to improve the 3D-edge rendering capability compared to the original T-pad.

Provancher et al. [63] designed a tactile device, called the contact location display (Fig. 1.5(b)), which uses tactile feedback to render the location of the contact centroid moving on the user's fingertip. They found, through a human perception experiment with virtual environment, that users are able to distinguish between objects of different curvature, as well as the interaction types using such a contact location

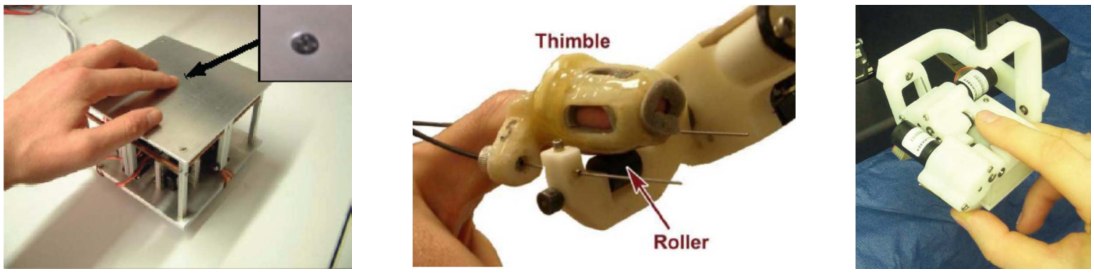

Figure 1.5: (a) Multiple-contact shear display using mechanical linkages and servo motos (b) Contact location display (c) 2-D slip display. Photos adapted from [15], [59], and [87] respectively.

display.

Webster et al. [87] use two DC motors to drive a ball using contact friction, as shown in Fig. 1.5(c). The ball is positioned under the user's fingerpad, and rotation of the ball reproduces the sensations of sliding contact and slip. They found that human study participants are able to use the combination of slip and force feedback to complete a virtual paper manipulation task with lower applied force compared to force feedback alone.

Kajimoto et al. [32] developed an electrotactile display that is compose of skin surface electrodes. They proposed an algorithm that uses real-time impedance sensing to vary the duty-cycle of a pulse-width modulation to minimize the variance in tactile sensation due to spatial and temporal difference in skin impedance.

1.3.4 Feedback of force information in Surgical Teleoperation Systems

1.3.4.1 Force and Tactile feedback in robotic surgery

Kinesthetic force feedback had been found to be useful in surgery. The force feedback helps to reduce interaction forces [82] while improving task performance such as

tissue characterization [79] and suture manipulation [36][76]. However, due to several issues, which include the stability of the system, current surgical teleoperation systems do not incorporate force feedback [56]. To overcome this issue, McMahan et al. [51] studied the feedback of interaction information through vibrotactile feedback in surgical teleoperation systems. Instead of relaying the whole spectrum of interaction force information, they focus particularly on the sensing and feedback of high-frequency vibration during the performance of a task. Accelerometers were placed on the patient-side robot of a clinical da Vinci system to sense the tool acceleration, and this information is fed back and displayed through vibrotactile actuators on the master tool manipulator. They found that such tactile feedback improves the surgeon's concentration and situation awareness, while maintaining task performance when working on a teleoperated surgical task.

Besides conveying information related to interaction with objects in the surgical environment, King et al. [35] conveyed tactile information related to grasping. They used a piezoresistive force sensor to measure the grip force on the patient-side robot of the da Vinci surgical teleoperation system, and pneumatic balloon actuators on the master side manipulator to feed back the grip force information to the user. The display of gripping force information through such tactile approach decreases the gripping force during execution of a peg-transfer task.

Meli et al. [61] used the same sensory subtraction approach, as described in section 1.3.1, to perform a task in which users insert rings onto pegs, emulating the Peg-board module of the da Vinci Surgical Simulator (Intuitive Surgical, Inc.). They found that sensory subtraction reduces insertion forces and time when compared to the case with just visual feedback.

Other methods have been developed for conveying tactile information in tasks that are surgically motivated, such as palpation and lump detection, though these systems were not integrated and tested with actual surgical teleoperation systems. Gwilliam et al. [25] developed an air jet lump display that uses an air jet directed through an aperture to create sensations of lumps of different hardness and size. Serio et al. [71] developed a fabric yielding tactile display, shown in Fig. 1.6(a), that is able to vary the contact area spread rate during palpation to display surfaces of different

compliance. Such methods were also used by Kimura et al. [34] who employ a flexible surface to wrap around the fingers (Fig. 1.6(b)), and Yazdian et al. [93] who use a tilting plate to vary the contact area spread rate during palpation (Fig. 1.6(c)).

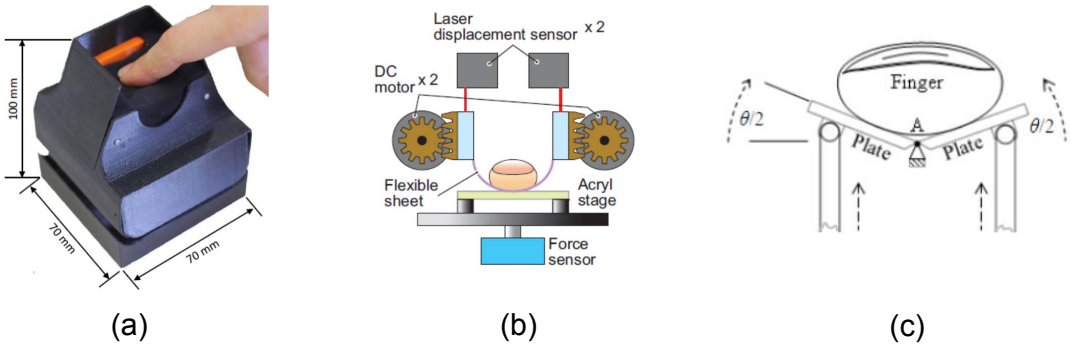

Figure 1.6: (a) Fabric yielding softness display (b) Softness display that uses a flexible surface to wrap around fingers (c) Tilting plate softness display. Photos adapted from [71], [34], and [93] respectively.

1.3.4.2 Visual feedback in robotic surgery

Besides conveying force information through the haptic modality, Gwilliam et al. [24] and Reiley et al. [66] implemented a system that is able to graphically display interaction force information to the user, shown alongside the surgeons' view of the surgical environment through either a force bar display or a visual color indicator. Such vision-based display of interaction force information decreased interaction forces and lowered surgeon's mental workload during performance of surgical task. Tavakoli et al. [78] performed telemanipulated suturing experiment with visual force feedback and found the same decrease in interaction force. However, he found that such performance benefits are only obtained if the surgeons paid attention to the visual force feedback, resulting in higher mental workload for the surgeons.

1.4 Dissertation Overview

This thesis consists of six chapters. In Chapter 1, which is this introduction, we presented the motivation for our research of using tactile feedback for sensory substitution and augmentation of force feedback. We also presented prior work on the various types of tactile feedback devices and prior work on providing interaction force information in robot-assisted minimally invasive surgery.

Chapter 2 describes how tangential skin stretch feedback can be rendered together with force feedback to increase stiffness perception of virtual rendered surfaces. We performed human user experiment to determine how human perception of stiffness of objects are affected by additional skin stretch cues. We also derived a model utilizing the framework of multi-sensory integration to characterize the shift in stiffness perception due to skin stretch augmentation.

Our results from Chapter 2 highlighted the promising approach of using fingerpad skin deformation for force feedback substitution and augmentation. In Chapter 3, we describe a 3-Degree-of-Freedom (DoF) skin deformation tactile device that is able to communicate 3-DoF force information for sensory substitution or augmentation of force feedback. We performed human user experiment that evaluated participants' ability to interpret the 3-DoF force information to locate a feature in a virtual environment, and how participants' task performance can be improved by augmenting force feedback with skin deformation feedback and vice versa.

While skin deformation tactile feedback can be used to convey 3-DoF force information, a similar approach can be used to convey 3-DoF torque information, or 6-DoF force and torque information to the user. This information can be used for sensory substitution and augmentation of forces and torques. In Chapter 4, we present a skin deformation tactile device that can convey 6-DoF force and torque information. We performed a human user experiment to verify the device's capability as well as participants' ability to interpret the 6-DoF force and torque information to perform a peg-in-hole task.

In Chapter 5, we integrated the 3-DoF skin deformation tactile device with a surgical teleoperation system. The viability of using skin deformation tactile feedback,

as well as its usefulness, was evaluated via a human user experiment in which participants performed surgically related tasks with force and/or skin deformation tactile feedback.

Chapter 6 summarizes the results of this research, reviews the contributions made in this dissertation, and provides suggestions for future work.

Chapter 2

Augmentation of Stiffness with Tangential Skin Stretch

In Chapter 1, we presented prior work on using tactile feedback for sensory substitution and augmentation of force feedback, and prior work on various types of tactile devices. A particularly interesting form of tactile feedback is skin stretch feedback. In this chapter, we investigate the use of skin stretch tactile feedback to augment the perception of stiffness of rendered virtual surfaces.

The rendering of stiffness surfaces using kinesthetic force feedback devices has been an important area of research in the field of haptics. High stiffness rendering is associated with a higher transparency of the system. However, the rendering of high stiffness surfaces is plagued by many factors that affect its stability, such as position sensing resolution, time delay, haptic feedback control loop rate, and the inertial and damping properties of the kinesthetic force feedback device [88][14]. To maintain stability of the rendering, the maximum rendered stiffness is often lowered. The end result is that the kinesthetic force-feedback device is limited in the magnitude of the force it can display and the stiffness of the environment it can render stably. All of these factors can degrade the rich information that the sense of touch provides, which may introduce significant sensory and perceptual cost [43] and effect task performance [91].

In this chapter, we use a 1-degree-of-freedom (DoF) tactile skin stretch device

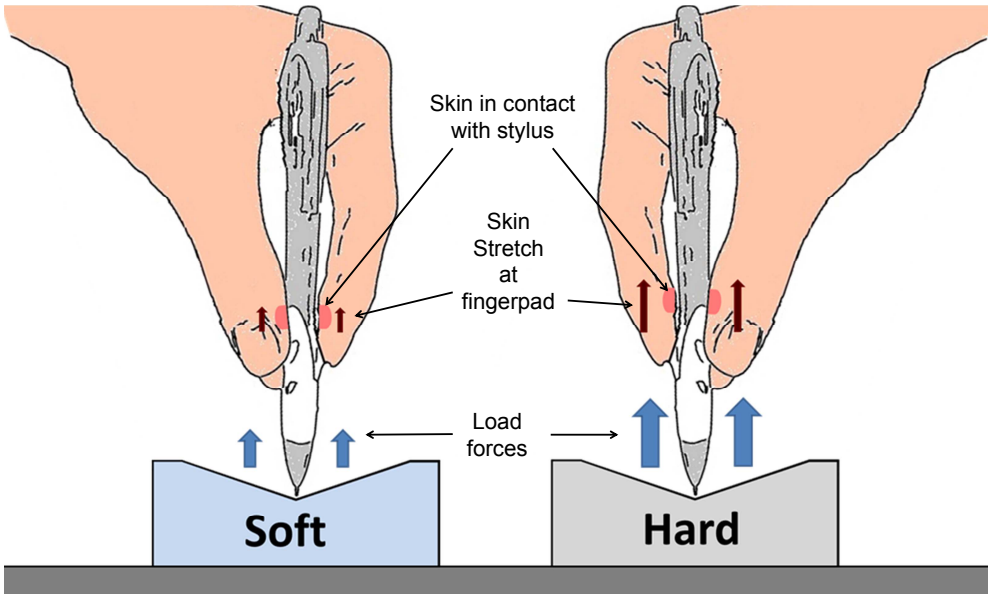

Figure 2.1: Skin stretch is a tactile sensation that provides information regarding the stiffness of an object. As we interact with a stiffer object using a stylus, for the same penetration distance, we experience a larger load force and hence a larger shear force and larger skin stretch on the fingerpad.

to render skin stretch together with forces to augment the perception of stiffness of virtual surfaces. In Fig. 2.1, schematic representations of interactions with soft and hard objects demonstrate that, when a person uses a stylus-like device to interact with the environment, for the same penetration distance, a stiffer environment results in a larger load force. The larger load force causes a larger shear force between the fingerpad and the stylus, and hence, a larger amount of fingerpad skin stretch. Prior studies have shown that humans obtain information from multiple sensory modalities [29] and integrate them in a statistically optimal [16] or sub-optimal [40] fashion to form a single percept. In addition, studies have shown that tactile cues play a role in the discrimination of stiffness information [74][4]. Skin stretch, in particular, has been shown to increase the perception of friction when rendered in conjunction with forces [62].

From these prior results, we hypothesized that skin stretch is a tactile stimulus that is integrated with kinesthesia to form the perception of force, and, when combined with displacement information, contributes to the perception of stiffness. By

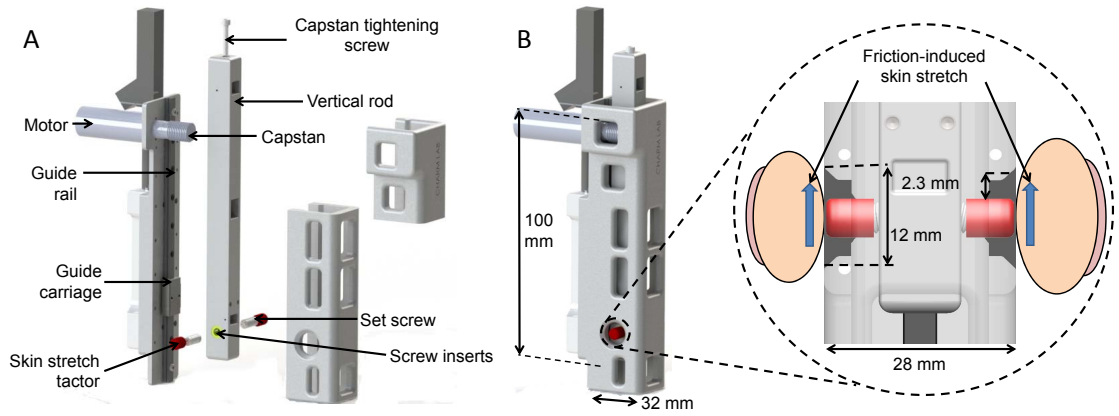

Figure 2.2: Exploded and assembled view of the Skin Stretch Stylus. A: The device consists of a vertical rod attached to a linear guide carriage, which slides along the linear guide rail. A DC motor actuates the vertical rod through a cable capstan mechanism. Skin stretch tactors are attached to the side of the rod. B: Movement of the tactors stretch the skin of the users fingerpad while the users fingers are locally grounded on the outer aperture.The skin stretch tactor movement was software-limited to -2.3 mm in order to prevent the tactor from hitting the sides of the aperture.

rendering skin stretch (using tactor displacement) in conjunction with force, we can modulate the perceived stiffness of the object. We also proposed a model that can explain the effect of artificial tactor displacement-induced skin stretch on the perception of stiffness.

2.1 1-Degree-of-Freedom Skin Stretch Device Design and Control

We designed and built a 1-Degree-of-Freedom tactile device that can impart tangential skin stretch to the users fingerpad skin, shown in Fig.2.2. The device consists of a linear guide rail fixed onto a rapid prototyped plastic backing. A vertical bar, fixed to the carriage of the linear guide, slides along the guide rail. The vertical bar is actuated by a 16 mm geared DC motor (Portescap 16G88214E with gear ratio of 27:1) through a cable capstan drive. The vertical rod consists of screw holes at one end of the rod, where 10-32 set screws are inserted to create two protrusions. Skin stretch tactors,

which are rubber Lenovo Trackpoint Classic dome tactors with a rounded surface and a rough, sandpaper-like texture, are placed over the set screws. Movement of the vertical bar shifts the skin stretch tactors, and friction between the tactors and the skin stretches the users fingerpads tangentially. The tactors are surrounded by conical apertures (each with a 12 mm diameter) on the outer shell covering the device. These apertures allow users to have a firm grip on the device, while grounding the user's fingerpads locally to the outer shell so that the skin stretch tactors stretch the skin of the user within the aperture.

The Skin Stretch Stylus is attached to the end of a Phantom Premium 1.5 haptic device (Fig. 2.3(a) and Fig. 2.3(b)). The Phantom Premium provides force feedback and measurements of the users hand position, while the Skin Stretch Stylus imparts skin stretch to the users fingerpad through tactor displacement during interaction with a virtual environment. CHAI3D [11] is used to render the virtual environment, which consists of a horizontal virtual surface with programmable stiffness. The visual display gives a top-down view of the surface, as shown in Fig. 3(a), so that users can visualize the desired workspace in which they should maintain the device. This view does not provide any visual cues about the stiffness properties of the virtual surface.

The force f rendered by the Phantom Premium is

$$f = kx, \tag{2.1}$$

where x [m] is the amount of penetration into the horizontal virtual surface and k [N/m] is the stiffness of the virtual surface. The amount of tactor displacement rendered by the Skin Stretch Stylus can be calculated in two ways:

$$x_{\text{ss}} = Rf, \tag{2.2}$$

or

$$x_{\text{ss}} = Gx, \tag{2.3}$$

where x_{ss} [mm] is the desired tactor displacement, R is the ratio of applied tactor displacement to applied force, which we call tactor displacement ratio, and G [mm/m]

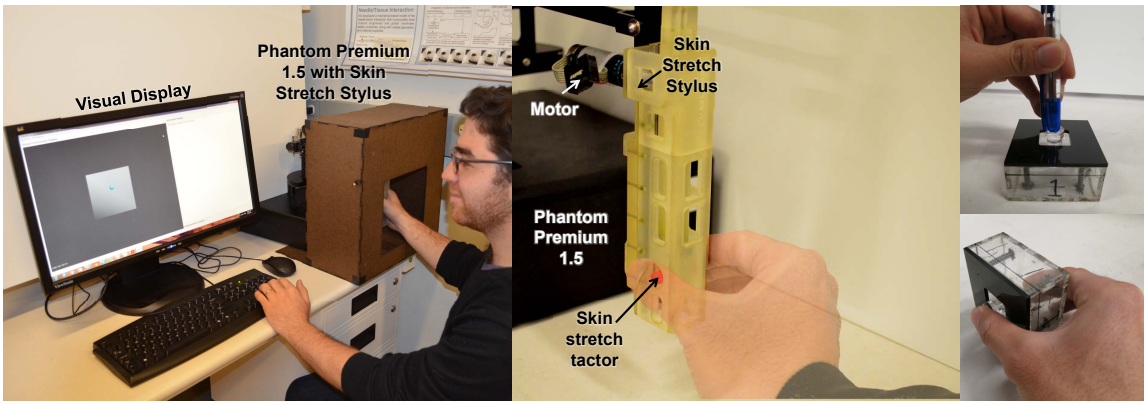

Figure 2.3: (a) The Skin Stretch Stylus attached to the Phantom Premium 1.5. The visual display shows a top-down view of the surface presented to the user. (b) Subjects are advised to hold the Skin Stretch Stylus by gripping the stylus with a force of approximately 2 N, with the thumb and index finger completely covering the aperture. (c) Subjects probed stiffness boxes to understand the concept of stiffness and familiarize themselves with the desired grip force prior to the main study.

is the ratio of applied tactor displacement to penetration depth, which we call tactor displacement gain. The desired tactor displacement is converted to a desired motor angle through the device kinematics. A proportional-integral-derivative (PID) controller calculates the torque to be applied to the motor in order to move the tactor to the desired location.

We performed an experiment to verify accurate control of the skin stretch tactor motion when subjected to shear forces from the user's fingerpad. A series of sinusoidal desired tactor positions, with a position amplitude of 2 mm and a frequency range of 1-5Hz, were commanded. This range of tactor displacement amplitude and movement frequency is typical of the maximum tactor displacement and movement frequency that will be rendered by the device when users interact with the virtual surface. The total error, including the control error and error due to backlash, was less than 10% of the commanded input. Due to these errors, the actual amount of tactor displacement rendered to the user was lower than the commanded amount.

2.2 Effect of skin stretch on perception of stiffness

2.2.1 Study Description

The experiment protocol was approved by the Stanford University Institutional Review Board.

2.2.1.1 Participants

Twelve right-hand-dominant subjects (9 males and 3 females) between the ages of 18 and 41 participated in our experiment after giving informed consent.

2.2.1.2 Experiment Methods

The goal of the experiment was to determine the shift in subjects' perception of stiffness when tangential skin stretch is applied to the fingerpads during the exploration of a kinesthetically rendered surface. Prior to the start of the experiment, subjects probed two physical springs with different stiffness values using a physical stylus, and were asked to determine which of the two surfaces was stiffer. They were coached if they answered incorrectly. This ensured that all subjects had a common interpretation of the concept of stiffness. Subjects were then instructed to hold the skin stretch stylus using their right hand, as shown in Fig. 2.3(b). Prior to the start of the experiment, we trained the grip force of the subject to be approximately 1-2 N by asking them to press on a spring-loaded mechanism, shown in Fig. 2.3(c). The spring-loaded mechanism is designed such that user will grip the mechanism in a similar manner to the way they grip the aperture. Subjects underwent further training during breaks in the experiment to ensure consistent stylus grip force throughout the experiment.

To assess the effect of adding artificial skin stretch on perception of stiffness, we employed a two-alternative, forced-choice paradigm with the method of constant stimuli. We used subjects' responses to fit psychometric curves that describe their perception of stiffness as a function of the level of imposed fingerpad skin stretch. In this experiment, subjects were presented with two surfaces for each trial: a reference and a comparison. The reference surface had a kinesthetic stiffness (k) of 125 N/m

and skin stretch ratios (R) of 0, 0.2, 0.4, and -0.4 mm/N. Each of the reference stimuli was compared with each of the kinesthetic-only stimuli with values of 10, 50, 90, 110, 130, 150, 170, 190, 210, 230, 270, and 310 N/m, for a total of 144 trials per skin stretch ratio. The trials were presented in balanced, predetermined, pseudo-random order, which was the same across all participants. Subjects were given as much time as they desired to interact with each surface, but were not allowed to answer which surface was stiffer until they had spent a minimum of 3 seconds interacting with each surface. The experiment consisted of a total of 576 trials, comprising 12 repetitions of the 12 comparison stiffness values for each of the 4 different skin stretch ratios. The experiment was divided into two 1.5- to 2-hour sessions of 288 trials each, completed on different days. After every 30 trials, subjects were given a 3-minute break during which they rested and underwent reinforcement training on the desired stylus grip force.

2.2.1.3 Data Analysis

To assess the effect of the addition of artificial skin stretch on perception of stiffness, we used subjects' responses to calculate the Point of Subjective Equality (PSE), the point at which subjects, judged the reference to be equal to the comparison. For our experiment, the PSE represents the stiffness-only stimuli that is perceptually equivalent to the reference stimuli (kinesthetic force feedback combined with skin stretch). We fit psychometric curves to the subjects' responses using the psignifit toolbox version 2.5.6 [89], and extracted the PSE at the point where the fit function crosses the 0.5 value. We calculated confidence intervals using the accelerated and bias-corrected bootstrap method described in [90]. Examples of psychometric curve fit to subjects' response are shown in Fig. 2.4.

Statistical analysis was performed using MATLAB anovan, ttest, and custom-written functions. To statistically test the effect of the skin stretch ratio on perceived level of stiffness, we used repeated-measures one-way ANOVA [49][18]. We used the Greenhouse-Geisser correction to adjust for the degrees of freedom in the repeated-measures ANOVA (due to homogeneity assumption) [49], and the p-values calculated

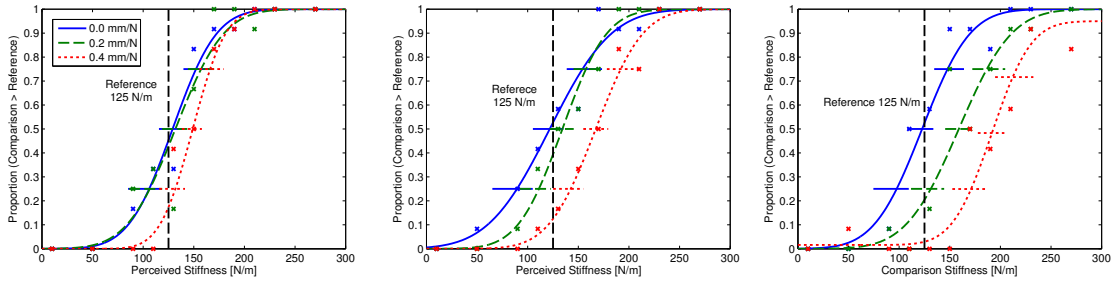

(a) Weakly affected subject (b) Moderately affected subject (c) Strongly affected subject

Figure 2.4: Example psychometric curves for different skin stretch ratios for subjects weakly, moderately, and strongly affected by skin stretch. Symbols are data extracted from subject, curves are fit psychometric functions, and horizontal lines are 95% confidence intervals for estimation of 0.5 threshold value. The shift of the psychometric curve to the right of the 125 N/m reference indicates that the subject feels the combination of kinesthetic force and skin stretch feedback creates a perceptually stiffer surface

using this adjustment are referred to as p_{adj}. We performed multiple post-hoc comparisons to test the statistical significance of contrasts between different skin stretch ratios, and used Bonfferoni correction for family-wise error. Statistical significance was determined at the 0.05 level.

2.2.2 Results and Discussions

Fig. 2.5a shows the PSE values for all subjects and for all skin stretch ratios. The diagram showed that six out of twelve subjects show a positive shift in perceived stiffness that increased with increasing skin stretch ratio. However, there is a large intra-subject variability in perception for the negative skin stretch ratio of -0.4 mm/N. Therefore, we did not include the negative skin stretch ratio of -0.4 mm/N results in our statistical analysis.

Fig. 2.5b shows the the mean and the 95% confidence interval for the estimated mean of the perceived stiffness of the reference stimuli for all subjects. When averaged across all subjects, we found a statistically significant increase in the mean PSE when artificial skin stretch is applied to the subjects fingerpads ($p = 0.001$), and that the effect increases as larger skin stretch is applied using a higher skin stretch ratio. The

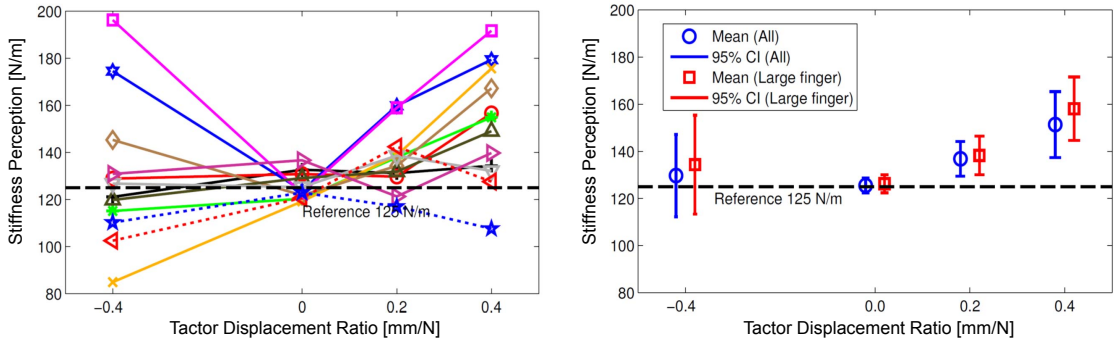

(a) (b)

Figure 2.5: (a) Individual trends for stiffness perception for all 12 subjects. (b) Mean and 95% confidence intervals for the perceived stiffness for tactor displacement ratios of -0.4, 0.0, 0.2, and 0.4 mm/N for all subjects and for large finger subjects. There is a significant increase in the mean perceived stiffness when tactor displacement is being applied.

results of repeated measures one-way ANOVA together with post-hoc comparisons between different skin stretch ratio groups are presented in Table 2.1.

A detailed examination of Fig. 2.5a reveals that some of the subjects showed relatively small perceptual effects (shown with dashed lines in Fig. 2.5a). A possible explanation for such a lack of perceptual effect could be the size of the subjects' fingerpads. The shift in perceived stiffness for a skin stretch ratio of 0.4 mm/N as a function of the measured user finger size is shown in Fig. 2.6. There is a statistically significant positive correlation between the size of the fingerpad and the shift in stiffness perception ($R = 0.76$, $p = 0.0045$). We believe that the subjects with very small fingerpads did not properly experience the effects of skin stretch because their fingers were too small to hold on securely to the device's apertures. In that case, the fingers would move with the the skin stretch tactors, preventing tactor motion from imposing additional skin stretch. These subjects therefore experienced a fundamentally different experiment due to the lack of finger restraint from apertures that were not properly sized for their fingers. Based on this result, we repeated the statistical analysis excluding subjects with index finger width less than 14 mm (small finger group, $n = 2$, '$\times$' symbols and dashed lines in Fig 2.5a). This was based on the device aperture size of 12 mm and a 1 mm overlap between finger and device

	All subjects			**Large finger subjects**		
Group Analysis	$F_{2,22}$	p	p_{adj}	$F_{2,18}$	p	p_{adj}
ANOVA	9.54	0.0010	0.0041	14.9	$1.53 * 10^{-4}$	0.0013
Post-hoc analysis	Effect [N/m]	t_{22}	p	Effect [N/m]	t_{18}	p
$\mu_{0.2} > \mu_{0.0}$	11.33	2.70	0.0065	12.01	2.88	0.0050
$\mu_{0.4} > \mu_{0.2}$	14.52	3.46	0.0011	19.84	4.76	$7.86 * 10^{-5}$
$\mu_{0.4} > \mu_{0.0}$	25.84	6.16	$1.67 * 10^{-6}$	31.85	7.64	$2.35 * 10^{-7}$

Table 2.1: Results for the repeated measures one-way ANOVA, together with the post-hoc analysis with the appropriate Bonfferoni correction, for all subjects and large finger subjects. There is statistically significant difference between the mean PSE values across all three comparisons when considering all subjects and when considering only large finger subjects.

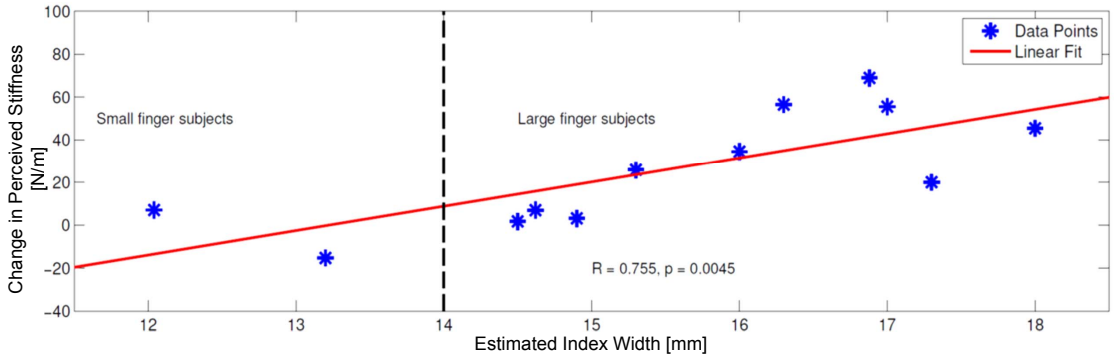

Figure 2.6: Correlation between the estimated size of the subjects fingertip and the shift in stiffness perception for a skin stretch ratio of 0.4 mm/N. There is a statistically significant positive correlation between subjects fingerpad size and shift in stiffness perception.

at each side of the aperture. The results for the group of subjects with large fingers (n = 10) are depicted in Fig. 2.5b (squares) and on the right side of Table 2.1, and are qualitatively similar but more pronounced than the results of all subjects taken together.

2.3 Modeling of skin stretch augmentation

2.3.1 Model for stiffness perception with skin stretch augmentation

We propose a model for the perception of stiffness based on force and skin stretch information using the framework of multisensory integration. We assume that the force information that is communicated via kinesthesia, $F_{\text{kinesthesia}}$, and the shear force information that is communicated via tactile mechanoreceptors, $F_{\text{cutaneous}}$, are combined into a single percept by some weighting rule, such as:

$$F_{\text{perceived}} = wF_{\text{kinesthesia}} + (1 - w)F_{\text{cutaneous}}, \tag{2.4}$$

where $F_{\text{perceived}}$ is the perceived force and w is a weight that depends on many factors, such as the density of tactile mechanoreceptors in the skin, the relative reliability of the cutaneous and kinesthetic information, and other factors such as cognitive strategy. All factors that contribute to the weighting rule are subject-specific. For our device, the shear force on the fingerpad mechanoreceptors, $F_{\text{cutaneous}}$, is a combination of the shear force applied by the force feedback device via contact with the aperture, F_{aperture}, and the shear force, F_{tactor}, caused by displacement of the tactor. Fig. 2.7 shows the distribution of the shear force on the fingerpad when subjected to a load force F_{load} and tactor displacement x_{ss}. Since the tactile device does not impart additional forces to the user, the forces transferred from the stylus to the user via the fingerpad skin-stylus interface (the sum of F_{aperture} and F_{tactor}) is equal to the load force F_{load}. The kinesthetic force $F_{\text{kinesthetic}}$ experienced by the user is therefore also equal to F_{load}.

Bergmann Tiest et al. showed that there is a significant effect of the area of distribution of cutaneous force on weight perception [5]. Due to the difference in area in which the tactor shear force and the load force acts on the fingerpad, we assumed that

$$F_{\text{cutaneous}} = \gamma F_{\text{aperture}} + \eta F_{\text{tactor}}, \tag{2.5}$$

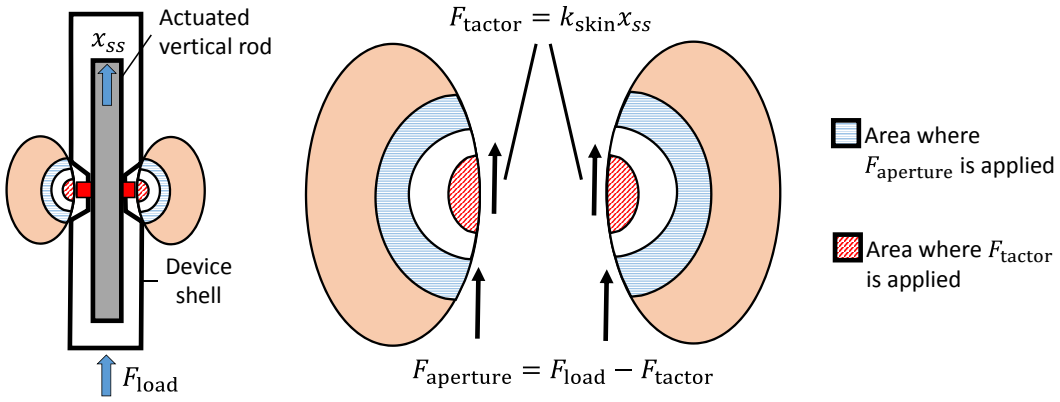

Figure 2.7: Free body diagram of the fingerpad when subjected to a load force acting on the stylus and a tactor displacement of x_{ss}.

where γ and η are additional weighting factors caused by the difference in area in which the shear force is applied. Considering the relation that $F_{\text{kinesthetic}} = F_{\text{load}}$, $F_{\text{aperture}} = F_{\text{load}} - F_{\text{tactor}}$, and substituting Equation (2.5) into Equation (2.4), yields:

$$F_{\text{perceived}} = (\gamma + w - \gamma w)F_{\text{load}} + (1 - w)(\eta - \gamma)F_{\text{tactor}}, \tag{2.6}$$

If we model the skin-tactor interface as an ideal linear spring, and assuming no slip at the skin-tactor interface, we get

$$F_{\text{perceived}} = (\gamma + w - \gamma w)F_{\text{load}} + (1 - w)(\eta - \gamma)k_{\text{skin}}x_{\text{SS}}, \tag{2.7}$$

where k_{skin} is the skin stiffness (also subject specific) and x_{SS} is the amount of tactor displacement. To obtain a model of the perceived stiffness, we divide the perceived force by the penetration depth:

$$k_{\text{perceived}} = \beta k_{\text{load}} + \alpha G, \tag{2.8}$$

where $k_{\text{perceived}}$ is the overall stiffness percept, k_{load} is the stiffness resulting from force feedback, $\beta = (\gamma + w - \gamma w)$ is the coefficient relating the ratio of actual rendered stiffness perceived by users, and $\alpha = (1 - w)(\eta - \beta)k_{\text{skin}}$ is the coefficient parameter relating the tactor-displacement gain, G, to the shift in stiffness perception. We note

that the parameter α is equal to the parameter $b_{i,j,\text{slope}}$ used in our regression model. Therefore, in accordance with this model, the shift in perceived stiffness, Δk, from Equations (2.11) and (2.12), will depend on the tactor displacement gain:

$$\Delta k = \alpha G, \tag{2.9}$$

The above model implies that the additional skin stretch induced by tactor displacement will have an additive effect on stiffness perception, independent of surface stiffness. This model motivates the use of tactor displacement gain in this study, instead of tactor displacement ratio in the first study. Using tactor displacement gain allows us to model the effect of tactor displacement-induced skin stretch on stiffness perception in a way that is independent of the surface stiffness. The tactor displacement gain G, which is the ratio of tactor displacement to penetration depth, is analogous to stiffness (ratio of force to penetration depth), and the coefficient α determines how we integrate this information to form the perception of stiffness. As the coefficient α depends on many subject-specific biomechanical and neural factors, we expect large inter-subject variability in the estimated value of this coefficient. Therefore, we expect that the Linear Mixed Model will yield statistically significant dependence on G and on the interaction between s (subject) and G.

2.3.2 Study Description

The study protocol was approved by the Stanford University Institutional Review Board.

2.3.2.1 Participants

A total of 15 subjects (3 females and 12 males) between the ages of 22 to 32 participated in the study after providing written consent.

2.3.2.2 Pre-Study Procedures

Prior to the beginning of the study, we measured the size of the index finger and thumb of the subject. Subjects then went through a familiarization protocol consisting of the following steps. They were first told to probe two spring-loaded boxes (depicted in Fig. 2.3(c)), which differed in their physical stiffness, and reported the box with the higher stiffness. Subjects were corrected if they responded incorrectly. This step ensures that subjects have a common and correct interpretation of stiffness prior to the start of the study. Subjects were then instructed to squeeze one of the spring-loaded boxes to a desired level of about 2 N (indicated by visual markings on the side of box). The spring-loaded boxes were designed such that the user's grip is similar to the grip they used later to hold the Skin Stretch Stylus. Subjects were reminded by the experimenter to maintain this grip force throughout the study. The target 2 N grip force was chosen because, with a maximum tactor displacement of 2.3 mm, the estimated applied normal force on the tactor to prevent slip between the tactor and the fingerpad is approximately 1.97 N [19]. This normal force was computed based on prior work: the mean fingerpad stiffness in the radial and ulnar direction is 1.37 and 1.18 N/mm respectively, while the friction coefficient between the fingerpad skin and the tactor surface is > 1.6 [20].

After the first two steps, to familiarize themselves with the study procedures, subjects performed an initial training phase consisting of 36 trials. In these trials, subjects were presented with pairs of virtual surfaces, and asked to choose which of the two surfaces was stiffer. During this phase, the grasp, posture, and interaction manner of the subject were visually monitored by the experimenter. Subjects were instructed to hold the device as shown in Fig. 2.3(b). Any undesirable grasp or interaction behaviors, such as tilting the device away from the vertical position or gripping the tactor instead of the aperture, were corrected. This training lasted about 5 minutes, and was included so that subjects fully understood the experiment procedure and the manner in which they should grip the device to interact with the virtual surface before proceeding to the main study.

2.3.2.3 Study Procedure

In the main study, we employed a two-alternative, forced-choice paradigm using the 1-up, 1-down adaptive staircase method to determine the effect that tactor displacement-induced skin stretch has on the perceived stiffness of virtual surfaces. Subjects were presented with two surfaces: a reference surface and a comparison surface, in a random order. The reference surface displayed force and tactor displacement, while the comparison surface displayed only force feedback. In a 1-up, 1-down adaptive staircase method, when subjects answered that the reference surface is stiffer, the stiffness of the comparison surface was increased by one step size. Similarly, when subjects answered that the comparison surface was stiffer, the stiffness of the comparison surface was decreased by one step size. Using the 1-up, 1-down method, the 50% point on the psychometric function, called the Point of Subjective Equality (PSE), is obtained. This is the surface stiffness that subject feels is equivalent to the reference surface with force and tactor displacement. The adaptive staircase method was chosen because the PSE can be estimated using a small number of trials, which allowed us to determine the PSE at multiple reference stiffness levels and multiple tactor displacement gains without having to perform a long and fatiguing study. To reduce the error caused by habituation and expectation, we performed two sets of adaptive staircase trials for each reference with low and high initial stiffness.

In each trial, subjects were given 3 seconds to interact with each of the two virtual surfaces. Then, the subject had to select which of the two surfaces was stiffer. The comparison stiffness value changed according to the subject's response, and the study continued until the termination criterion of 10 reversals was met. A reversal was defined as changing the direction of the comparison stiffness step size from positive to negative, or vice versa.

The reference surface conditions were surface stiffness of 60, 120, and 180 N/m with tactor displacement gains of 0, 40, 80, 120, and 160 mm/m. These reference surface stiffness values were chosen because they are near the lower end of stiffness values that can be rendered by many commercial force-feedback haptic devices. In addition, the above tactor displacement gains were chosen such that, with the maximum value of 160 mm/m, subjects' interaction with the virtual surface will lead to

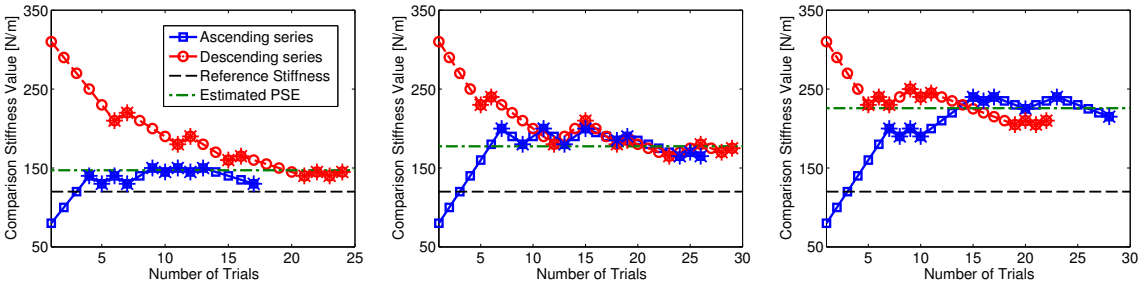

(a) Weakly affected subject (b) Moderately affected subject (c) Strongly affected subject

Figure 2.8: Example of comparison stiffness values versus number of trials, together with the estimated Point of Subjective Equality (PSE) value, for subjects who are (a) weakly, (b) moderately, and (c) strongly affected by tactor displacement-induced skin stretch. Each dot marks a trial, while each asterisk marks a reversal point. The tactor displacement gain value for these data are 80 mm/m. The graphs illustrate the feasibility of using the 1-up 1-down adaptive staircase method, with both low and high initial comparison stiffness values, to determine the PSE value.

saturation of the tactor displacement. In the first set of trials, the comparison stiffness was set to a low initial stiffness value of 40, 80, and 140 N/m respectively, and in the second set, the comparison stiffness was set to a high initial stiffness values of 250, 310, and 370 N/m, respectively, for the 60, 120, and 180 N/m reference stiffness levels. Prior to the first reversal, the comparison stiffness changed by a large step size of 20 N/m. The step size was reduced to 10 N/m after the first reversal, which was then subsequently reduced to 5 N/m after the fourth reversal. Fig. 2.8 provides an example of the adaptive staircase method, with the ascending and descending series, used in our study.

The entire study consists of 15 parameter combinations (5 tactor displacement gains over 3 reference stiffness levels), with each parameter combination consisting of a staircase sequence that starts from a low and a high initial stiffness level. Each sequence lasted about 3-4 minutes for each subject. The order in which the 30 sequences were presented to the subject was randomized for each subject. The overall study took a total of 1.5 to 2 hours, with each subject completing the study over 1 or 2 days. During the entire study, subjects wore noise-canceling headphones to minimize the effect of environmental or device motor noise on the study results.

2.3.2.4 Data Analysis

To assess the effect of adding tactor displacement-induced skin stretch on perception of stiffness, we calculated the Point of Subjective Equality (PSE) of each subject for each reference stiffness value and tactor displacement gain. The PSE was obtained by averaging the last 6 out of the 10 reversal stiffness values for the ascending and descending sequence of trials:

$$\text{PSE} = \frac{1}{12}\left(\sum_{n=5}^{10} k_{a,\text{trans},n} + \sum_{n=5}^{10} k_{d,\text{trans},n}\right), \tag{2.10}$$

where $k_{a,\text{trans},n}$ is the reversal stiffness for the ascending sequence, $k_{d,\text{trans},n}$ is the reversal stiffness for the descending sequence, and n is the reversal trial number. The shift in perceived stiffness, Δk, was then calculated by subtracting the PSE from the surface stiffness value k:

$$\Delta k = \text{PSE} - k, \tag{2.11}$$

We employed a Linear Mixed Model to assess the dependence of the shift in perceived stiffness, Δk, on reference stiffness r, and tactor displacement gain G. The independent variables in our analysis are the categorical variable of reference stiffness r (fixed effect), continuous variable of tactor displacement gain G (fixed effect), and categorical variable of subject, s (random effect). We include in the analysis first-order interaction between G and r (fixed effect) and between s and G (random effect). This analysis can be interpreted as a Linear Mixed Model that allows subject and stiffness-specific intercepts and slopes with respect to tactor displacement gain. The method is described mathematically as

$$\Delta k_{r=i,s=j} = \underbrace{(b_0 + b_{r_i} + b_{s_j})}_{b_{i,j,\text{intercept}}} + \underbrace{(b_G + b_{Gr_i} + b_{Gs_j})G}_{b_{i,j,\text{slope}}G}, \tag{2.12}$$

where $\Delta k_{r=i,s=j}$ is the shift in stiffness perception for a particular subject i and reference stiffness j, b_0 is the average intercept, b_r is the reference stiffness specific

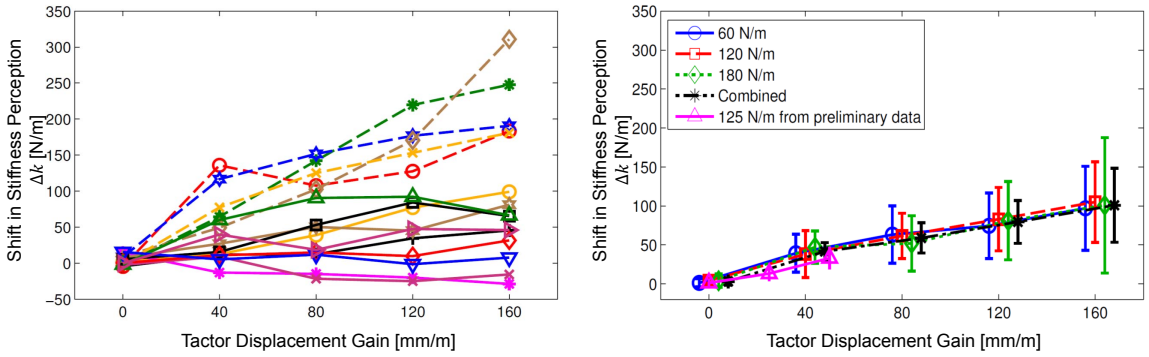

(a) (b)

Figure 2.9: (a) Individual results for the shift in stiffness perception versus tactor displacement gain, averaged across the 3 reference stiffness levels. (b)The means and 95% confidence intervals for the shift in stiffness perception across all subjects for the 60, 120, 180 N/m reference stiffness levels and the overall combined average. Data from a preliminary study is presented for comparison.

intercept, b_s is the subject specific intercept, b_G is the average slope, b_{Gr} is the reference specific slope, b_{Gs} is the subject-specific slope, and G is the tactor displacement gain. The above model can also be interpreted as fitting a regression line between the shift in stiffness perception and tactor displacement gain for each combination of reference stiffness and subject, in which $b_{i,j,\text{intercept}}$ is the intercept and $b_{i,j,\text{slope}}$ is the slope for a particular subject i and reference stiffness j. Statistical analysis of the data based on the above model was performed using the MATLAB fitlme function, with statistical significance determined at the 0.05 level.

2.3.3 Results

Fig. 2.8 shows the progression of the change in comparison stiffness value as a function of the trial number for the initial low and high stiffness sequence of three representative subjects that are weakly affected, moderately affected, and strongly affected by the tactor displacement. Each of the diagrams illustrates the convergence of the curves for the low and high initial comparison stiffness set to the Point of Subjective Equality (PSE) value. The estimated PSE is also shown in the diagram, illustrating the feasibility of using the adaptive staircase method to estimate the PSE.

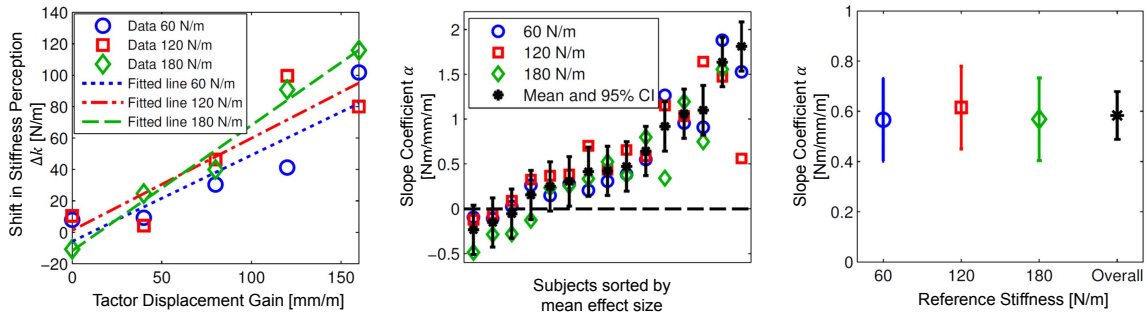

(a) (b) (c)

Figure 2.10: (a) Example subject data and the linear fit by the statistical model.(b)The means, 95% confidence intervals, and individual slope coefficients α for the three reference stiffness values and for all subjects, shown in order of increasing mean subject α to improve readability. The mean slope coefficient α for individual subjects varies from -0.23 N/m to 1.81 N/m per mm/m of tactor displacement gain. (c) Mean and 95% confidence intervals for the slope coefficient α averaged across all subjects for the three reference stiffness levels and the overall data combining the results for the three reference stiffness levels.

Fig. 2.9a shows the perceived stiffness for all subjects averaged across the three reference stiffness cases for different amount of skin stretch gains. The diagram shows that adding tangential skin stretch in conjunction with force feedback increases the perception of stiffness of a virtual surface. The effect is also close to linear, with large inter-subject variability. By averaging the data across subjects instead of reference stiffness level, Fig. 2.9b shows the shift in stiffness perception versus tactor displacement gains for the three reference stiffness levels. The data averaged across the three reference stiffness levels is also shown in the same figure. The result shows that the average shift in perceived stiffness as a function of tactor displacement gain is consistent between the three reference stiffness levels. The result of our preliminary study that was conducted using a different device, subject pool, and experimental paradigm is also depicted. The comparison shows that the effect is robust and independent of the experimental methodology and subject pool.

Fig. 2.10a shows the shift in perceived stiffness of a typical subject, together with the linear regression fit to obtain the slope coefficient $b_{i,j,\text{slope}}$. Both the data and the

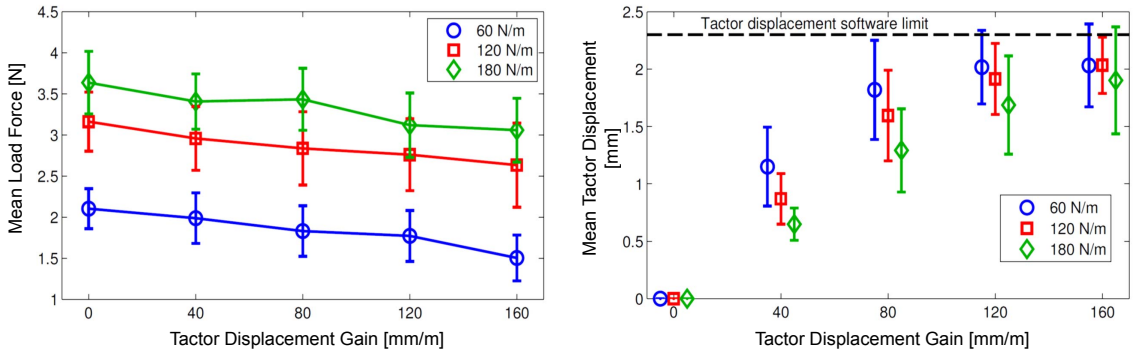

(a) (b)

Figure 2.11: The means and 95% confidence intervals for (a) the maximum load force that subjects experienced, and (b) the maximum amount of tactor displacement that subjects experienced for the 60, 120, and 180 N/m reference stiffness levels. There is a statistically significant decrease in load force as the tactor displacement gain increases.

linear fit show a consistent increase in the perceived stiffness when the same tactor displacement gain is used across the three reference stiffness levels. This within-subject consistency is a characteristic seen in most of the subjects, as evident in the close clustering of the slope coefficients for the three reference stiffness levels for most of the subjects, as depicted in Fig. 2.10b. The 95% confidence intervals of the estimated mean slope of each subject show that 5 subjects were not statistically significantly affected by tactor displacement, while 10 subjects were positively affected by tactor displacement. The consistency of the perceptual effect across different levels of force

Name	Estimates	StdErr	t-stats	DOF	p-value
(Intercept)	10.15	4.72	2.15	219	0.033
G	583.21	154.71	3.77	219	< 0.001
Ref-120	-0.40	6.55	-0.061	219	0.951
Ref-180	-0.93	6.55	-0.143	219	0.886
G*Ref-120	-17.10	66.81	-0.256	219	0.798
G*Ref-180	31.82	66.81	0.476	219	0.634

Table 2.2: Results for the Linear Mixed Model based on our proposed statistical model. The mean slope coefficient is statistically significantly different from zero. There is no statistically significant effect of reference surface stiffness on the intercept and slope of the model.

feedback reference stiffness is also highlighted in Fig. 2.10c, where the slope coefficients averaged across subjects are presented for the three different reference stiffness values. The mean slope coefficient is statistically significantly different from zero, with a value of 0.58 N/m shift in perceived stiffness per mm/m of tactor displacement gain.

Table 2.2 shows the results of the Linear Mixed Model that supports our qualitative observations in Fig. 2.9b, 2.10b, and 2.10c: there is a statistically significant effect of tactor displacement gain, no significant effect of reference stiffness, and no significant interaction between reference stiffness and tactor displacement gain. Using the likelihood ratio test, the effect of subject on the intercept of the model is not significant ($p \approx 1$), while the effect of subject on the slope of the model is significant ($p < 0.001$). These results are consistent with the prediction from our proposed model, in which there is a subject-dependent effect of tactor displacement on stiffness perception, and that the stiffness perception at zero tactor displacement gain is subject independent.

The mean and 95% confidence intervals for the maximum load force and tactor displacement experienced by the subjects are shown in Fig. 2.11a and Fig. 2.11b, respectively. Not surprisingly, the load forces increased as the reference stiffness of the surface increased. In addition, for all reference stiffness levels, there was a small but significant decrease in the load force as the tactor displacement gain increased ($F_{1,13} = 36.04, p < 0.001$). The maximum amount of tactor displacement rendered to the subjects increased as the tactor displacement gains increased, with gradual saturation to the software limit of 2.3 mm as higher gains were used.

2.3.4 Discussions

2.3.4.1 Skin stretch augmentation

Perceived stiffness is affected by tactor displacement In the first study, we found that applying additional skin stretch on the fingerpad of participants through tactor displacement caused a shift in perceived stiffness, and that the larger the tactor displacement ratio, the larger is the shift in perceived stiffness. However, rendering tactor displacement in the opposite direction to the rendered force does not have

any significant effect on perceived stiffness. This may be because imposing tactor displacement-induced skin stretch in the direction opposite to the applied force is not consistent with skin stretch that occurs during natural interactions. Several participants perceived the negative skin stretch cue as an indication of deeper penetration into the surface, resulting in a lower perceived stiffness, while other subjects perceived the negative skin stretch cue as a larger force acting on the stylus and hence a higher perceived stiffness. These results indicate that it would not be possible to consistently decrease a user's perception of stiffness by rendering skin stretch in a direction opposite to the direction of applied kinesthetic force.

In the second study, we found that applying additional skin stretch on the fingerpad of subjects through tactor displacement caused a shift in perceived stiffness that was linearly related to the tactor displacement gain and independent of the underlying surface stiffness. We also found that while the average slope of this linear relationship was positive and statistically significantly different from zero, there was large inter-subject variability, and 5 out of the 15 subjects did not experience a statistically significant effect on perceived stiffness. These results are consistent with our proposed model in Equation (2.9), in which the shift in stiffness perception is linear with respect to tactor displacement gain, and that the slope is subject dependent.

Inter-subject variability The large inter-subject variability in the slope coefficient can be attributed to the inherently large inter-subject variation in skin properties such as fingerpad stiffness, tactile sensitivity, fingerpad size, and cognitive interpretation. Wang et al. [85] characterized human fingerpad skin stiffness and found large inter-subject variability. Other experimental studies involving the fingerpad investigated the absolute psychophysical threshold for mechanical stimulus amplitude and neurological threshold [30][44], and found large inter-subject variability. Loesch and Martin found that fingerpad tactile sensitivity is also affected by factors such as ridge patterns [45]. The above studies indicate that there are many potential sources of variation between subjects that can result in differing effects of tactor displacement-induced skin stretch on perceived stiffness. Similar factors are likely responsible for the large inter-subject variability that was recently reported for the perception of force [81].

In addition, it is likely that cognitive factors play a part in the inter-subject variability of the perceptual effect. Post-study interviews revealed that two of the subjects were aware of the additional tactor displacement cues and actively tried to ignore the sensation provided by the additional cue. These two subjects had the lowest, and negative, slope coefficients in Fig. 2.10(b). Such a strategy could have also affected other subjects' responses.

Moreover, the way in which subjects gripped onto the device may have contributed to the inter-subject variability of the perceptual effect. While we trained subjects to hold onto the device with a minimum of 2 N of grip force, individual subject's grip force may have varied. This variation could cause underestimation of the effect of skin stretch on stiffness perception, as a reduction in grip force will cause slip between the tactor and the fingerpad skin, reducing the effect of skin stretch on stiffness perception. A higher grip force, however, will not increase the effect, as subjects' fingerpads are grounded locally on the aperture. Although it may be possible to reduce the inter-subject variability through regulating the grip force of the user, such regulation may not thoroughly reflect the effect of tactor displacement-induced skin stretch when used in real-world applications.

Perception of force with skin stretch Our proposed computational model is based on the assumption that kinesthetic and tactile information are integrated to form the perception of force. Several other studies have found supporting evidence for this assumption. Jones et al. [31] found that subjects tend to underestimate the force magnitude when the tactile sensation is removed from the fingerpad of their index finger. Provancher et al. [62] found that by rendering additional skin stretch via tactor displacement together with force, the perceived friction felt by users can be increased. The statistically significant decrease in load force when tactor displacement is applied provides further evidence for this assumption. From the force constancy hypothesis [8], users tend to apply a constant maximum force when interacting with surfaces of different stiffness. However, our results showed that there is a decrease in load force as tactor displacement gain increases, even though the underlying surface stiffness is the same. This behavior indicates that subjects are interpreting the additional tactor

displacement-induced skin stretch as additional force information.

2.3.4.2 Device design and control considerations

Aperture size versus fingerpad size of users Our results in the first study indicate that there is a relationship between the fingerpad size of the user and the amount of increase in perceived stiffness when skin stretch is applied. Although prior work by Gleeson et al. [21] indicated that aperture size does not affect the perceptual effect of skin stretch, there is a difference between the way in which subjects grasped the device in Gleeson's study and in our work. In Gleeson's device, the subject's fingerpad was placed on a stationary aperture plate that was grounded globally and with their arm on an arm rest, and the tactor moved to stretch the skin of the subject's fingerpad. In our device, subjects had to grasp the Skin Stretch Stylus in a precision grip and move the device around to explore the virtual environment. The skin stretch tactor moved relative to the device, inducing skin stretch on the subject's fingerpad that is grounded locally to the outer cover of the Skin Stretch Stylus. A large fingerpad size relative to the aperture size is therefore essential for good engagement between the aperture and the finger for skin stretch rendering. It is also important for the user to have a solid grip of the Skin Stretch Stylus so that force can be applied to the user via the force feedback device. The size of the aperture relative to the width of the index finger can be optimized and tailored to the user to maximize the effect of tactor displacement on perceived stiffness.

Underestimation of perceptual effect due to device limitations The perceptual effect due to tactor displacement that is reported in this study is possibly an underestimation of the effect of skin stretch on perceived stiffness. This is due to three factors: First, due to backlash and control error, the actual rendered tactor displacement is lower than the commanded value. Reducing this error will increase the actual rendered tactor displacement and hence possibly further increase in the perceptual effect.

Second, the amount of tactor displacement subjects received reaches the software saturation limit of 2.3 mm as higher tactor displacement gain is used, as shown in

Fig. 2.11(b). Due to saturation, the effective tactor displacement gain – the amount of tactor displacement divided by the penetration depth, is lower than the rendered tactor displacement gain when the saturation point is reached. Therefore, for high tactor displacement gain values of 120 mm/m and 160 mm/m, the perceptual effect obtained in this study may be an underestimation of the actual effect when there is no saturation of rendered tactor displacement.

Third, we attempt to render skin stretch by displacing the tactor relative to the fingerpad. With no slip, the amount of skin stretch will be equal to the tactor displacement. However, in an actual rendering scenario, some slip will occur between the tactor and the user's fingerpad. The amount of slip depends on the fingerpad stiffness, fingerpad size, and the grip force that users applied on the device aperture. Such slippage will cause actual skin stretch experienced by the subject to be lower than the amount of tactor displacement. Therefore, the perceptual effect in this study would likely be greater if no slip occurred between the tactor and the skin of the fingerpad. It is possible to eliminate the slippage by gluing the tactor to the finger of the user [6]. The resulting evaluation of the effect of skin stretch on perceived stiffness will be more accurate, but the results will not be directly relevant for use in practical applications. We chose instead to focus on evaluating the (skin stretch mediated) effect of tactor displacement on the perception of stiffness.

Tactor displacement ratio versus gain In the first study, we used tactor displacement ratio (ratio of tactor displacement to applied force), while in the second study, we used tactor displacement gain as the independent variable in our analysis. The use of tactor displacement gain allows us to obtain insight on the effect of tactor displacement on perceived stiffness regardless of the underlying surface stiffness level. In practical applications, the use of tactor displacement gain or ratio depends on the application. For haptic rendering in virtual environments, the use of tactor displacement gain is possible since the amount of penetration into virtual surfaces is known. In teleoperation, tactor displacement ratio can be used instead since the amount of force to be rendered on the master side haptic device can be determined from the teleoperation controller / force sensors.

Calibration of gain to suit sensitivity of individual user Our results show that, for individuals who are affected by the tactor displacement-induced skin stretch, the effect on stiffness perception is consistent across different reference stiffness values. This consistency implies that only a single calibration curve needs to be obtained for each user in order to determine the effect that tactor displacement-induced skin stretch has on the users perception of stiffness. The tactor displacement ratio / gain could be adjusted based on this calibration curve in a user-specific manner to suit the tactile sensitivity of each user. The capability to tune the gain to suit individual tactile sensitivity is analogous to the volume, mouse movement sensitivity, and brightness adjustment used in common devices such as speakers, computer mice, and monitors. Such adjustment is natural in the design and use of human-computer interfaces.

2.3.4.3 Using skin stretch in practical applications for sensory augmentation

Our results show that rendering additional skin stretch through tactor displacement can augment perceived stiffness without increasing the force applied by the force feedback display. This may be used in practical applications such as remote teleoperation or robot-assisted surgery. Skin stretch feedback can be used in conjunction with force feedback where force feedback is weak due to actuator or stability limitations [42], in which skin stretch feedback can convey force information to the user while the limited physical resistance would still be provided by the force feedback device. Given that current commercial teleoperation systems do not utilize tactile displays, skin stretch feedback can be a practical and viable method to augment force feedback.

2.4 Conclusions

A Skin Stretch Stylus was built to render shear forces to the user's fingers via tactor displacement. Studies were carried out to determine the effect that tactor displacement-induced skin stretch has on the perception of stiffness of virtual surfaces. The results showed that adding tactor displacement-induced skin stretch in the direction of force-feedback increases the perceived stiffness of the virtual surface,

and that the larger the tactor displacement ratio, the larger is the shift in perceived stiffness. Rendering tactor displacement-induced skin stretch in the direction opposite to the direction of force-feedback has no significant effect on perceived stiffness of the surface.

A model for the integration of force and skin stretch feedback for stiffness perception is proposed. This model, together with the results, showed that the effect of tactor displacement-induced skin stretch has an additive effect on stiffness perception that is independent of the baseline force-feedback stiffness, and that the effect is a linear, subject-specific function of tactor displacement gain. There is also large inter-subject variability in the magnitude of the perceptual effect, which can be attributed in part to the various physiological, biomechanical, neural, and cognitive factors that could not be controlled in this study.

The results in this chapter showed that skin stretch feedback is a type of tactile feedback that is fundamentally linked with how we perceived forces and stiffness. This showed that skin stretch feedback can be an intuitive feedback modality for sensory substitution or augmentation of force feedback in virtual environment or teleoperation. However, manipulation and interaction with objects involves forces in 3-DoF, and a 1-DoF skin stretch tactile device do not have the bandwidth to convey the information for sensory substitution or augmentation of force feedback. This limitation will be addressed in the next chapter.

Chapter 3

Using Skin Deformation Feedback for Sensory Substitution and Augmentation of 3-Degree-of-Freedom Forces

The results in Chapter 2 showed that tangential skin stretch feedback is fundamentally linked to how humans perceived forces and stiffness. This indicates that tangential skin stretch can be an effective and intuitive method to substitute for the force information provided by force feedback (defined as force-feedback sensory substitution), or to augment force feedback with additional force information (defined as force-feedback augmentation) during haptic interaction. Sensory substitution and augmentation of interaction forces and torques using tactile feedback requires tactile devices that can convey 3- or 6-Degree-of-Freedom information. However, the 1-DoF tangential skin stretch tactile device is unable to reproduce the tactile sensations that results from interaction with a 3-DoF spatial environment.

In this chapter, we propose to use skin deformation tactile cues as a form of tactile feedback for sensory substitution and augmentation of interaction forces information. Skin deformation is a type of tangential skin stretch and normal skin deformation tactile cues that one obtains while interacting with the environment. From Fig. 3.1,

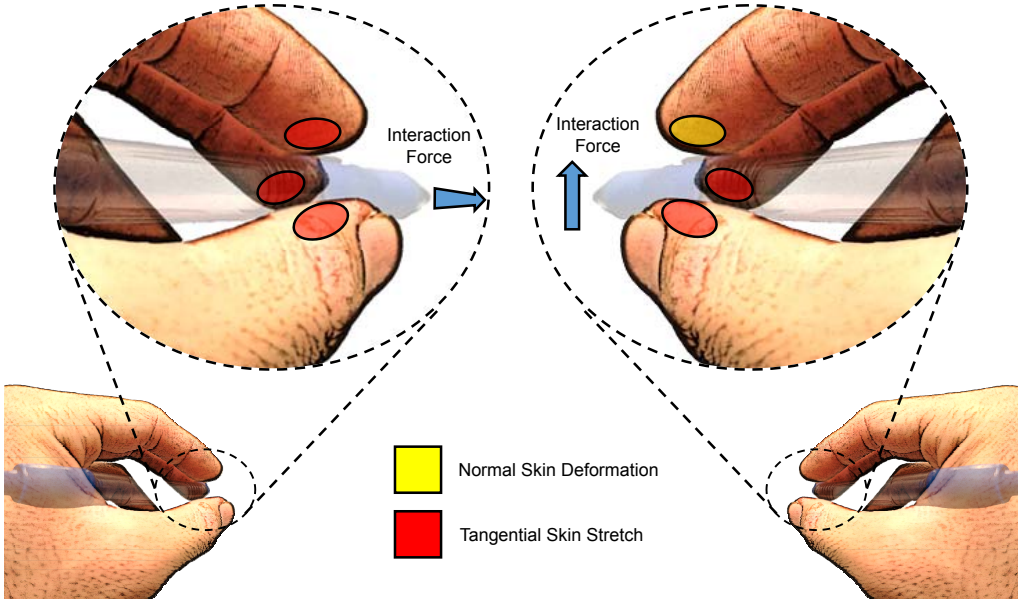

Figure 3.1: Tangential skin stretch (red) and normal deformation (yellow) cues that occur during natural interaction (upper panel). Different interaction forces magnitude and direction result in different patterns of skin stretch and normal deformation on the fingerpads.

we see that while interacting with objects in the environment using a stylus, different interaction forces and torques results in different patterns and intensities of fingerpad skin deformation. Based on this observation, we hypothesized that we can provide effective and intuitive sensory substitution or augmentation of interaction force information by reproducing the skin deformation cues on the fingerpads.

3.1 3-Degree-of-Freedom Skin Deformation Tactile Device

The goal of our tactile device is to impart skin deformation tactile sensations while users grasp the device using a precision grip that involves the thumb, index finger, and middle finger. This type of precision grip is analogous to the way users typically grasp a stylus-like tool. Skin deformation tactile sensations are created by translating a high friction surface relative to the fingerpad skin. We apply the aperture and tactor

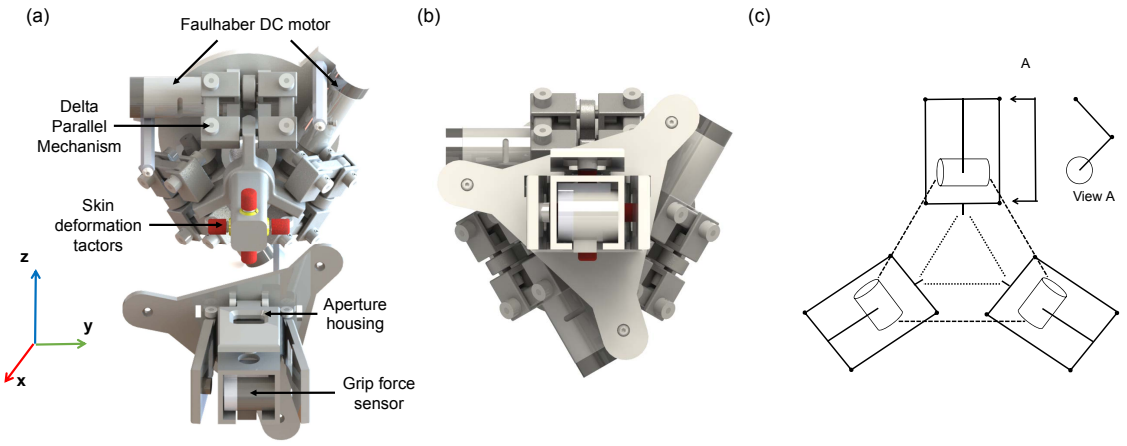

Figure 3.2: Design of the 3-DoF skin deformation tactile device. The device consists of a Delta parallel mechanism actuated by 3 geared DC motors. (a) Exploded view of the device, (b) assembled device, (c) kinematic diagram of the Delta parallel mechanism.

design used in [21] for our device. Due to the size of the tactors (∼7 mm in diameter), and the size of the aperture (∼12 mm in diameter), the end-effector of the tactile device is limited to a translational workspace of about 5×5×5 mm. This workspace is appropriately matched to the size of the human fingerpad and the amount of skin deformation that can be achieved, considering skin mechanics and user comfort. In addition, the device should also be as compact and lightweight as possible. With the requirement of a compact mechanism, small workspace, and high mechanical stiffness, a parallel kinematic mechanism is well suited for this purpose. We choose to base our design on the Delta parallel mechanism, which offers three degrees of freedom of translation, together with well understood kinematics and control [46].

The design of the skin deformation device is shown in Fig. 3.2. The device consists of a Delta-type parallel mechanism actuated by three Faulhaber 1516 DC-micromotors with 141:1 gear ratio. Skin deformation tactors, which are rubber Lenovo Trackpoint Classic dome tactors with a rounded surface and a rough, sandpaper-like texture, are attached to the end-effector of the skin deformation device (termed as the tactor base). An aperture housing, which consists of four beveled, square-shaped apertures, is rigidly attached to the base of the Delta mechanism, and which surrounds the tactor base such that the four skin deformation tactors protrude through the apertures.

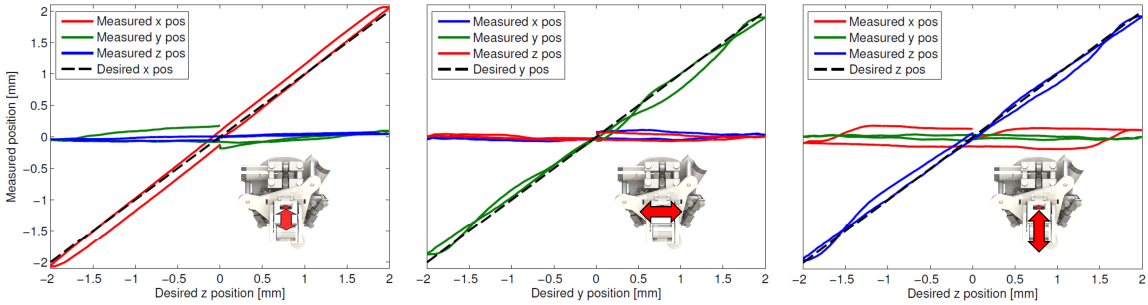

(a) Movement in X direction (b) Movement in Y direction (c) Movement in Z direction

Figure 3.3: Commanded and measured position of the end-effector of the 3-DoF skin deformation device when the device is in the unloaded state. The maximum error in the commanded direction of motion is 0.25 mm, while the maximum error in the non-commanded direction is 0.19 mm.

Users grasp the device with three fingerpad contacts at the locations of the top, left, and right tactors. Users are able to mechanically ground their fingerpad locally on the aperture housing while the tactors translate to deform the users' fingerpads. Shear forces are induced on the fingerpad due to friction between the fingerpad and a skin deformation tactor surface when a tactor moves tangentially to the fingerpad. Normal forces act on the fingerpad when a tactor moves in a direction normal to the fingerpad. An ATI Nano-17 force sensor measures the amount of grip force that users exert on the device. The force that a user exerts on the aperture is transmitted to the force sensor through a lever mechanism on the aperture housing.

The skin deformation device is attached to the end-effector of a Force Dimension Omega.3 force-feedback haptic device. The Omega.3 provides force feedback and measurement of the user's hand position in space, while the skin deformation device provides skin deformation feedback to the user's fingerpads. The weight of the device is approximately 260 g, and active gravity compensation is provided by the Omega.3 to balance the weight of the device.

3.1.1 Kinematic Verification

To verify the kinematic accuracy of the skin deformation device, we measured the position of the end effector using a Force Dimension Omega.3 (with position sensing resolution of less than 0.01 mm), and compared it to the position specified by the kinematic model under a no-load condition. The end-effector of the skin deformation device was commanded, in each of the three axis, from the zero position to the positive 2 mm position, followed by the -2 mm position, and back to the zero position. The non-commanded axis was held at 0 mm. The result of a single verification run is shown in Fig. 3.3. The position of the end-effector agrees well with the kinematic model. With a commanded amplitude of 2 mm, the maximum error in the commanded direction of motion is 0.25 mm, while the maximum error in the non-commanded direction is 0.19 mm. A small amount of hysteresis is also observed. It should be noted that under actual usage conditions, in which a user's fingerpad presses on the device aperture, due to the additional forces on the tactor by the fingerpads, the actual skin deformation rendered to the user depends on the normal and tangential stiffness of the user's fingerpad skin.

3.1.2 Using Skin Deformation Feedback to Convey Force Information

Fig. 3.4 shows illustrations of how the 3-DoF skin deformation tactile device can be used to convey force information to the user. In order to create the same skin deformation sensation that one felt when using a stylus-like tool to interact with objects in the environment, the end-effector of the tactile device will translate in the direction of the interaction force. For a larger interaction force magnitude, the end-effector will translate further to create a more intense skin deformation sensation.

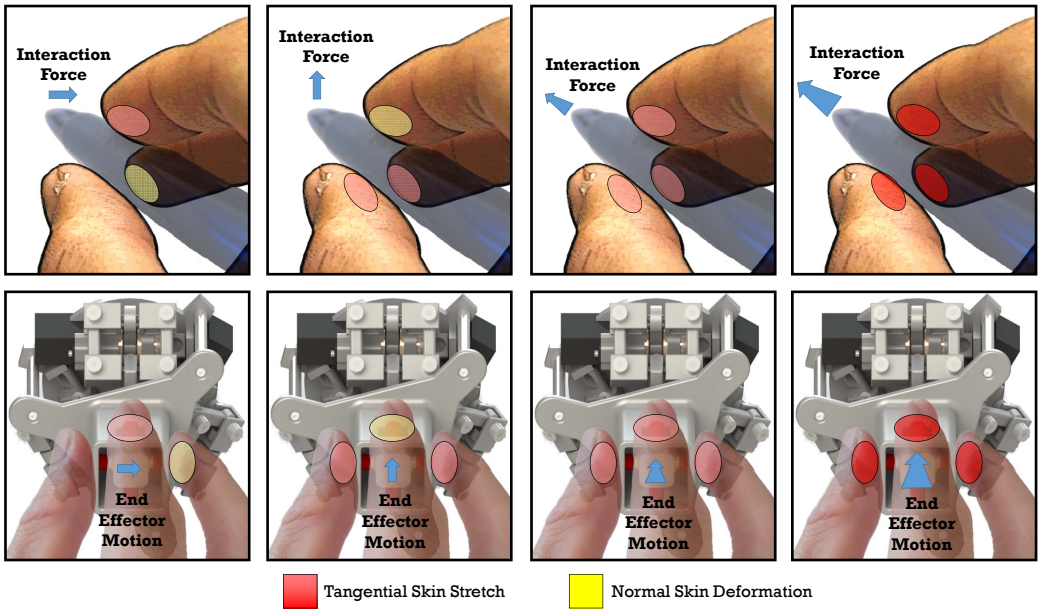

Figure 3.4: Illustration of how the tactile device can convey skin deformation tactile sensation analogous to the sensations that one felt when subjected to interaction forces while using a stylus-like tool. Skin deformation sensations caused by interaction forces of different magnitude and direction can be created by the tactile device.

3.2 Sensory Substitution of Forces using 3-Degree-of-Freedom Skin Deformation Feedback

3.2.1 Study Description

The goal of this study is to determine whether participants can interpret the 3-DoF skin deformation cues for 3-DoF force-feedback sensory substitution. We performed this study using a version of the 3-DoF skin deformation device that uses RC-servos and which does not have grip force sensing. The experiment protocol was approved by the Stanford University Institutional Review Board.

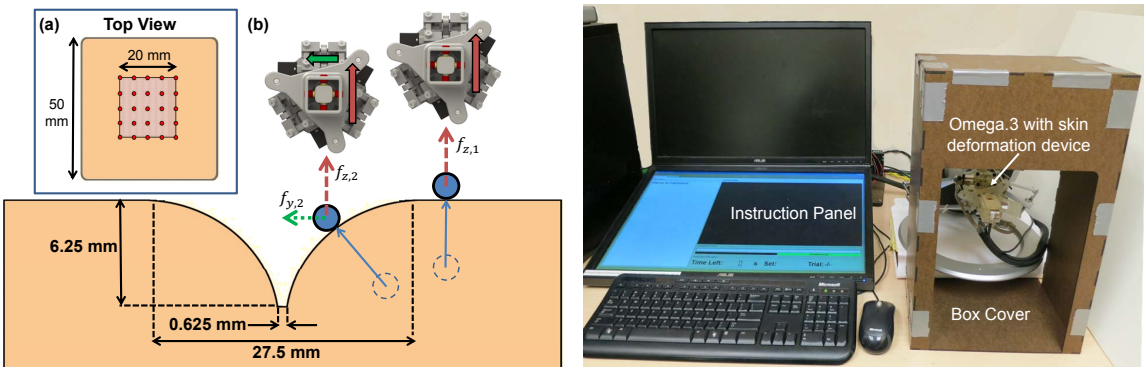

(a) (b)

Figure 3.5: (a) Profile of the rendered contoured hole that is located by users in the experimental task. The top left diagram illustrates 25 different locations in which the center of the contoured hole may be placed. When user interacts within the hole profile, the god-object algorithm renders force in the X and Y directions toward the center of the hole. These forces are applied as a physical force or skin deformation cue that the user can interpret to locate the hole center. (b) Setup for the sensory substitution experiment.

3.2.1.1 Participants

A total of 9 participants (6 males and 3 females) between the ages of 21 to 34 participated in the experiment after giving informed consent. Eight of the participants were right-hand dominant.

3.2.1.2 Apparatus and Set-up

In this experiment, we wanted to determine whether participants can interpret the 3-DoF information provided by our tactile device to locate a feature in a 3-DoF virtual environment. Participants interacted with a virtual surface to determine the center of a contoured hole, shown in Fig. 3.5a. This task was chosen because it can be completed using either 1-DoF or 3-DoF feedback, with 3-DoF feedback providing additional information that can be used by participants to improve task performance. Therefore, if participants can interpret the 3-DoF skin deformation feedback provided by our tactile device, they will be able to perform the task better than with the corresponding 1-DoF skin deformation feedback.

The experiment conditions consist of four different feedback types: 1-DoF kinesthetic force feedback, 3-DoF kinesthetic force feedback, 1-DoF skin deformation feedback, and 3-DoF skin deformation feedback. For 1-DoF kinesthetic force feedback, the Omega.3 provides force feedback in the z-direction. For 3-DoF kinesthetic force feedback, the Omega.3 provides force feedback in all directions. For 1-DoF skin deformation feedback, the tactile device provides skin deformation feedback in the z-direction, while for 3-DoF skin deformation feedback, the tactile device provides skin deformation feedback in all directions. The force feedback is included as a control to show that the task performance difference using 1-DoF feedback versus 3-DoF feedback, and to act as a baseline for task performance comparison with skin deformation feedback. The 1-DoF and 3-DoF skin deformation feedback are used to test our experiment hypothesis.

The virtual surface was displayed to the participant through a monitor placed flat on the table (as shown in Fig. 3.5b), and the virtual environment was rendered to spatially match the participant's view. This configuration eliminates visual depth information, which could be used by participants to determine the hole center. Shadows in the virtual environment are eliminated so that participants could only see a plain surface on the monitor. The virtual surface was a 50 mm×50 mm square, with the hole in one of the 25 locations that was constrained on a 20 mm×20 mm square. The scale of the surface displayed visually to the participant is magnified by a factor of 4.

We use the CHAI3D framework to render the virtual environment to the participant [11], and the proxy algorithm [95] to render the force feedback according to

$$\vec{f_p} = K\vec{x}_p, \tag{3.1}$$

where K [N/m] is the stiffness of the rendered surface and $\vec{x}_p$ [m] is the vector from the haptic interaction point (HIP) to the proxy. The desired position of the end-effector relative to its centered position (position where all tactors are at the center of their corresponding aperture) is obtained from

$$\vec{x}_{\text{sd}} = R\vec{f_p}, \tag{3.2}$$

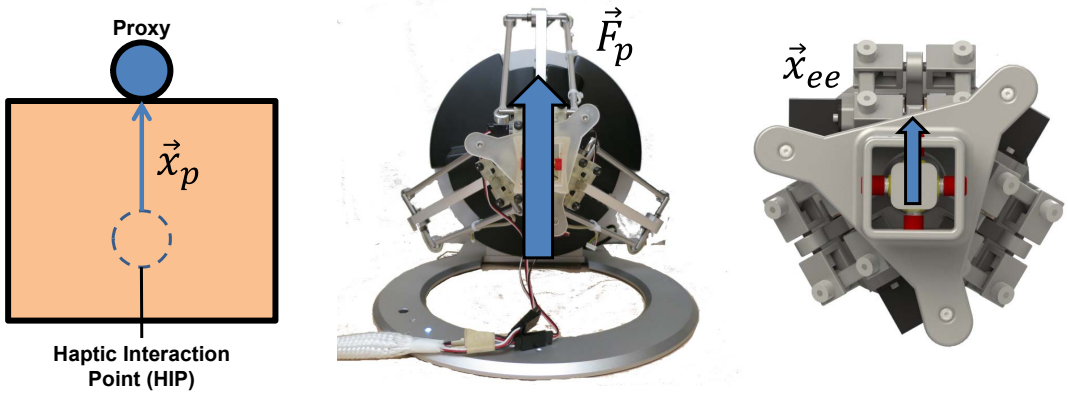

Figure 3.6: The proxy algorithm renders the force according to the difference in position between the haptic interaction point and proxy position (left). The force is applied by the Omega.3 (middle) for the force feedback case, while the skin deformation algorithm in Equation (2) substitutes the forces with the movement of the end-effector, which moves the tactors and deforms the fingerpad of the user (right).

where R [mm/N] is the skin deformation-to-force ratio and $\vec{x}_{\text{sd}}$ is the desired position of the end-effector of the skin deformation device. Combining Equations (3.1) and (3.2), we get a mapping from the proxy-HIP position difference to skin deformation:

$$\vec{x}_{\text{sd}} = RK\vec{x}_p \tag{3.3}$$

An illustration of the rendering algorithm for both the force and skin deformation cues is shown in Fig. 3.6.

The stiffness of the virtual surface, K, was set to 300 N/m, and the skin deformation-to-force ratio, R, was 2.0 mm/N in all directions. The value of 2.0 mm/N was determined during pilot studies, such that participants are able to obtain perceptible skin deformation feedback during interaction while avoiding device saturation as much as possible.

3.2.1.3 Experimental Procedure

Participants were first given two minutes to learn the hole localization task, with the contoured hole center shown on the screen as a circle for each feedback type. This familiarized participants with the different feedback types and how the feedback can

be used to locate the hole center. Then, participants performed a 20-trial training session, which consisted of 5 trials with each of the 4 feedback types. During the training, participants were shown the exact location of the hole after each trial. This training served to familiarize participants with the experimental procedures. It also provided participants with baseline experience in using the information from different feedback types to locate the hole center without the contoured hole center visible on the screen.

After the training, participants performed the main experiment, consisting of 25 trials for each of the 4 different feedback types. Each of the 25 contoured hole locations in Fig. 3.5a was presented once with each feedback type, and all feedback types and locations were pseudo-randomly interleaved. Before the beginning of each trial, participants were asked to take note of the feedback type presented on the monitor screen. They were given a maximum of 30 seconds to interact with the virtual surface and locate the hole center, after which the haptic feedback was turned off. Participants were asked to bring the cursor to their estimated hole location to complete the trial whenever they felt confident of the hole location, or after haptic feedback was turned off. No visual feedback of the hole location was provided during the main experiment. Participants were instructed prior to the experiment to place first priority on locating the hole accurately, and second priority on the speed which they took to locate the hole. The experiment took approximately 40-60 minutes to complete.

3.2.1.4 Data Analysis

The performance metrics for the experiment were the error between the participant-specified location and the actual location of the hole center, and time to complete a trial. The error, e, for each trial is calculated as

$$e = |\vec{x}_{\text{reported}} - \vec{x}_{\text{actual}}|_2, \tag{3.4}$$

where $\vec{x}_{\text{reported}}$ is the x, y coordinate of the participant reported location, $\vec{x}_{\text{actual}}$ is the x,y coordinate of the actual hole location, and $|.|_2$ is the Euclidean 2-norm. Because

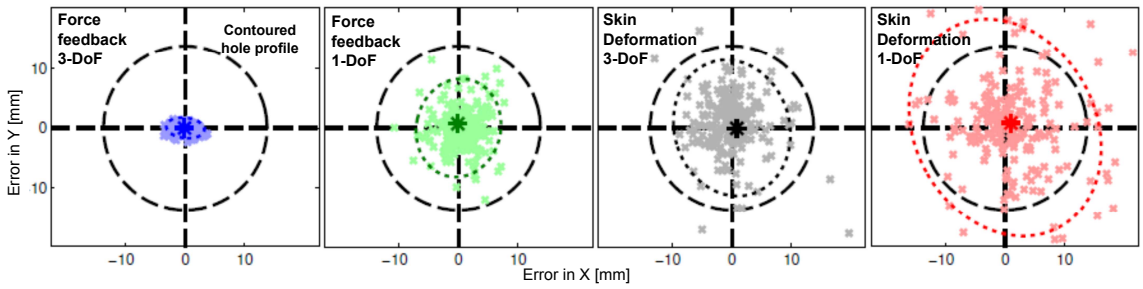

Figure 3.7: Error relative to the target hole center for all participants and all trials (crosses) for the sensory substitution study. Mean errors (asterisks) indicate that participants are accurate in their response. The dashed circle indicates the contoured hole profile. The dotted ellipses indicate the 95% confidence regions. Reproduced from [65] ©IEEE 2014.

there is a trade-off between speed and accuracy, we combine the two metrics together by multiplying the two metrics to form a single performance metric of error-time.

We performed the repeated-measures 2×2 ANOVA to compare the error-time performance metric across different feedback types and device degrees-of-freedom. The independent variables in our analysis are the categorical variable of degree-of-freedom (fixed effect with 2 levels), categorical variable of feedback type (fixed effect with 2 levels), and categorical variable of subject (random effect). We used the Kolmogorov-Smirnov test for normality of the data. Whenever the ANOVA result was significant, we performed a pairwise comparison between 3-DoF and 1-DoF force or skin deformation feedback, and between force and skin deformation feedback. Statistical analysis was performed using MATLAB `fitrm` and `ranova` functions, with statistical significance determined at the 0.05 level with the appropriate Bonferroni correction.

3.2.2 Results

The X and Y errors relative to the location of the hole, for all trials and for all participants, are shown in Fig. 3.7. The figure shows that for all feedback types, participants' responses are generally symmetrically distributed around the center of the hole. There is also no bias in participants' responses, as indicated by participants' average errors in the X and Y directions (dark asterisks in Fig. 3.7), which are close to zero. Participants demonstrated the highest precision when using 3-DoF force

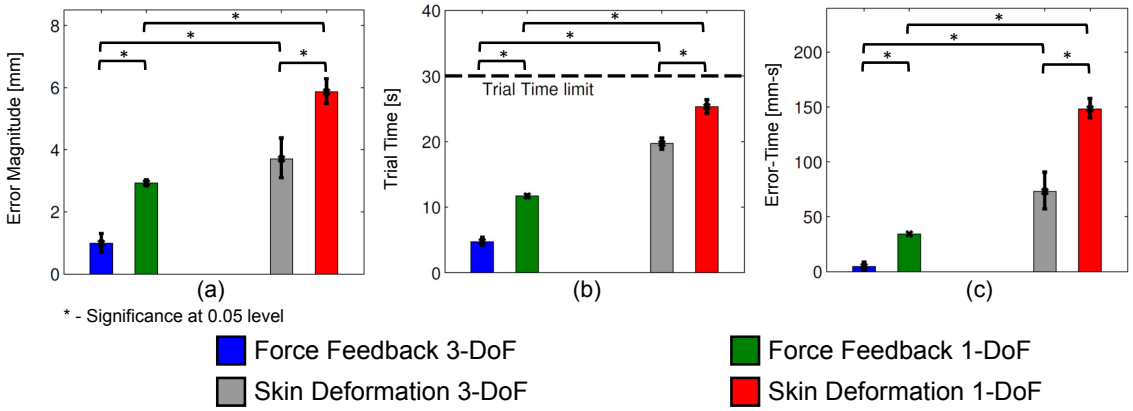

Figure 3.8: Mean performance metrics: (a) error distance, (b) trial time, (c) error-time averaged across all subjects. The errorbars indicate 95% confidence intervals.

feedback, followed by 1-DoF force feedback, 3-DoF skin deformation feedback, and 1-DoF skin deformation feedback.

Figure 3.8 shows the error distance, trial time, and error-time performance metric, while Fig. 3.9 shows the mean error distance as a function of time averaged across all subjects and all trials. These figures show that subjects had the best precision, accuracy, and were the fastest in locating the hole center for 3-DoF force feedback, followed by 1-DoF force feedback, 3-DoF skin deformation feedback, and 1-DoF skin deformation feedback.

Before performing the repeated-measures two-way ANOVA on the performance metric, we tested the data for normality using the Kolmogorov-Smirnov test and examined the size of the standard deviations. Table 3.1 shows the resultant p-values when using the raw error-time data and the p-values after performing a log-transformation. With the logarithmic transform, the distribution is closer to normal and the variances are more homogeneous. Therefore, we used the log-transformed error-time data for statistical analysis. There was a statistically significant effect of the feedback type ($F_{1,8} = 1148.6, p < 0.001$), statistically significant effect of feedback degrees of freedom ($F_{1,8} = 280.6, p < 0.001$), and statistically significant effect of interaction of feedback type and feedback degrees of freedom ($F_{1,8} = 15.2, p = 0.005$). Fig. 3.8c shows the paired t-test comparisons of the error-time performance metric

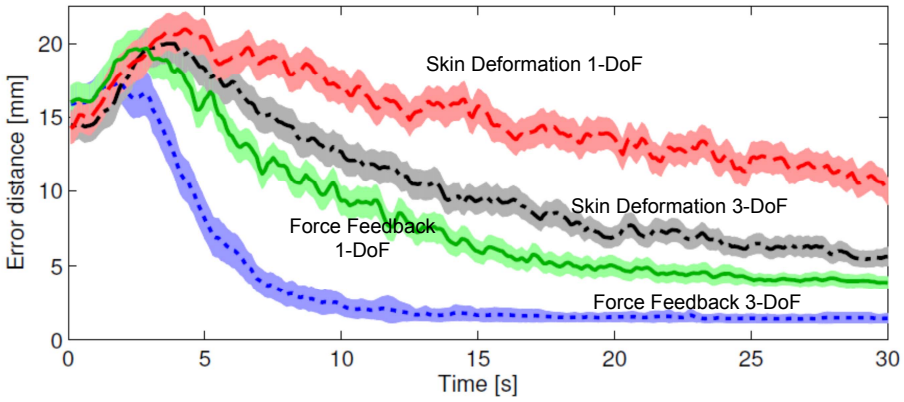

Figure 3.9: Mean trial profile for error averaged across all participants and all trials for the sensory substitution study. The shaded area indicates 95% confidence intervals. On average, participant converge to the feature most accurately and quickly using 3-DoF Force feedback, followed by 1-DoF Force feedback, 3-DoF Skin deformation, and 1-DoF Skin deformation.

	Raw		Transform	
	p-value	σ	p-value	σ
3-DoF Force feedback	2.60×10^{-4}	4.76	0.63	0.78
1-DoF Force feedback	1.15×10^{-4}	37.07	0.66	0.82
3-DoF Skin deformation	7.69×10^{-6}	92.79	0.05	0.92
1-DoF Skin deformation	1.30×10^{-5}	168.63	0.80	0.86

Table 3.1: Normality tests and comparison of standard deviation for the error-time performance metric for the sensory substitution study.

with the appropriate Bonferroni corrections for multiple comparisons.

3.2.3 Discussions

3.2.3.1 3-DoF versus 1-DoF feedback

The results from the sensory substitution of force experiment show that participants have the best performance using FF-3dof, followed by FF-1dof, SD-3dof, and SD-1dof. This finding is consistent with our hypothesis that the cues provided by the additional DoFs help the user to locate the center of the hole. For force feedback, the

lateral forces provided by FF-3dof pushed the user towards the hole center, while the lateral skin deformation cue provided by SD-3dof allowed the user to quickly form a rough estimate of the hole location and to spend more time exploring near the hole center. For their 1-DoF counterparts, users had to explore the entire surface in order to form a mental model of the hole and to estimate the location of the hole center, resulting in increased trial time and lower accuracy. The improvement in performance of 3-DoF skin deformation feedback over its 1-DoF counterpart also provides evidence that users are able to interpret the additional cues provided by our device to infer more information about the environment.

While the additional information can be due to additional direction information or an increase in feedback information, prior work by by Guinan et al. [22] had showed that with a 5-DoF back-to-back skin stretch device, participants are able to discriminate between the different directional information provided to them. The improvement in performance for 3-DoF skin deformation compared to 1-DoF skin deformation feedback can therefore be attributed mostly to the additional directional information provided by 3-DoF skin deformation feedback.

3.2.3.2 Force versus skin deformation feedback

The better performance of force feedback compared to skin deformation feedback can be attributed to the physical resistance provided by force feedback in the direction normal to the virtual surface. The physical resistance allows users to glide the device easily along the surface and makes exploring the surface easier and faster. For skin deformation feedback, users had to make an effort to physically constrain their motion to the plane of the surface in order to obtain interpretable skin deformation cues. This increases both the physical and mental effort of the user, resulting in their overall poorer performance (both error and time) for skin deformation feedback. Our results are consistent with [83][82], in which physical constraint provided by force feedback helped to reduce the mental workload during task execution.

3.2.3.3 Familiarity with skin deformation feedback

For most participants, this experiment was the first time in which they had experienced skin deformation feedback without the corresponding kinesthetic force feedback. Through appropriate training, it is expected that participants' performance using skin deformation feedback would improve over time.

3.3 Sensory Augmentation of Forces using 3-Degree-of-Freedom Skin Deformation Feedback

In section 3.2, we used the skin deformation tactile feedback as a form of sensory substitute to provide interaction force information to the user. In this section, we augment kinesthetic force feedback with additional force information through the tactile device.

3.3.1 Study Descriptions

The goal of this study is to determine the effect of augmenting force feedback (of different force-feedback gains) with skin deformation. The experiment in this study is performed using the DC motor powered version of the tactile device with grip force sensing.

3.3.1.1 Participants

A total of 14 participants (12 males and 2 female) between the ages of 21 to 30 participated in the experiment after giving informed consent. All but one of the participants were right-handed. The experiment procedure was approved by the Stanford University Institutional Review Board.

3.3.1.2 Apparatus and Set-up

In this experiment, we wanted to determine whether the addition of skin deformation feedback to force feedback can improve task performance. Participants perform a

path-following task by moving the haptic device from an initial 3D position to a target position via a specified path, subjected to force feedback (with varying force-feedback fidelity), and/or skin deformation feedback that acts as forbidden region virtual fixture [1] to prevent movement away from the specified path. The initial position of the path is $\vec{p}_{\text{path,start}} = (0, 0, 0)$. The path in space $\vec{p}_{\text{path}}$ is

$$\vec{p}_{\text{path}} = \begin{bmatrix} x_{\text{path}} \\ y_{\text{path}} \\ z_{\text{path}} \end{bmatrix} = \begin{bmatrix} x_{\text{hand}} \\ y_{\text{mag}} \sin(2\pi y_{\text{freq}} x_{\text{hand}}) \\ z_{\text{mag}} \sin(2\pi z_{\text{freq}} x_{\text{hand}}) \end{bmatrix}, \tag{3.5}$$

y_{path} and z_{path} are the desired y and z position of the path in space, y_{mag}, z_{mag}, y_{freq}, z_{freq} are the parameters defining the path, and x_{hand} is the x coordinate of the participant's hand as measured by the haptic device. Therefore, participants are able to move freely along the x axis, while the haptic feedback guides the participant towards the desired y and z coordinates of the path in space. Throughout the path, the guidance force is

$$\vec{f}_{\text{guide}} = \begin{bmatrix} 0 \\ K(y_{\text{path}} - y_{\text{hand}}) \\ K(z_{\text{path}} - z_{\text{hand}}) \end{bmatrix}, \tag{3.6}$$

in which y_{hand} and z_{hand} are the y and z coordinates of the hand position, measured by the Omega-3, and K is the stiffness of the virtual fixture. At the end of the path, a virtual wall is shown to the participant. The additional force output by the virtual

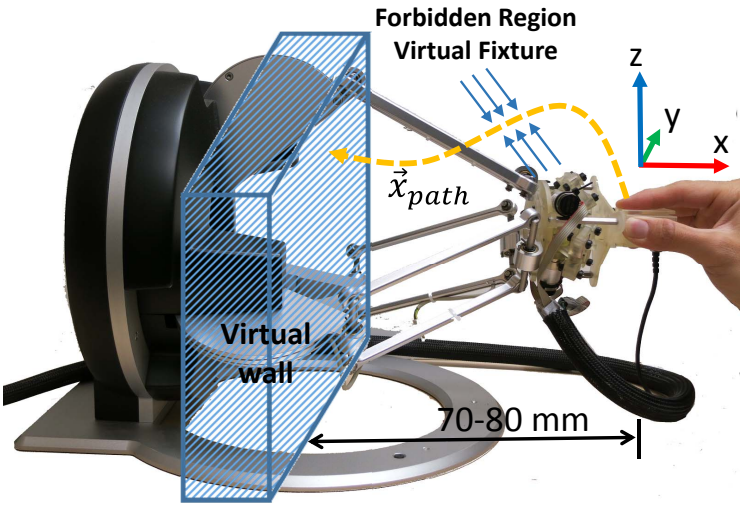

Figure 3.10: Illustration of the path-following task with forbidden virtual fixture guidance and the virtual wall in which participants had to detect that indicates the end of the path.

wall, $\vec{f}_{\text{wall}}$, is

$$\vec{f}_{\text{wall}} = \begin{cases} \begin{bmatrix} K(x_{\text{path,end}} - x_{\text{hand}}) \\ 0 \\ 0 \end{bmatrix}, & \text{if } x_{\text{path,end}} \leq x_{\text{hand}} \\ \begin{bmatrix} 0 \\ 0 \\ 0 \end{bmatrix}, & \text{otherwise} \end{cases}, \tag{3.7}$$

in which $x_{\text{path,end}}$ is the x coordinate of the virtual wall (which indicates the end of the path), and x_{hand} is the x coordinate of the participant's hand in space. An illustration of the experiment task is shown in Fig. 3.10.

The force rendered by the Omega.3 force-feedback device is

$$\vec{f}_{\text{Omega}} = G(\vec{f}_{\text{guide}} + \vec{f}_{\text{wall}}), \tag{3.8}$$

Table 3.2: The seven feedback conditions for the sensory augmentation of kinesthetic force feedback study.

No.	Name	Feedback Condition	
1	Force 100%	$G = 1.0$	$R = 0$ mm/N
2	Force 66%	$G = 0.66$	$R = 0$ mm/N
3	Force 33%	$G = 0.33$	$R = 0$ mm/N
4	Force 100% + Skin deformation	$G = 1.0$	$R = 2.0$ mm/N
5	Force 66% + Skin deformation	$G = 0.66$	$R = 2.0$ mm/N
6	Force 33% + Skin deformation	$G = 0.33$	$R = 2.0$ mm/N
7	Skin deformation only	$G = 0.0$	$R = 2.0$ mm/N

where $\vec{f}_{\text{Omega}}$ is the force output by the force-feedback device, and G is the force-feedback ratio. For the skin deformation tactile feedback, the movement of the end-effector is

$$\vec{x}_{\text{ee,sd}} = R(\vec{f}_{\text{guide}} + \vec{f}_{\text{wall}}), \tag{3.9}$$

where $\vec{x}_{\text{ee,sd}}$ is the displacement of the tactile device's end-effector, and R is the skin deformation-to-force ratio.

Participants performed the task under seven different feedback conditions. These seven feedback conditions include force feedback with different force-feedback gains, with and without the addition of skin deformation feedback. The parameters for each of the seven feedback conditions are summarized in Table 3.2. We choose the stiffness of the virtual fixture K to be 220 N/m as it is the minimum amount of stiffness found in [57] that is required for object detection. This value of stiffness is also found during pilot studies to be a value of stiffness such that reduced force-feedback gains with force-feedback ratio of 66% and 33% will give a decrease in path tracking and virtual wall penetration performance.

3.3.1.3 Experiment Procedure

The experiment started with a familiarization procedure in which a participant freely explored the task for each of the seven feedback conditions. During this period, the experimenter explained to the participants how to interpret the different feedback

conditions. Participants were also instructed to grasp the device with a precision grip using the thumb, index, and middle finger. In addition, participants were told to exert a 1 N minimum grip force on the device, which was measured and displayed through the graphical interface using a bar graph. After the familiarization procedure, participants proceeded to the main experiment.

In the main experiment, participants performed the trials in seven sets, with each set corresponding to each of the seven different feedback conditions. The seven sets were presented to the participants in a Latin square order. For each set, participants performed a total of 17 trials. The first 5 trials are included to familiarize participants with the feedback condition and are not included in the data analysis. Participants, however, are not informed of these training trials. For all 17 trials, the parameters y_{freq} and z_{freq} are randomly chosen between the values 1.5 to 4, the parameters y_{mag} and z_{mag} are randomly chosen between the values -0.05 to 0.05 m, and the parameter $x_{\text{path,end}}$ is randomly chosen between the values -0.07 to -0.08 m.

Prior to the start of each trial, the Omega.3 force-feedback haptic device is placed in position control and the device moves the participant's hand towards $\vec{x}_{\text{path,start}}$, the starting point of the path. Next, the participant pressed a keyboard command to start the trial, after which he/she started the path-following task while force feedback and/or skin deformation feedback are provided to guide the participant towards the desired path in space. Participants were given unlimited time to perform the task, and were instructed to place priority on tracing the path as accurately as possible and to avoid penetrating the virtual wall at the end of the path. When a participant felt the virtual wall (and hence reached the end of the path), he/she pressed a keyboard key to end the trial. Throughout the experiment, the participants relied on haptic feedback provided by the Omega.3 and the skin deformation device. No visual information was provided for all feedback cases.

At the end of the experiment, participants were asked to rank the seven feedback conditions according to how they felt the feedback helped them in the path-following and wall penetration task. They ranked the feedback from "1 to 7", with a higher number corresponding to a feedback condition that helps them perform better in the task.

3.3.1.4 Data Analysis

Throughout each trial, the participant's interaction information was recorded every 1 ms. We used several metrics to assess task performance:

- ***Mean path-following error*** between the desired path $\vec{x}_{\text{path}}$ and the participant's hand position $\vec{x}_{\text{hand}}$ is:

$$e_{\text{mean}} = \frac{1}{N}\sum_{n=1}^{N}(|\vec{x}_{\text{path}}[n] - \vec{x}_{\text{hand}}[n]|_2), \tag{3.10}$$

  where N is the number of data points recorded for the path, $\vec{x}_{\text{path}}[n]$ and $\vec{x}_{\text{hand}}[n]$ are the desired path and actual hand position at sample n, and $|.|_2$ is the l^2-norm.

- ***Trial time normalized for path length*** was calculated as trial completion time divided by the length of the desired path.

- ***Error-time*** was calculated as the product of mean path-following error and trial time normalized for path length.

- ***Wall penetration*** is the maximum amount of penetration into the virtual wall at the end of the path.

In addition to the above performance measures, we also used the grip force sensor to measure participant's' grip force on the device throughout the experiment. This grip force information is not used to evaluate participants' performance.

We used the Kolmogorov-Smirnov test for normality prior to the statistical analysis, and where necessary, we log-transformed the data to mitigate violations of the assumption of normality. We performed five repeated-measure one-way ANOVA with the mean error, trial time normalized for path length, error-time, wall penetration, and grip force as the dependent variables, and feedback type as an independent categorical factor with 7 levels. We used the Greenhouse-Geisser correction to adjust for the degrees of freedom in the repeated-measures ANOVA. Statistical analysis was performed using MATLAB `fitrm` and `ranova` functions, with statistical significance determined at the 0.05 level with the appropriate Bonferroni correction.

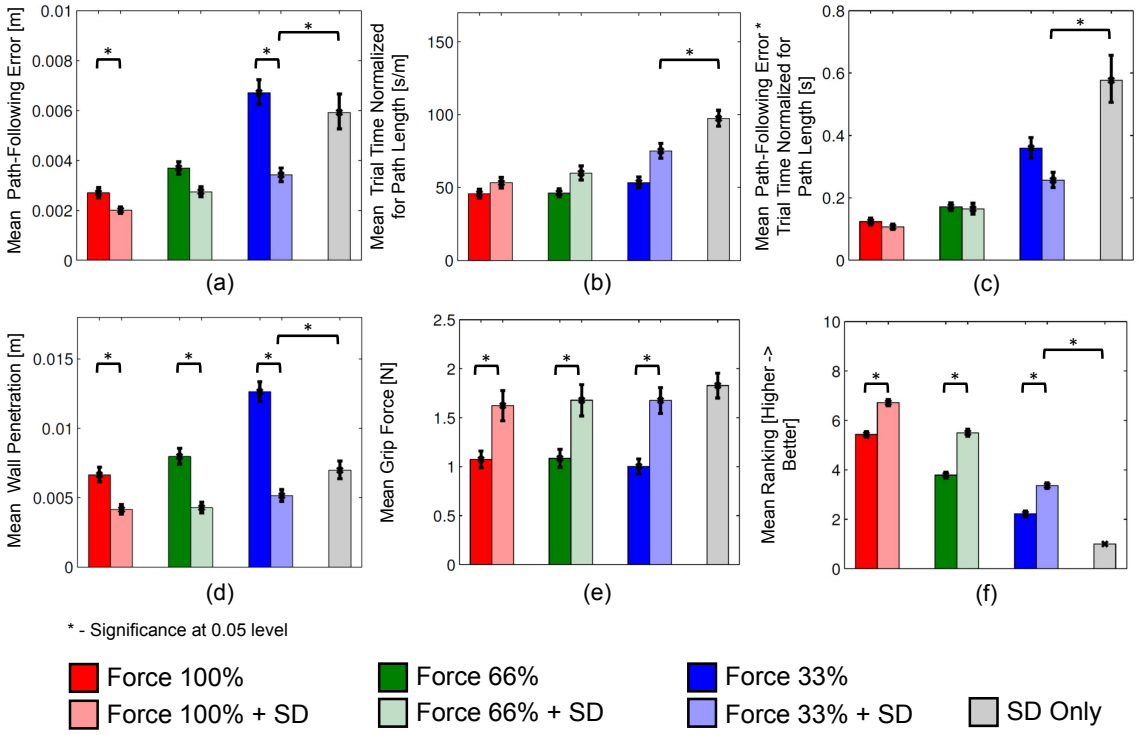

Figure 3.11: (a) Mean path-following error, (b) Mean trial time normalized for path length, (c) Mean path-following error * trial time normalized for path length (d) Mean wall penetration (e) Mean grip force (f) Mean ranking averaged across all participants for the sensory augmentation study. The error bars indicate 95% confidence intervals. The path-following error and trial time normalized for path length plots are obtained by backtransforming the mean and 95% confidence interval obtained from the log-transformed data.

3.3.2 Results

Before performing the analysis, we tested the data for normality using the Kolmogorov-Smirnov test and examined the size of the standard deviations. Table 3.3 shows the p-values and the standard deviations for the error, normalized time, and the penetration performance metric. The distribution approaches normal and the standard deviation becomes closer to equal with the logarithmic transform. We therefore used the log-transform data for the statistical analysis of error, normalized time, and penetration performance metric. The error-time and the grip force data satisfy the normality assumption for all cases and is not log-transformed for the statistical analysis.

When skin deformation is added to force feedback, the mean path-following error

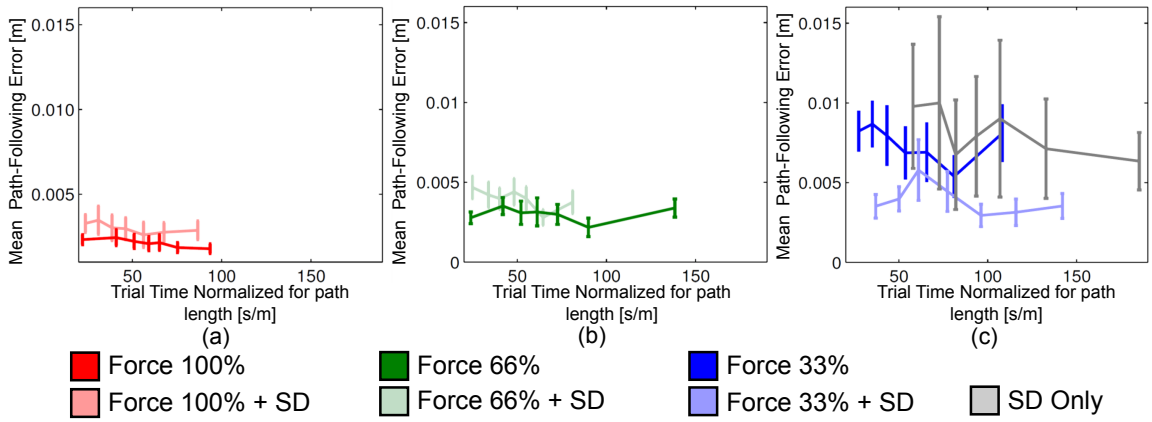

Figure 3.12: Mean path-following errors and 95% confidence intervals across trial time normalized for path length for the sensory augmentation study. (a) Force 100% versus Force 100% with skin deformation, (b) Force 66% versus Force 66% with skin deformation, (c) Force 33% versus Force 33% with skin deformation versus skin deformation only. The mean path-following error is obtained by sorting the data according to their trial time normalized for path length, combining them into bins of 12 trials, and obtaining the statistics for each bin.

decreases for all force-feedback ratios. This result is shown in Fig. 3.11a, which gives the mean and 95% confidence interval for the path-following error for each feedback types. The ANOVA analysis on path-following error shows a statistically significant effect of feedback type ($F_{1.9,24.6} = 28.6, p < 0.001$). Post-hoc comparisons showed that there is statistically significant difference between Force 100% and Force 100% with skin deformation, between Force 33% and Force 33% with skin deformation, and between Force 33% with skin deformation and skin deformation feedback case. Due to non-normality of the data for the Force 100% case, we performed additional sign-rank test between Force 100% and Force 100% with skin deformation, and obtained statistical significant difference between the two cases ($p <= 0.001$).

Adding skin deformation to force feedback increases the mean trial time normalized for path length, for all force-feedback ratios. Fig. 3.11b shows the mean and 95% confidence interval for the trial time normalized for path length for all feedback types. The ANOVA analysis confirmed a statistically significant effect of feedback type ($F_{2.7,35.3} = 17.9, p < 0.001$). Post-hoc comparisons showed statistically significant difference between the Force 33% with skin deformation and the skin deformation

only case.

Our results show that adding skin deformation to force feedback decreases path-following error but increases trial time normalized for path length. However, it is unlikely that the decrease in path-following error is due to the increase in trial time normalized for path length, as we did not observe a speed-accuracy tradeoff in this task. Fig. 3.12 shows the mean path-following error as a function of trial time normalized for path length, for Force 100% versus Force 100% with skin deformation (Fig. 3.12a), Force 66% versus Force 66% with skin deformation (Fig 3.12b), and Force 33% versus Force 33% with skin deformation versus skin deformation only (Fig 3.12c). In general, there is no speed-accuracy tradeoff between path-following error and trial time normalized for path length for all feedback types. For all force-feedback ratios, augmenting force feedback with skin deformation feedback decreases path-following error across a range of trial time normalized for path length. Fig 3.11c shows the result when we combined both the path-following error metric and the trial time normalized for path length metric. ANOVA analysis on error-time showed that there is a statistically significant effect of feedback type ($F_{1.4,17.8} = 16.7, p < 0.001$). Post-hoc comparisons showed statistically significant difference between the Force 33% with skin deformation and the skin deformation only case.

There is a decrease in virtual wall penetration when skin deformation feedback is added to force feedback. This result is shown in Fig 3.11d, where the mean and 95% confidence interval for the wall penetration is depicted for all feedback types. ANOVA analysis on wall penetration showed that there is a statistically significant effect of feedback type ($F_{3.0,38.8} = 29.7, p < 0.001$). Post-hoc comparisons also showed that there is statistically significant difference when skin deformation feedback is added to force feedback for all force-feedback ratio, and between Force 33% with skin deformation and the skin deformation only case. Due to non-normality of the data for the Force 100% case, Force 66% case, and skin deformation only case, we performed additional signrank test between Force 100% and Force 100% with skin deformation, Force 66% and Force 66% with skin deformation, and Force 33% with skin deformation and skin deformation only case. We obtained statistical significant difference for all three comparisons ($p <= 0.001$).

There is an increase in the grip force when skin deformation feedback is added to force feedback for all force-feedback ratio (Fig. 3.11e). From the ANOVA analysis, there is a statistically significant effect of the presence of skin deformation feedback on grip force ($F_{3.4,44.1} = 17.9, p < 0.001$). Post-hoc comparisons also showed that there is statistically significant difference when skin deformation feedback is added to force feedback for all force-feedback ratio. In addition, for all feedback types, participants applied a mean grip force above the specified mean grip force of 1 N.

The results of the post-experiment ranking survey is shown in Fig. 3.11f. Participants indicated that the additional skin deformation for all force-feedback ratios helped them achieve a better performance in path-following and wall penetration.

3.3.3 Discussions

3.3.3.1 Performance improvement with combined feedback

Augmenting force feedback (of all force-feedback ratios) with skin deformation feedback decreases path-following error and wall penetration compared to force feedback alone. The decreases in path following error and wall penetration are most significant when skin deformation feedback is added to force feedback with force-feedback ratio of 33%. These results illustrate that, while adding skin deformation feedback to force feedback improves task performance across all force-feedback levels, the benefits of augmenting force feedback with skin deformation feedback is most prominent when skin deformation feedback is used to augment force feedback with reduced force-feedback gains. Augmenting force feedback with skin deformation feedback is therefore useful in systems in which reduced force-feedback is desired. Such systems include teleoperation system with communication delay, in which reduced force-feedback is required to maintain stability of the system [42].

On the other hand, the addition of a small amount of force feedback can greatly improve both the path-following error, trial time normalized for path length, and wall penetration, as shown in Fig. 3.8a, Fig. 3.8b, and Fig. 3.8d. This trend is consistent with the results obtained by [58] and [25], in which the combination of tactile feedback with force feedback decreases penetration distance into virtual tissue and improves

Table 3.3: Kolmogorov-Smirnov test for normality of path-following error, trial time normalized for path length, and wall penetration performance metric.

	Path-Following Error				Trial Time Normalized for Path Length				Wall Penetration			
	Raw		Transformed		Raw		Transformed		Raw		Transformed	
	p-value	σ	p-value	σ	p-value	σ	p-value	σ	p-value	σ	p-value	σ
Force 100%	< 0.01	0.0016	0.66	0.49	0.14	21.1	0.40	0.42	< 0.01	0.0046	0.64	0.53
Force 100%+SD	0.03	0.0010	0.93	0.44	0.68	22.1	< 0.01	0.46	< 0.01	0.0045	< 0.01	0.57
Force 66%	0.01	0.0018	0.91	0.44	0.24	18.3	0.32	0.38	0.04	0.0044	0.46	0.48
Force 66%+SD	< 0.01	0.0015	0.76	0.48	0.02	36.0	0.15	0.54	< 0.01	0.0047	0.02	0.62
Force 33%	0.14	0.0036	0.77	0.49	0.08	27.0	0.61	0.46	0.24	0.0048	0.20	0.37
Force 33%+SD	< 0.01	0.0026	0.46	0.53	0.06	35.7	0.14	0.45	< 0.01	0.0043	0.25	0.53
SD Only	< 0.01	0.0094	0.04	0.78	< 0.01	41.8	0.57	0.37	< 0.01	0.0065	0.01	0.62

directional recognition compared to just tactile feedback alone.

3.3.3.2 Force constraint versus force information

Skin deformation feedback alone results in smaller wall penetration than the 33% and 66% force feedback cases, and larger wall penetration than the 100% force feedback case. However, for path-following error, participants' performance with skin deformation feedback is worse than the 100% and 66% force feedback cases, and better than the 33% force feedback case. A possible reason for participants' better performance in reducing wall penetration with skin deformation feedback is the fundamental nature of force feedback [83] and skin deformation feedback. Force feedback provides both force information and physical constraint, while skin deformation feedback provides only force information to the user. For the virtual wall detection task, the primary factor affecting performance is the sensing of the force information. From Fig. 3.8b, the mean trial time normalized for path length across all feedback types is higher than 45 s/m. This corresponds to a mean insertion speed of 22 mm/s or lower. Such a slow insertion speed indicates that for the virtual wall detection task, the physical constraint provided by force feedback does not offer a significant advantage in lowering wall penetration. The observation that the amount of wall penetration increases as the force feedback ratio decreases further strengthens the point that the primary factor affecting the wall penetration task is the sensing of force information. As the force feedback ratio decreases, it takes a larger penetration for user to feel a certain minimum force threshold in order to detect the wall force and hence notice the virtual wall. Skin deformation feedback alone therefore provides sufficient force information that informs the user about the presence of the virtual wall.

For the path-following task, however, the physical constraint provided by force feedback inherently prevents the user from deviating too far away from the desired path. This physical force constraint is absent in skin deformation feedback. Force feedback (for all force-feedback ratios) therefore achieved better path tracking performance than skin deformation feedback alone.

The concept of force constraint and force information can also be used to explain the performance improvement observed when skin deformation feedback is used to

augment force feedback. When force-feedback ratio is decreased, the physical constraint and the information provided by force feedback becomes weaker. A greater position difference (either between the hand and path in the y and z direction, or between the hand and the wall in the x direction) is needed for participants to feel the same force information. This explains the degradation in performance when force-feedback ratio is decreased, for both path-following error and wall penetration. When skin deformation feedback is used to augment force feedback, skin deformation provides force information that is lacking in reduced-gain force feedback. Therefore, augmenting force feedback with skin deformation feedback decreases path-following error and wall penetration, due to the additional force information provided by skin deformation feedback. The performance improvement provided by the additional skin deformation feedback becomes more prominent as force feedback ratio decreases.

On the other hand, by including a small amount of force feedback to skin deformation feedback, the additional physical constraint provided by force feedback helped improved overall performance compared to just skin deformation feedback alone.

3.3.3.3 Feedback sensitivity

Due to the design of our task, the primary form of skin deformation feedback that a user receives during path following is normal skin deformation, while the primary form of skin deformation feedback that a user received during wall penetration is tangential skin stretch in the x direction. Biggs et al. [6] showed that humans are more sensitive to tangential displacement than normal displacement, and more sensitive to normal forces than tangential forces. The lower sensitivity to normal skin deformation, and the higher sensitivity to tangential skin stretch, might have caused the lower performance in path-following and the better performance in wall penetration for the skin deformation feedback case compared to the other feedback types.

In addition, users received feedback from all three fingerpads for tangential skin stretch in the x direction, while they received feedback from one to three fingerpads with a combination of tangential skin stretch and normal skin deformation in the y and z directions. Montandon et al. [53] have shown that simultaneous cues through

multiple fingerpads result in higher accuracy in a direction identification task than a single fingerpad alone. The higher number of fingerpads involved in the x direction might have contributed to the higher sensitivity, and hence the better performance for wall penetration.

The above issues motivate the potential use of a larger skin deformation ratio in the y and z directions, which are mainly involved in providing normal skin deformation feedback, and which received feedback cues mostly on a single fingerpad.

3.3.3.4 Grip force adjustment

We found that participants exerted a larger grip force on the device in cases when skin deformation feedback is used to augment force feedback, even though participants were instructed in both cases to maintain a minimum of 1 N grip force on the device. A higher grip force has previously been found to be correlated to a higher impedance of the wrist [38]. With a higher impedance, the restoring force due to force feedback will not be able to push the participant's hand towards the desired path as easily as when the impedance of the participant's hand is low. Our results, however, showed that participants achieved a statistically significant decrease in mean error when skin deformation feedback is present. As such, these results suggest that participants are using the additional skin deformation feedback to stay in the desired path.

In addition, previous work has shown that people increased their arm impedance in response to perturbations from the environment [7]. Previous work has also shown that augmenting force feedback with skin stretch feedback increases the perception of friction [62], stiffness [64], and force [48]. Therefore, augmenting force feedback with skin deformation feedback might have increased the perception of restoring force by participants. Participants therefore increases their grip force and hence wrist impedance in response to this higher perception of restoring force from the environment.

3.4 Conclusions

We designed a 3-DoF skin deformation tactile haptic device that is able to provide 3-DoF sensory substituted force information to the user. The device uses a Delta-parallel mechanism to actuate skin deformation tactors in 3-DoF, creating skin deformation to the fingerpads which are grounded locally on the aperture restraints. Two experiments were performed to determine the capability of our approach to provide sensory substituted force information to the user, and to use this information to augment force feedback. In our first experiment, users had to determine the location of a contoured hole using 3-DoF and 1-DoF force or skin deformation feedback. Results showed that users achieved better performance when 3-DoF feedback is used compared to 1-DoF feedback (for both force and skin deformation feedback), indicating that users are able to interpret the multi-DoF force information provided by our tactile device.

The second experiment measured the effects of augmenting force feedback with skin deformation feedback on a virtual fixture-guided path-following task. By augmenting force feedback with skin deformation feedback, participants were able to follow the path more accurately and decrease the amount of penetration into the virtual wall. The improvement in performance over force feedback was most significant when skin deformation feedback is added to force feedback with reduced force-feedback fidelity.

Our results motivate the integration of skin deformation feedback with force feedback in teleoperation systems. In a teleoperation system, for example, high-fidelity force feedback is not implemented partly due to the potential instability that force feedback can bring to the teleoperation system. As such, it might be possible to provide 3-DoF sensory substituted force information to the user via skin deformation feedback, or to use skin deformation to augment a reduced-gain force feedback teleoperation for both performance and stability improvements.

Chapter 4

Using Skin Deformation Feedback for Sensory Substitution and Augmentation of 6-Degree-of-Freedom Forces and Torques

Our work in Chapter 4 showed that skin deformation tactile cues can be used to convey force information to the user to substitute force feedback, or to augment force feedback with additional force information during task manipulation. In this chapter, we proposed to use the same skin deformation tactile cues for sensory substitution and augmentation of both interaction force and torque information.

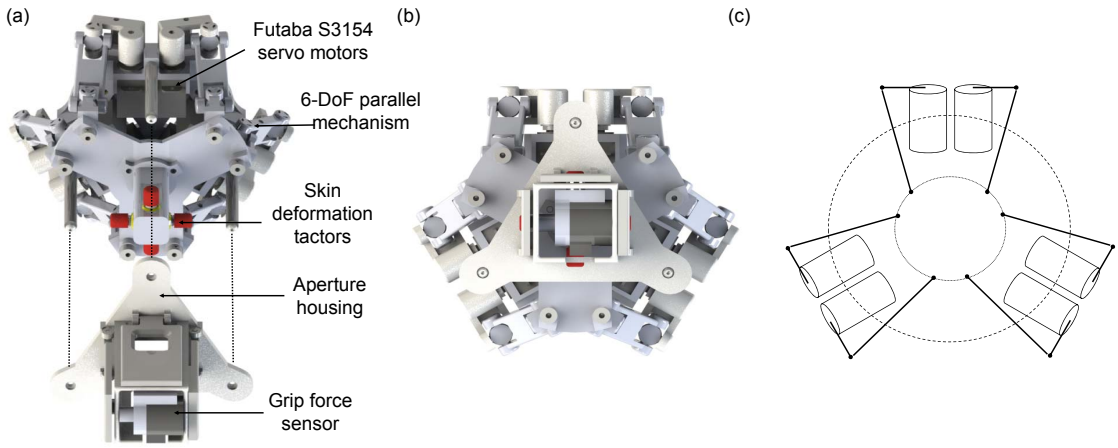

Figure 4.1: Design of the 6-DoF skin deformation tactile device. The device consists of a Hunt-Typed 6-Rotational-Universal-Spherical (6-RUS) parallel mechanism actuated by 6 servo motors. (a) Exploded view of the device, (b) assembled device, (c) kinematic diagram of the Hunt-Typed 6-RUS parallel mechanism.

4.1 6-Degree-of-Freedom Skin Deformation Tactile Device

4.1.1 Device Design

The design requirement for the 6-DoF skin deformation tactile device is similar to the 3-DoF skin deformation tactile device, in that both devices has to be compact, exhibit high mechanical stiffness, and has to be designed such that users will grasp it in a stylus-like manner using the thumb, index, and middle finger. The main difference between the 6-DoF and the 3-DoF skin deformation tactile device is that the end-effector of the 6-DoF device must be able to translate and rotate in space. We chose the Hunt-Type 6-Rotational-Universal-Spherical (RUS) parallel mechanism [17] due to the mechanism's capability to translate and rotate in all 6-DoFs, and its potential for a compact design using rotary actuators.

Fig. 4.1 shows the design of the 6-DoF tangential and normal skin deformation tactile feedback device. The device is a Hunt-Type 6-RUS parallel kinematic mechanism actuated by six Futaba S3154 RC servo motors. A detailed analysis of the

kinematics of the Hunt-Type 6-RUS parallel kinematic mechanism is shown in Appendix A. The 6-DoF tactile device is attached to the end-effector of the master manipulator of the da Vinci Research Kit [33], as shown in Fig. 4.2. The master manipulator measures position and orientation of the user's hand and provides force and torque output, while the tactile device provides skin deformation feedback by translating and rotating the tactors relative to the user's fingerpads. The tactile device weighs approximately 200 g, and gravity compensation is provided by the master manipulator to compensate for both the weight of the manipulator and the tactile device.

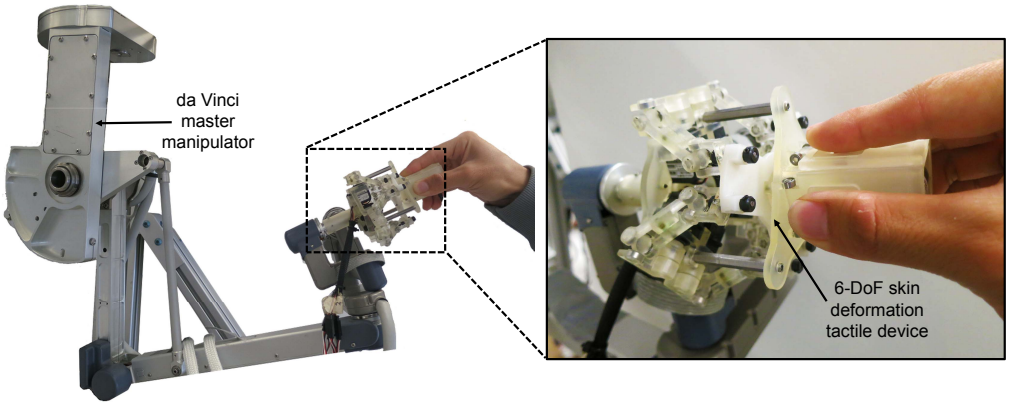

Figure 4.2: The 6-DoF tactile feedback device attached to the end-effector of the master manipulator of the da Vinci Research Kit. Gravity compensation is provided by the master manipulator to compensate for the weight of the tactile device.

4.1.1.1 Kinematic Verification

To determine the kinematic accuracy of the device, we measured the position and orientation by attaching the end-effector of the tactile device to the end-effector of a Phantom Premium with gimbal attachment. The Phantom Premium with gimbal attachment had a position resolution of 0.03 mm and a rotation resolution of 0.008°. The result agrees with our kinematic model, with a maximum translation error of 0.4 mm in the commanded axis of motion and 0.15 mm in the non-commanded axis, for a commanded translation range between -3 mm and +3 mm. The maximum rotation error in the commanded axis of motion is 0.85°, and 0.5° in the non-commanded

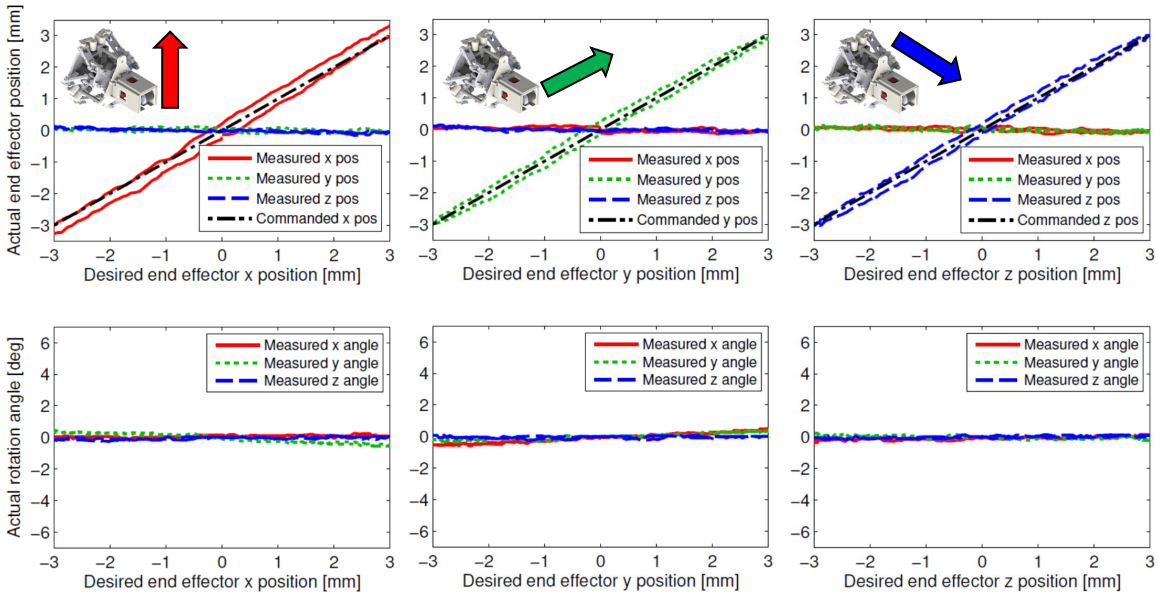

(a) Translation in X,Y, and Z direction

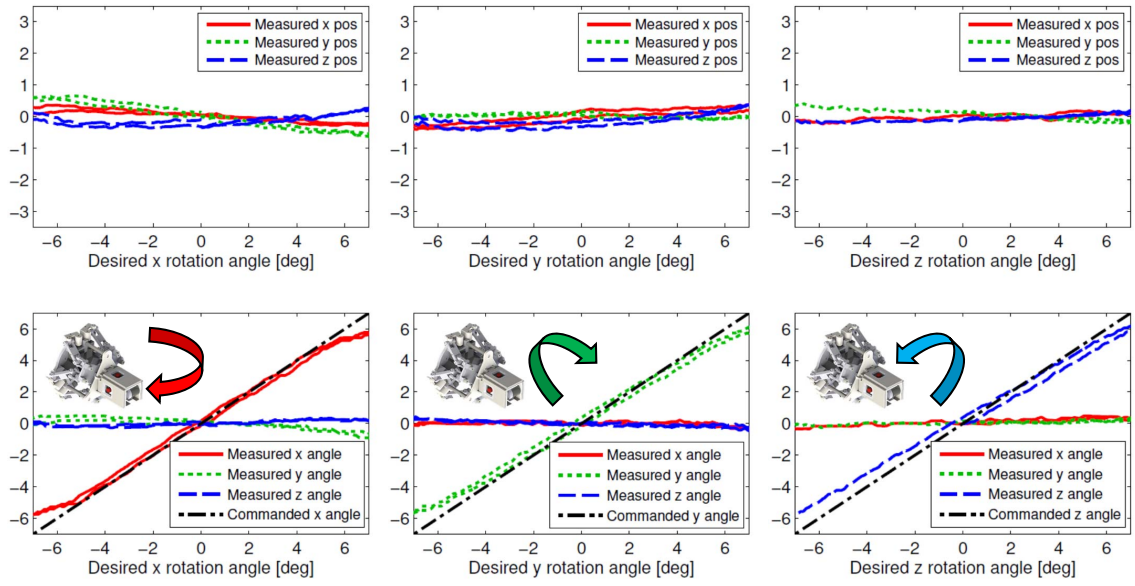

(b) Rotation in X, Y, and Z direction

Figure 4.3: Commanded and measured translation and rotation of the end-effector of the 6-DoF skin deformation device when the device is in the unloaded state. For a commanded translation range between -3 mm to 3 mm.

axis of motion, for a commanded rotation range between -6° and +6°.

4.1.1.2 Device Saturation

The skin deformation tactile device experiences device saturation when one or more of the tactors hit the side wall of the aperture on the aperture housing. A diagram of device saturation in the translational and rotational degree of freedom is illustrated in Fig. 4.4. The square aperture on the aperture housing has a length of 10 mm, while the skin deformation tactor has a diameter of 6 mm. Therefore, the device is restricted to a maximum translation of 2 mm in all directions. In addition, the distance from the center of the end-effector to the tip of the tactors is 18 mm. The device therefore has a maximum rotation of 6°. When the device translates and rotates simultaneously, the maximum translation and rotation is dependent on the specific configuration, and is less than or equal to 2 mm and 6° for all axes.

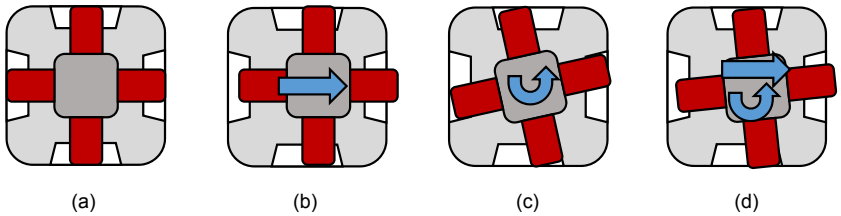

Figure 4.4: Illustration of device saturation: (a) Device in equilibrium position (b) Device saturation in a translational degree of freedom (c) Device saturation in a rotational degree of freedom (d) Device saturation under both translation and rotation.

4.1.1.3 Using Skin Deformation Feedback to Convey Force and/or Torque Information

Fig. 4.5 shows illustrations of how the 6-DoF skin deformation tactile device can be used to convey force, torque, and both force and torque information to the user. In order to create the same skin deformation sensation that one felt when using a stylus-like tool to interact with objects in the environment, the end-effector of the tactile device will translate, rotate, or translate and rotate in the direction of the interaction force/torque. For a larger interaction force/torque magnitude, the end-effector will translate/rotate further to create a more intense skin deformation sensation.

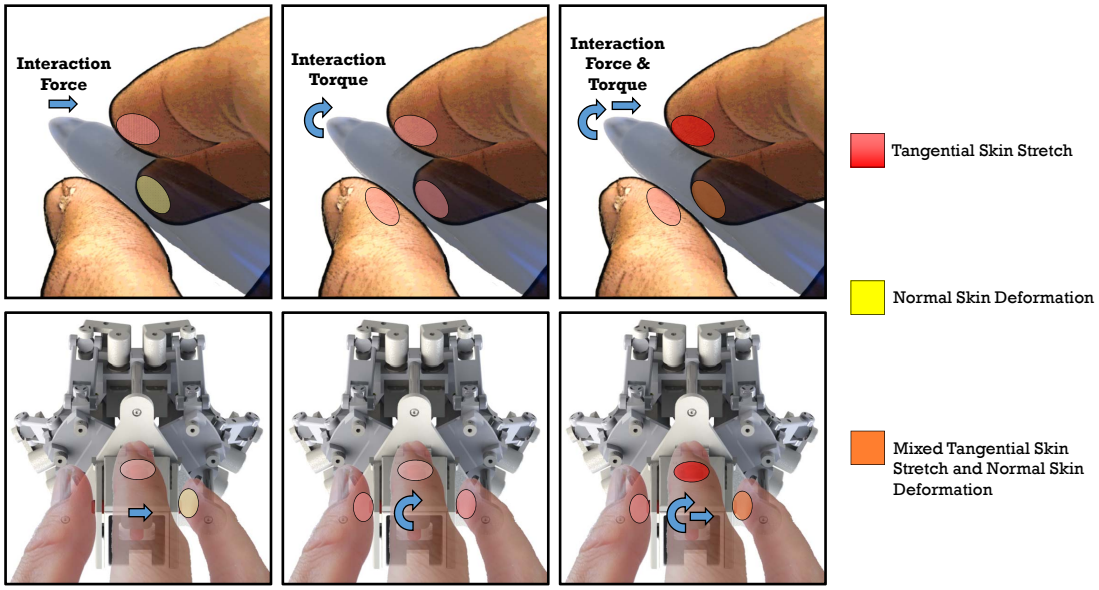

Figure 4.5: Illustration of how the 6-DoF skin deformation tactile device can convey skin deformation tactile sensation analogous to the sensations that one felt when subjected to interaction forces and torques while using a stylus-like tool.

4.2 Sensory Substitution of Forces and Torques using 6-Degree-of-Freedom Skin Deformation Feedback

4.2.1 Study Description

4.2.1.1 Participants

A total of 14 participants (10 males and 4 females) took part in the experiment after giving informed consent. All but one participants are right-handed. The experimental protocol was approved by the Stanford University Institutional Review Board.

4.2.1.2 Experiment Task

In this experiment, the goal was to determine participants' ability to interpret the skin deformation cues provided by the tactile device for force and torque sensory substitution. Participants performed a peg-in-hole insertion task in a virtual environment, illustrated in Fig. 4.7. The virtual environment was displayed to the participants using the high definition stereo vision display of the da Vinci Research Kit.

Although there has been work to model the interaction forces encountered during performance of a 2-D and 3-D peg-in-hole task [50] [75], in this study, we used CHAI3D [11] and Open Dynamics Engine to render the peg-in-hole task in a virtual environment, and used the proxy algorithm to render the force-torque feedback according to

$$\begin{bmatrix} {}^0\vec{F} \\ {}^0\vec{\tau} \end{bmatrix} = \begin{bmatrix} K_{\text{force}} & 0_{3\times3} \\ 0_{3\times3} & K_{\text{torque}} \end{bmatrix} \begin{bmatrix} {}^0\vec{x}_{\text{p}} \\ {}^0\vec{\theta}_{\text{p}} \end{bmatrix} \tag{4.1}$$

in which ${}^0\vec{F}$ and ${}^0\vec{\tau}$ is the interaction force and torque vector in the global frame, K_{force} is a 3×3 virtual coupling linear stiffness matrix, K_{torque} is a 3×3 virtual coupling torsional stiffness matrix, ${}^0\vec{x}_{\text{p}}$ is the vector from the haptic interaction point to the proxy, expressed in the global frame, and ${}^0\vec{\theta}_{\text{p}}$ is the difference in orientation between the haptic interaction point and the proxy, expressed in the axis-angle format in the global frame:

$${}^{\text{HIP}}\vec{\theta}_{\text{p}} = \text{AxisAngle}({}^0R_{\text{HIP}}{}^T{}^0R_{\text{virtual tool}}), \tag{4.2}$$

$${}^0\vec{\theta}_{\text{p}} = {}^0R_{\text{HIP}}{}^{\text{HIP}}\vec{\theta}_{\text{p}}, \tag{4.3}$$

in which ${}^0R_{\text{virtual tool}}$ is the rotation matrix from the virtual tool frame to the global frame, and ${}^0R_{\text{HIP}}$ is the rotation matrix from the haptic interaction point frame to

the global frame.The force and torque output by the dVRK is

$$\begin{bmatrix} {}^{\text{dVRK}}\vec{F} \\ {}^{\text{dVRK}}\vec{\tau} \end{bmatrix} = \begin{bmatrix} H_{\text{force}} & 0_{3\times3} \\ 0_{3\times3} & H_{\text{torque}} \end{bmatrix} \begin{bmatrix} {}^{0}\vec{F} \\ {}^{0}\vec{\tau} \end{bmatrix}, \tag{4.4}$$

where H_{force} and H_{force} are indicator functions that specify whether the da Vinci master manipulator will render forces and/or torques.

Skin deformation tactile cues are rendered to inform participants of the force and torque they are exerting on the virtual environment. The translation and rotation skin deformation cue, used to convey force and torque information, is

$$\begin{bmatrix} {}^{sd}\vec{x}_{\text{e}} \\ {}^{sd}\vec{\theta}_{\text{e}} \end{bmatrix} = \begin{bmatrix} G_{\text{force}} & 0_{3\times3} \\ 0_{3\times3} & G_{\text{torque}} \end{bmatrix} \begin{bmatrix} {}^{\text{sd}}R_0 & 0_{3\times3} \\ 0_{3\times3} & {}^{\text{sd}}R_0 \end{bmatrix} \begin{bmatrix} {}^{0}\vec{F} \\ {}^{0}\vec{\tau} \end{bmatrix} \tag{4.5}$$

in which ${}^{\text{sd}}R_0$ is the rotation matrix from the global frame to the skin deformation device frame, G_{force} is the linear skin deformation-to-force ratio, and G_{torque} is the rotational skin deformation-to-torque ratio. An illustration of the rendering algorithm for kinesthetic force, kinesthetic torque, skin deformation force, and skin deformation torque cues is shown in Fig. 4.6.

Participants completed the task using 7 different types of feedback, shown in Table 4.1. The kinesthetic force and/or torque feedback are included as a control to see if task performance can be improved using force/torque feedback, and to act as a baseline to compare the performance with skin deformation feedback.

4.2.1.3 Experiment Procedure

The task and the different feedback types were explained to the participants at the beginning of the experiment. After that, participants spent a minute for each of the seven feedback types to perform the peg-in-hole task. These procedures familiarized participants with performing the task using the seven different feedback types. After the initial training, participants proceed to the main experiment.

The main experiment consists of seven sets of trials, corresponding to each of the

Table 4.1: The seven feedback conditions for the peg-in-hole study.

No.	Name	Feedback Condition	
1	Visual only	$H_{\text{force}} = 0_{3\times3}$	$G_{\text{force}} = 0\ mm/N$
		$H_{\text{torque}} = 0_{3\times3}$	$G_{\text{torque}} = 0\ rad/Nm$
2	Visual + kinesthetic force	$H_{\text{force}} = I_{3\times3}$	$G_{\text{force}} = 0\ mm/N$
		$H_{\text{torque}} = 0_{3\times3}$	$G_{\text{torque}} = 0\ rad/Nm$
3	Visual + kinesthetic torque	$H_{\text{force}} = 0_{3\times3}$	$G_{\text{force}} = 0\ mm/N$
		$H_{\text{torque}} = I_{3\times3}$	$G_{\text{torque}} = 0\ rad/Nm$
4	Visual + kinesthetic force and torque	$H_{\text{force}} = I_{3\times3}$	$G_{\text{force}} = 0\ mm/N$
		$H_{\text{torque}} = I_{3\times3}$	$G_{\text{torque}} = 0\ rad/Nm$
5	Visual + SD Force	$H_{\text{force}} = 0_{3\times3}$	$G_{\text{force}} = 1.0\ mm/N$
		$H_{\text{torque}} = 0_{3\times3}$	$G_{\text{torque}} = 0\ rad/Nm$
6	Visual + SD Torque	$H_{\text{force}} = 0_{3\times3}$	$G_{\text{force}} = 0\ mm/N$
		$H_{\text{torque}} = 0_{3\times3}$	$G_{\text{torque}} = 0.7\ rad/Nm$
7	Visual + SD force and torque	$H_{\text{force}} = 0_{3\times3}$	$G_{\text{force}} = 1.0\ mm/N$
		$H_{\text{torque}} = 0_{3\times3}$	$G_{\text{torque}} = 0.7\ rad/Nm$

seven feedback types. The seven sets were presented to the participants in a Latin square order. Each set of trials consisted of 4 training trials and 10 experiment trials. For each set, participants performed the training trials before the experiment trials. These training trials re-familiarized participants with the feedback type before the start of the experiment trials, and also familiarized participants with the experiment procedure. Before the start of each trial, participants moved the haptic device to a designated starting region, after which the virtual environment would be rendered and participants would start the peg-in-hole task. Participants were given unlimited amount of time to perform the task, and were instructed prior to the start of the experiment to place priority on minimizing the forces and torques during the insertion process. The trial ended when the participant inserted the peg fully into the hole.

For all trials, the translational virtual coupling stiffness was set at 220 N/m. The rotational virtual coupling stiffness was 1.0 Nm/rad. The translational skin deformation-to-force ratio was 1.0 mm/N while the rotational skin deformation-to-torque ratio was 0.7 rad/Nm for each axis. These values were determined during pilot studies to achieve good skin deformation perception while avoiding device saturation.

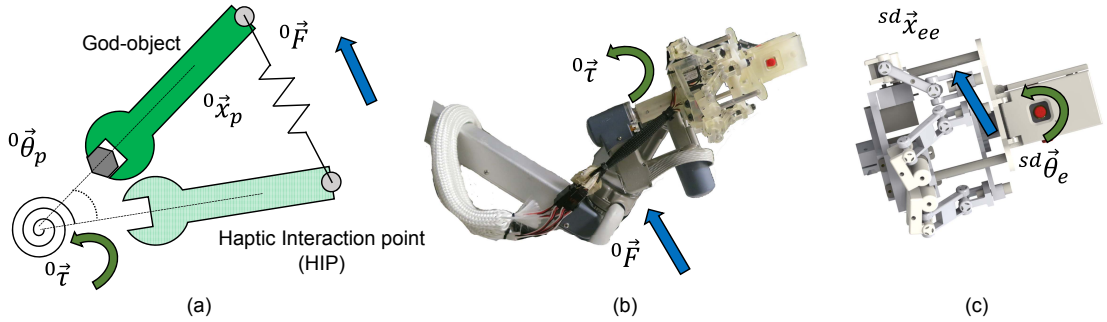

Figure 4.6: (a) Proxy algorithm for rendering forces and torques with the virtual environment. The solid-green object represents the actual location/orientation of the virtual tool while the light green tool represent the actual position/orientation of the tool. The forces/torques are rendered via (b) the master manipulator of the da Vinci or (c) the tactile skin deformation device.

4.2.1.4 Data Analysis

Participant's interaction information was recorded at 1 kHz. We used the following metrics to evaluate each participant's performance:

- ***Mean magnitude of force and torque*** that participants exert to insert the peg into the hole

$$F_{\text{mean}} = \frac{1}{N}\sum_{n=1}^{N} |\vec{F}[n]|_2, \ \tau_{\text{mean}} = \frac{1}{N}\sum_{n=1}^{N} |\vec{\tau}[n]|_2, \tag{4.6}$$

  where N is the number of data points recorded for the path, $\vec{F}[n]$ and $\vec{\tau}[n]$ are the interaction force and torque at sample n, and $|.|_2$ is the l^2-norm.

- ***Peak interaction force and torque*** that participants exert to insert the peg into the hole

$$F_{\text{peak}} = \max_n |\vec{F}[n]|_2, \ \tau_{\text{peak}} = \max_n |\vec{\tau}[n]|_2, \tag{4.7}$$

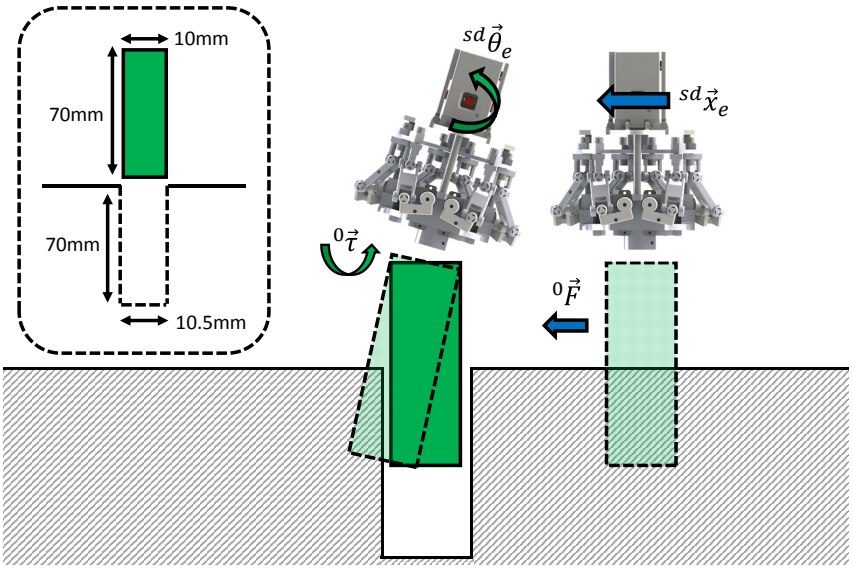

Figure 4.7: Peg-in-hole task performed by participants during the experiment. The force/torque calculated by the simulation is reflected back to the participants through the da Vinci Research Kit master manipulator and skin deformation tactile device. Participants can use these information to minimize the force/torque during the insertion process.

- ***Sum of squared force and torque*** was calculated by taking the sum of the square of the interaction force / torque:

$$SOSF = \sum_{n=1}^{N} |\vec{F}[n]|_2^2, \; SOST = \sum_{n=1}^{N} |\vec{\tau}[n]|_2^2, \tag{4.8}$$

  This performance metric was previously used to measure the performance of a 6-axis force-torque reflecting teleoperator [26], and it penalizes large interaction force/torque over completion time.

- ***Task completion time*** was calculated as the time that elapsed when participants placed the haptic device in the starting region, to the instant when participants inserted the peg fully into the hole.

- ***Path correlation***. Participants' hand positions after inserting the peg through the hole entrance was spatially sampled at distinct insertion length of 1 mm.

The correlation between the path vector fields is

$$\rho(U,Y) = \frac{Cov(U,Y)}{\sigma(U)\sigma(Y)}, \tag{4.9}$$

where U, and Y are the position vectors of participant's path. The covariance function and the standard deviation of an ordered set of vectors are calculated using the method described in [72].

We performed a repeated measures one-way ANOVA using the above metrics as dependent variables and feedback types as independent variables. Whenever the feedback effect was significant, we performed comparisons between visual feedback and visual with kinesthetic or skin deformation force and/or torque feedback. We also performed comparison between visual with skin deformation force or torque feedback, and visual with skin deformation force and torque feedback. These comparisons are made as we want to determine whether adding kinesthetic or skin deformation force and/or torque feedback affects task performance, and to determine whether rendering force and torque skin deformation cues together degrade participants' performance. We also wanted to compare the performance of kinesthetic and skin deformation feedback. Statistical analysis was performed using the MATLAB `fitrm` and `ranova` functions. Statistical significance was determined at the 0.05 level, with the appropriate Bonferroni correction for multiple comparisons.

4.2.2 Results

Participants decrease their interaction force and torque when force/torque feedback, either in the form of kinesthetic feedback or skin deformation cues, are rendered. This result is shown in Fig. 4.8a, where the mean and 95% confidence interval for the applied force and torque is illustrated. From ANOVA analysis, there is a statistically significant effect of feedback type on the mean force ($F_{6,78} = 116.5, p < 0.001$) and mean torque ($F_{6,78} = 76.8, p < 0.001$).

Fig. 4.8b shows the mean and 95% confidence interval for the peak applied force and torque. Again, participants are able to utilize the kinesthetic or skin deformation

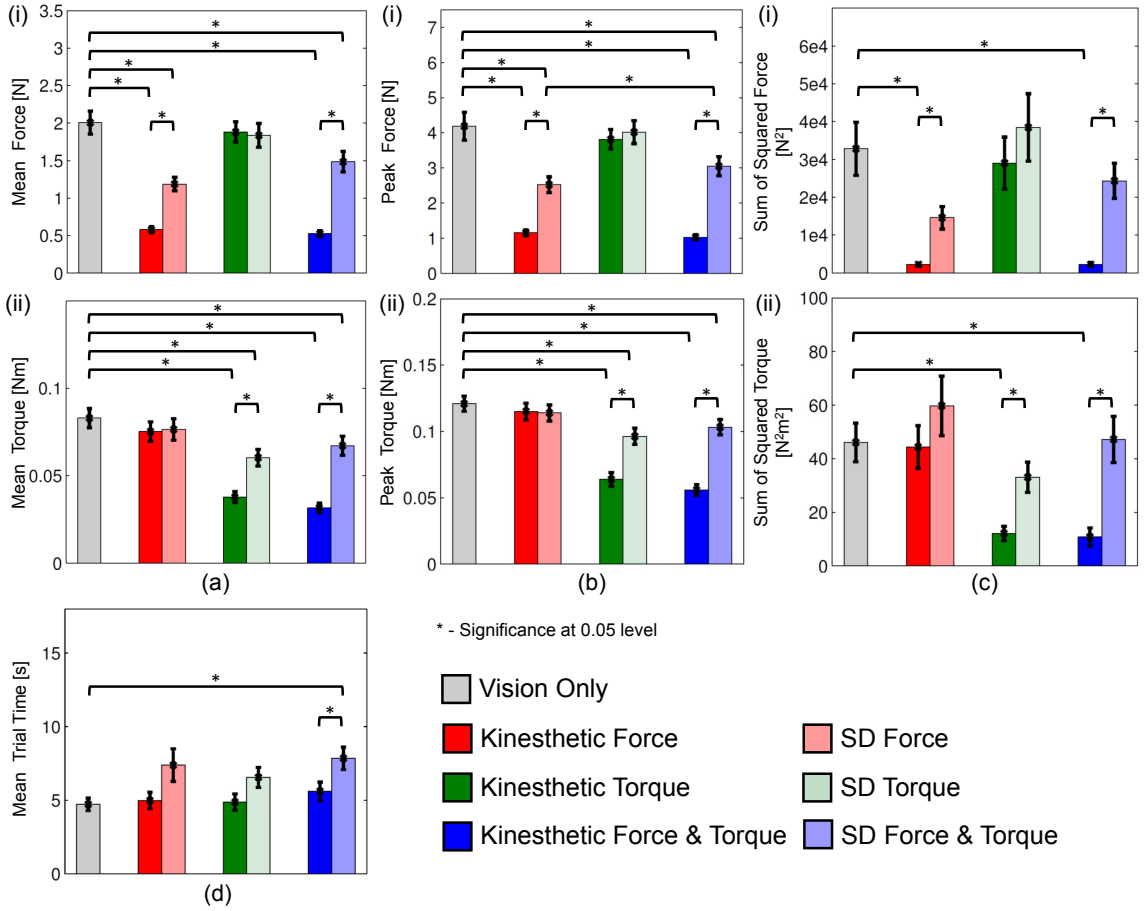

Figure 4.8: Mean and 95% confidence interval for the (a) mean magnitude of force and torque (b) peak magnitude of force and torque (c) sum of squared force and torque performance metric.

force/torque feedback to reduced peak force/torque. From ANOVA analysis, there is a statistically significant effect of feedback type on peak force ($F_{6,78} = 111.0, p < 0.001$) and peak torque ($F_{6,78} = 91.1, p < 0.001$).

Fig. 4.8c shows the mean and 95% confidence interval for the sum of squared force (SOSF) and torque (SOST) metrics. From ANOVA analysis, there is a statistically significant effect of feedback types on SOSF ($F_{6,78} = 10.2, p < 0.001$) and SOST ($F_{6,78} = 7.4, p < 0.001$). There is a decrease in SOSF when kinesthetic force or skin deformation force feedback are added. Skin deformation force and torque feedback also decreases SOSF, but with a smaller effect than when only skin deformation force

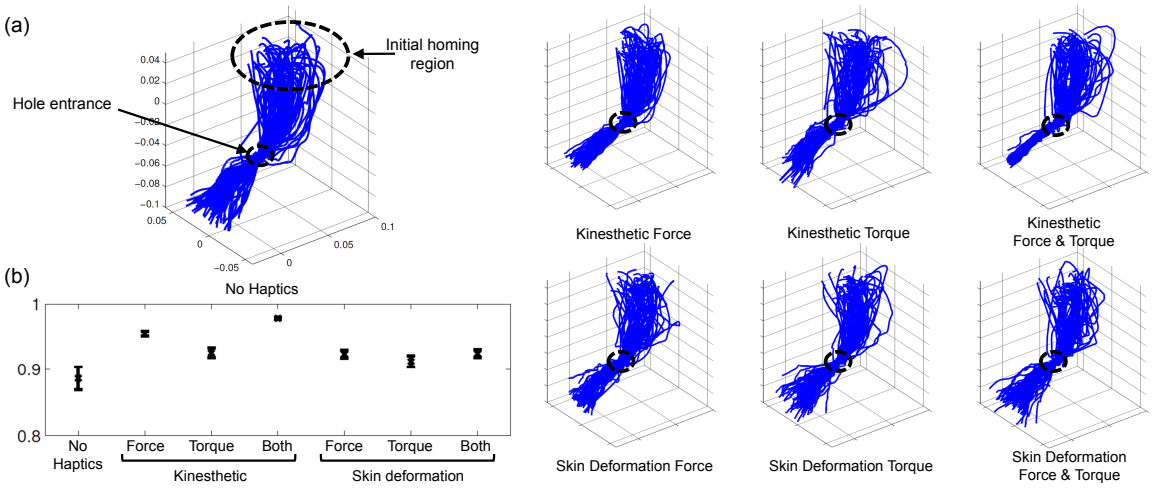

Figure 4.9: (a) Paths of the da Vinci manipulator (user's hand) for the seven feedback types. (b) Mean and 95% of the correlation between the paths for the seven feedback types. The addition of kinesthetic and skin deformation force and/or torque feedback significantly increases the correlation between the paths compare to visual only feedback.

feedback is used. For SOST, torque feedback in the form of kinesthetic torque or skin deformation feedback decreases SOST, but there is no difference in SOST when skin deformation force and torque feedback is used.

The mean and 95% confidence interval for the trial time is shown in Fig. 4.8d. ANOVA analysis shows that there is a statistically significant effect of feedback type on trial time ($F_{6,78} = 3.6, p = 0.003$). Participants took longer to perform the task when skin deformation cues, either in the form of force, torque, or force and torque, are added.

Fig. 4.10 shows the mean and 95% confidence interval for the percentage of time that participants saturate the da Vinci master manipulator or the tactile device during interaction, and the breakdown of the saturation of each individual force and torque components. There is a statistically significant increase in device saturation when both force and torque skin deformation cues are rendered, compared to the case when either force or torque skin deformation cues are displayed.

The path of the master manipulator position (the commanded position of the tool) for all subjects and all trials, together with the path correlation, is shown in Fig. 4.9.

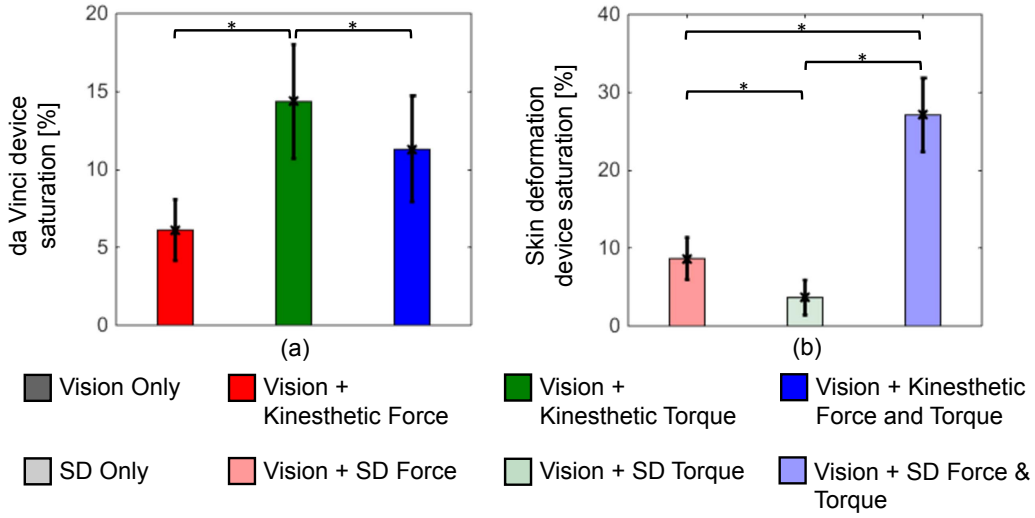

Figure 4.10: Mean and 95% confidence interval for the percentage of time that participants saturate the (a) da Vinci master manipulator, and (b) skin deformation tactile device. The brackets show comparisons that are statistically significant at the 0.05(*) level.

Adding kinesthetic or skin deformation force and/or torque feedback increase path correlation compared to visual-only feedback.

4.2.3 Discussions

4.2.3.1 Skin deformation feedback improves force or torque related performance metric

The addition of skin deformation force cues to visual feedback decreases mean force, peak force, and the sum of squared forces compared to visual feedback only. Similarly, the addition of skin deformation torque cues to visual feedback decreases mean torque, peak torque, and the sum of squared torques compared to visual feedback only. These results show that participants are able to interpret the corresponding skin deformation force/torque cues to decrease the applied force/torque during the peg-in-hole task. Participants are able to interpret the skin deformation force cues better than the torque cues to improve task performance, as shown by the larger difference in mean force, peak force, and the sum of squared forces between visual and visual with

skin deformation force feedback, compared to the smaller difference in mean torque, peak torque, and the sum of squared torques between visual and visual with skin deformation torque feedback. These results suggest that skin deformation force cues are more intuitive than skin deformation torque cues, and that perhaps more training should be given for users to interpret the skin deformation torque cues.

4.2.3.2 Coupling of skin deformation force and torque cues

When skin deformation force and torque feedback are rendered together, we observed a statistically significant increase in mean force, peak force, and the sum of squared forces compared to the case when only skin deformation force feedback is rendered. Similarly, we observed an increase in mean torque, peak torque, and the sum of squared torque compared to the case when only skin deformation torque feedback is rendered. The decrease in performance can be attributed to the increase in saturation of the tactile device when both force and torque cues are rendered, as shown in Fig. 4.10. This result shows that while force and torque skin deformation cues can be rendered simultaneously using the current tactile device, rendering both cues increase saturation and decrease cue interpret-ability. Future designs of the device can decouple the rendering of force and torque skin deformation cues to minimize the issue of device saturation.

4.3 Sensory Augmentation of Forces and Torques using 6-Degree-of-Freedom Skin Deformation Feedback

4.3.1 Study Description

4.3.1.1 Participants

A total of 16 participants (12 males and 4 females) took part in the experiment after giving informed consent. All participants are right-handed. The experimental protocol was approved by the Stanford University Institutional Review Board.

4.3.1.2 Experiment Task

In this experiment, the goal was to determine participants' change in performance when skin deformation cues are used in conjunction with kinesthetic force and torque feedback to augment force and torque information. Participants performed a peg-in-hole insertion task in a virtual environment, similar to the task used in the section 4.2. The force and torque feedback provided by the dVRK is

$$\begin{bmatrix} {}^{\text{dVRK}}\vec{F} \\ {}^{\text{dVRK}}\vec{\tau} \end{bmatrix} = G \begin{bmatrix} {}^{0}\vec{F} \\ {}^{0}\vec{\tau} \end{bmatrix} \tag{4.10}$$

The above equation is similar to that of equation 4.1, with the additional of a term G which we called the force/torque feedback ratio. The skin deformation tactile feedback is rendered according to equation 4.5.

Participants performed the task under eight different feedback conditions. These eight feedback conditions include force and torque feedback with different force-feedback fidelity, with and without the addition of skin deformation feedback. The parameters for each of the eight feedback conditions are summarized in Table 4.2.

4.3.1.3 Experiment Procedure

The experiment procedure is similar to the experiment procedure in section 4.2.1.3

4.3.1.4 Data Analysis

The performance metric used in this experiment is similar to the metric used in section 4.2.1.4, namely, the mean force and torque, the peak force and torque, the sum of squared force and torque, and the trial time. Besides the above performance metric, we also asked subjects to evaluate their perceived performance after the experiment. Subjects were asked to rate their performance (in terms of lowering interaction force, torque, and trial time) relative to the visual only case on a 7-degree Likert scale as the answer to the question:"How did you perceive your performance to be relative to the visual case for the different feedback types?",

Table 4.2: The eight feedback conditions for the sensory augmentation of kinesthetic force and torque feedback study.

No.	Name	Feedback Condition	
1	Visual + Force/Torque 100%	$G = 1.0$	$G_{\text{force}} = 0$ mm/N $G_{\text{torque}} = 0$ rad/Nm
2	Visual + Force/Torque 66%	$G = 0.66$	$G_{\text{force}} = 0$ mm/N $G_{\text{torque}} = 0$ rad/Nm
3	Visual + Force/Torque 33%	$G = 0.33$	$G_{\text{force}} = 0$ mm/N $G_{\text{torque}} = 0$ rad/Nm
4	Visual only	$G = 0.0$	$G_{\text{force}} = 0$ mm/N $G_{\text{torque}} = 0$ rad/Nm
5	Visual + Force/Torque 100% + Skin deformation	$G = 1.0$	$G_{\text{force}} = 0$ mm/N $G_{\text{torque}} = 0$ rad/Nm
6	Visual + Force/Torque 66% + Skin deformation	$G = 0.66$	$G_{\text{force}} = 0$ mm/N $G_{\text{torque}} = 0$ rad/Nm
7	Visual + Force/Torque 33% + Skin deformation	$G = 0.33$	$G_{\text{force}} = 0$ mm/N $G_{\text{torque}} = 0$ rad/Nm
8	Visual + Skin deformation	$G = 0.0$	$G_{\text{force}} = 0$ mm/N $G_{\text{torque}} = 0$ rad/Nm

We performed a repeated measures two-way ANOVA using the above metrics as dependent variables, force/torque feedback ratio as a categorical factor with 2 levels, and presence of skin deformation feedback. Whenever the feedback effect was significant, we performed comparisons between the case with and without skin deformation feedback for all force/torque feedback ratios. Statistical analysis was performed using the MATLAB `fitrm` and `ranova` functions. Statistical significance was determined at the 0.05 level, with the appropriate Bonferroni correction for multiple comparisons.

4.3.2 Results

Participants decrease their mean interaction force, peak interaction force, and sum of squared force when skin deformation feedback is added to kinesthetic force/torque feedback, for all force/torque feedback ratio. This result is shown in Fig. 4.11a(i), Fig. 4.11b(i), and Fig. 4.11c(i), which gives the mean and 95% confidence interval for

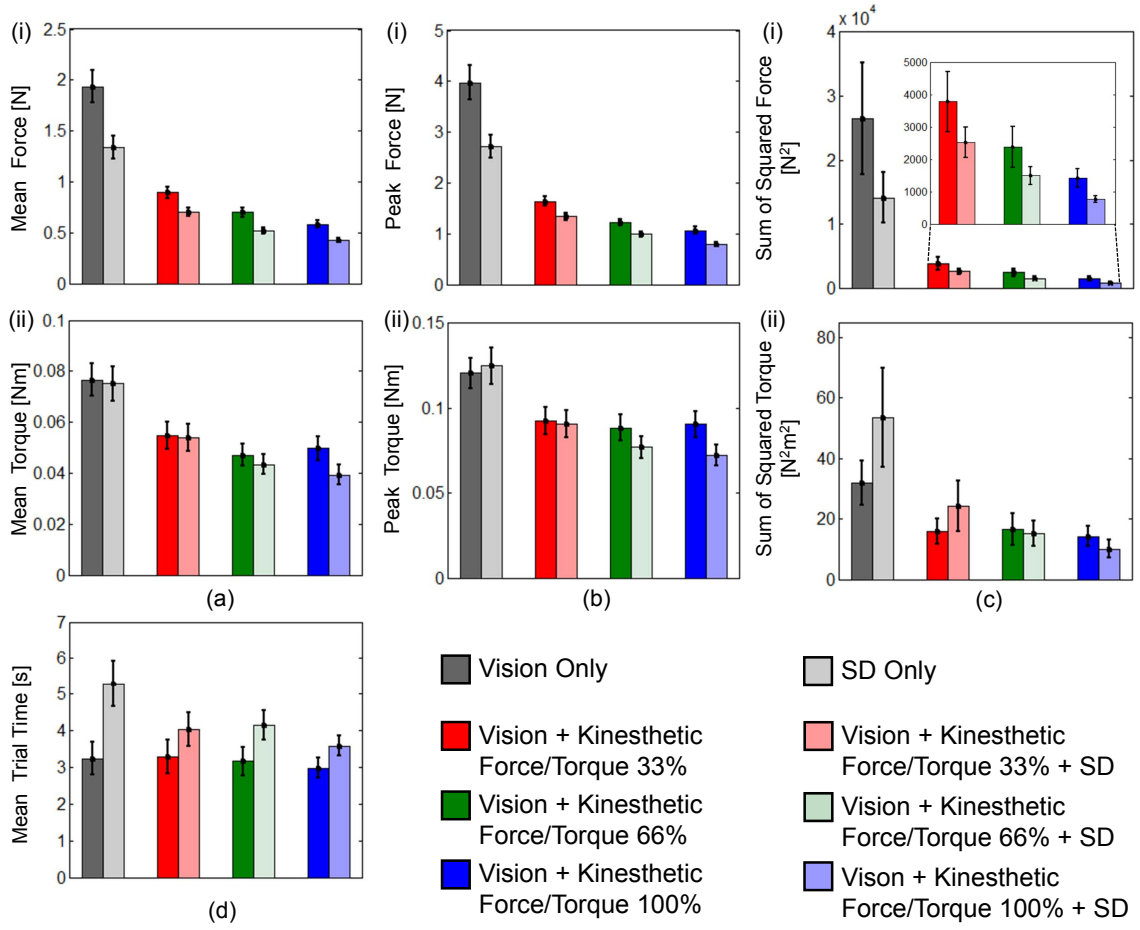

Figure 4.11: Mean and 95% confidence interval for the (a) mean magnitude of force and torque (b) peak magnitude of force and torque (c) sum of squared force and torque performance metric.

the mean applied force, peak applied force, and sum of squared force for each feedback types. ANOVA analysis shows a statistically significant effect of force/torque feedback ratio ($F_{3,45} = 177.14, p < 0.001$ for mean applied force, $F_{3,45} = 206.92, p < 0.001$ for peak applied force, and $F_{3,45} = 170.02, p < 0.001$ for sum of square force) and a statistically significant effect of the presence of skin deformation feedback ($F_{1,15} = 34.44, p < 0.001$ for mean applied force, $F_{1,15} = 33.41, p < 0.001$ for peak applied force, and $F_{1,15} = 8.24, p = 0.011$ for sum of square force).

For mean interaction torque, peak interaction torque, and sum of squared torque, however, there is no consistent trend in performance when skin deformation feedback

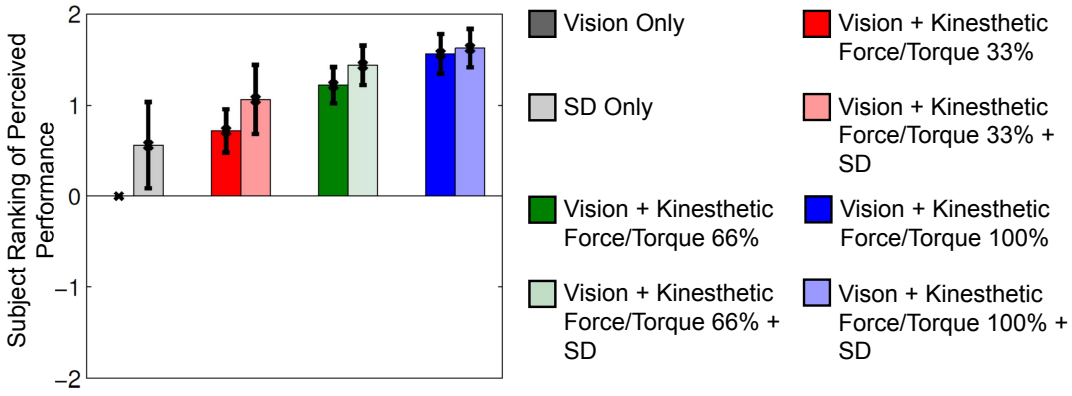

Figure 4.12: Mean and 95% confidence interval for the perceived performance rated by subjects. Subjects' perceived performance increases with force-feedback ratio, and increases with the addition of skin deformation feedback.

is added to kinesthetic force/torque feedback. The result is shown in Fig. 4.11a(ii), Fig. 4.11b(ii), and Fig. 4.11c(ii), which gives the mean and 95% confidence interval for the mean applied torque, peak applied torque, and sum of squared torque for each feedback types. ANOVA analysis showed statistically significant effect of force/torque feedback ratio ($F_{3,45} = 28.49, p < 0.001$ for mean applied torque, $F_{3,45} = 18.17, p < 0.001$ for peak applied torque, and $F_{3,45} = 26.67, p < 0.001$ for the sum of squared torques) and statistically significant effect of skin deformation feedback ($F_{1,15} = 5.16, p = 0.038$ for mean applied torque, $F_{1,15} = 6.19, p = 0.025$ for peak applied torque). However, there is no statistical significant effect of skin deformation feedback for the sum of square torque ($F_{1,15} = 0.45, p = 0.51$).

Participants increase their trial time when skin deformation feedback is added to kinesthetic force/torque feedback, for all force/torque feedback ratio. This result is shown in Fig. 4.11c, which gives the mean and 95% confidence interval for the trial time. ANOVA analysis on trial time showed a statistically significant effect of the presence of skin deformation feedback ($F_{1,15} = 23.35, p < 0.001$), but no statistically significant effect of force/torque feedback ratio ($F_{3,45} = 1.82, p = 0.18$).

Fig. 4.12 shows the perceived performance relative to the visual only case, for the different feedback types. Subjects' perceived performance increases with force-feedback ratio, and increases with the addition of skin deformation feedback.

For device saturation, Fig. 4.13a showed that the presence of skin deformation feedback has no statistically significant effect on the saturation of the da Vinci force feedback master device. However, there is a statistically significant effect of the force/torque feedback ratio on the saturation of the skin deformation tactile feedback device, with a larger force/torque feedback ratio leading to a lower saturation rate, as shown in Fig. 4.13b.

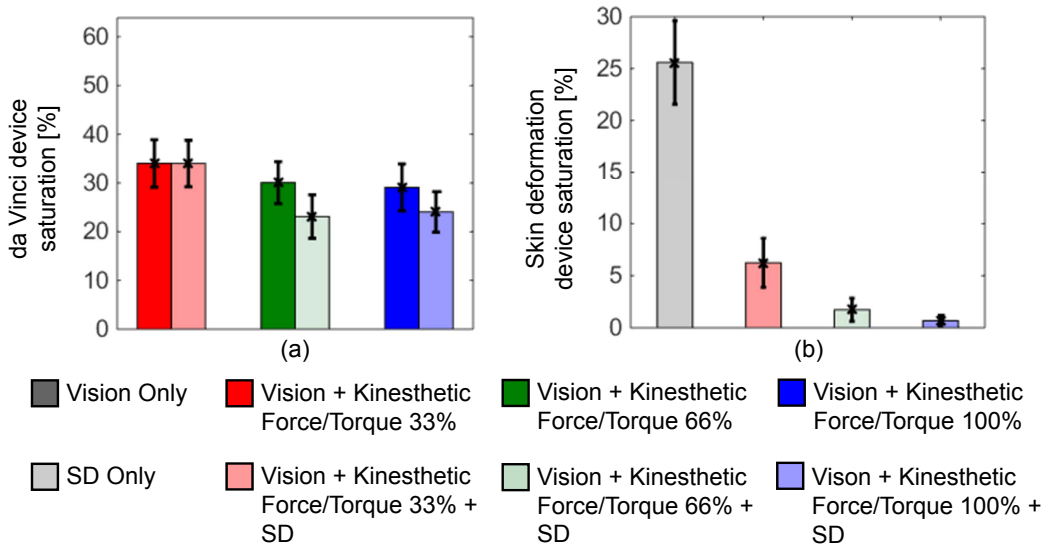

Figure 4.13: Mean and 95% confidence interval for the percentage of time that participants saturate the (a) da Vinci master manipulator, and (b) skin deformation tactile device.

4.3.3 Discussions

4.3.3.1 Improvement in force-related performance measure

When kinesthetic force/torque feedback is augmented with skin deformation tactile feedback, we see a decrease in the mean applied force, peak applied force, and sum of squared forces. However, there is no improvement in mean applied torque, peak applied torque, and sum of squared torques. This result can be attributed to the reason that participants placed higher emphasis on the skin deformation force cues rather than the torque cues when both force and torque skin deformation cues are

rendered, and the result of this experiment is consistent with the result obtained in the previous experiment in section 4.2.

The above issue can be solved by adjusting the relative ratio between the translational skin deformation-to-force ratio G_{force} and the rotational skin deformation-to-torque ratio G_{torque}. Lowering the relative ratio between G_{force} and G_{torque} will increase participants' sensitivity to the torque cues, and hence improve the torque related performance metric, while degrading the force-related performance metric.

4.3.3.2 Effect of tactile device saturation

As we increases the force/torque feedback ratio, Fig. 4.13 showed that there is a decrease in the saturation of the tactile device. At the same time, from Fig. 4.11a(ii), Fig. 4.11b(ii), and Fig. 4.11c(ii), we saw that there is a gradual improvement in the mean torque, peak torque, and sum of square torque performance metric for the combined feedback case compared to the case when only force/torque feedback is provided. Such a result provide evidence that saturation of the tactile device decreases the interpret-ability of the combined skin deformation force and torque cues, and that further improvement of the device should decouple the rendering of these two cues.

4.3.3.3 Relative ratio between translational/rotational skin deformation-to-force/torque ratio

In the sensory substitution and sensory augmentation study, we set the translational skin deformation-to-force ratio and the rotational skin deformation-to-torque ratio individually based on pilot studies. However, these ratios, which are set individually, might not be optimal when both force and torque skin deformation cues are rendered. Our results in Fig. 4.10 showed that when either force or torque skin deformation cues are rendered, participants achieved a higher saturation rate for the force cues compared to the torque cues. This indicates that the translational skin deformation-to-force ratio may had been set too high compared to the rotational skin deformation-to-torque ratio. Future studies could determine the optimal ratios between the two values to obtain the best improvement in both force and torque related performance.

4.3.3.4 Lost of contact between skin deformation tactors and fingerpads

When the tactors translate and rotate together to convey interaction force and torque at the same time, there may be situations in which the skin deformation tactors will lose contact with the fingerpad. For example, as illustrated in Fig 4.14(c), due to lose of contact between the tactor and the thumb, the interpretation of the rotational cues may be affected. This illustration shows that besides saturation, the coupling of the force and torque skin deformation cues introduces other issues such as the lost of contact between tactors and fingerpads that will decrease the interpret-ability of the cues.

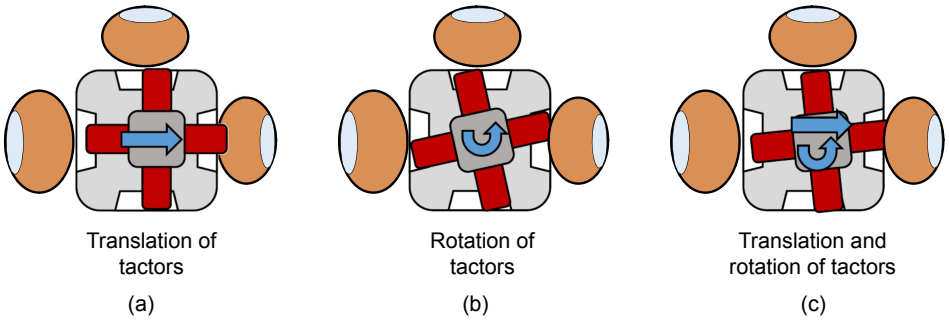

Figure 4.14: Illustration of how the tactors may lost contact with the fingerpads when both force and torque skin deformation cues are rendered. In (a) and (b), the tactors translate and rotate to convey interaction force and torque cues. In (c), when the tactors translate and rotate to convey both force and torque cues, there is lost of contact between the fingerpad and the tactor, resulting in a decrease in interpret-ability of the torque cues.

4.4 Conclusions

We designed a 6-DoF skin deformation tactile haptic device that is able to provide 6-DoF sensory substituted force and torque information to the user. The device uses a Hunt-Type 6-RUS mechanism to actuate skin deformation tactors in 6-DoF, creating skin deformation tactile cues to the fingerpads which are grounded locally on the aperture restraints. Two experiments were performed to determine the capability of our approach to provide sensory substituted force and torque information to the

user, and to use this information to augment kinesthetic force and torque feedback. In both experiments, users perform a peg-in-hole insertion task. Results from the sensory substitution study showed that participants are able to interpret the force and torque cues provided by the tactile device to improve their task performance. However, when both force and torque skin deformation cues are rendered, the interpret-ability of the skin deformation cues decreases, resulting in a decrease in task performance. This decrease in interpret-ability of the cues can be attributed to the increase in the rate of saturation of the tactile device.

For the sensory augmentation experiment, augmenting force/torque feedback with skin deformation feedback improves the force-related performance metric across all force/torque feedback ratio, but did not improve the torque-related performance metric. As the force/torque feedback ratio increases, we see a gradual improvement in the torque-related performance metric for the case when skin deformation feedback is used to augment kinesthetic force/torque feedback. This improvement can be attributed to the decrease in tactile device saturation as the stiffness of the kinesthetic force/torque feedback increases.

Overall in this chapter, we showed that skin deformation tactile feedback can be used for effective sensory substitution and augmentation of force and torque feedback.

Chapter 5

Skin deformation Feedback in Teleoperation Performing Surgery-Related Tasks

In traditional open incision surgery, surgeons performed a large incision on the patient's body and operated directly on it with surgical tools. Such an operation gives good visual and haptic feedback, and is very intuitive to the surgeon. Minimally invasive surgery (MIS) allows surgeons to insert a long, slim tool into the patient's body through a small incision. Using this approach, surgeons are able to see and touch body structures. However, the quality of the visual feedback is reduced, as visual information on the surgical site is captured using cameras, and displayed to the surgeon using a display monitor. The surgeons therefore loses the depth perception when performing MIS. Haptic feedback quality, the dexterity of manipulation, as well as the intuitiveness of manipulation are also reduced due to the fulcrum effect and scaling of forces that comes with the use of a telescopic tool. Robotic MIS was developed to address some of these issues present in traditional MIS. Through teleoperation and the use of high quality stereo vision cameras and 3D stereo displays, surgeons are now able to obtain high quality visual feedback of the surgery site, while at the same time regaining dexterity and intuitiveness of manipulation. Robotic MIS also brings about additional benefits, such as the removal of surgeon hand tremor.

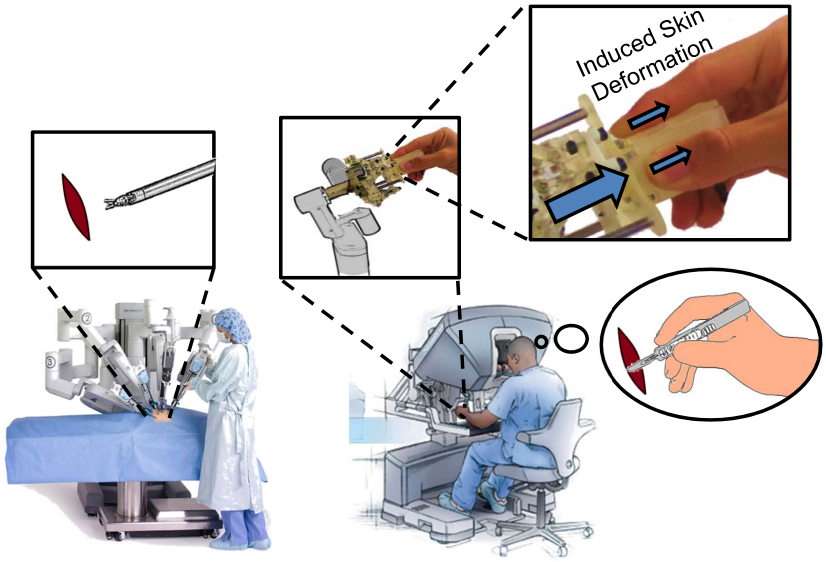

Figure 5.1: Surgical teleoperation system with fingerpad skin deformation feedback. Surgeons are able to feel the skin deformation tactile sensation analogous to the tactile sensation that they felt when using a stylus-like tool to physically interact with the surgical site, without the kinesthetic force components. Images derived from photographs provided by Intuitive Surgical, Inc. (©2015).

Despite the many benefits of robotic MIS, one major deficiency is the lack of both kinesthetic and tactile haptic feedback provided to the surgeon. Kinesthetic feedback provides forces and torques that affect the motion of the surgeon's hand/arm, while tactile feedback provides stimulation to the surgeon's skin on the fingers or hands. The lack of haptic feedback is due to issues on the sensing and display of forces in teleoperation systems. On the sensing side, force sensors can be integrated with the design of surgical instruments to allow teleoperation systems to measure the forces of interaction during surgery. However, due to reasons of cost, sterilizability, and biocompatibility, the implementation of such solution can be challenging [56]. Interaction force estimation, through the use of the difference between the position of the master and patient side robot, or the use of actuator current sensing, can also be implemented. Such methods often include the dynamic forces present in most robot, whose large magnitude can often mask the relatively smaller forces of interaction with the patient [47].

Regarding the display of force information, forces can be displayed to the surgeon through the use of force-feedback haptic devices. Bilateral force-reflecting teleoperation suffers from the fundamental limitation between stability and transparency [42]. As one pushes the limit of transparency, the stability of the bilateral teleoperation systems becomes sensitive to issues such as time delay, robot modeling accuracy, and the accuracy of interaction force estimation. The stability problem associated with force feedback can be overcome through the use of sensory substitution, in which force information are displayed through the use of visual, audio, or tactile cues. However, the problems with sensory substitution is that the use of other sensory modality to provide force information might not be intuitive. In addition, sensory substitution also does not provide the physical constraint that kinesthetic force feedback does.

In this chapter, we displayed interaction force information to the user through the use of fingerpad tactile skin deformation feedback. As shown in Fig. 5.1, the use of fingerpad skin deformation allows surgeons to experience the skin deformation tactile sensations when using a stylus-like tool to interact with tissues in the surgical site, without the corresponding kinesthetic force feedback. Through such a feedback method, we hypothesized it can increase the surgeon's awareness of the task and improve task performance, while maintaining the stability of the teleoperation system. To evaluate the effectiveness of this approach, we conducted a study that involved novice users and expert surgeons performing surgically related tasks with force feedback, skin deformation feedback, and the combination of force and skin deformation feedback. The tasks included in the study are: peg transfer, connection of flexible tubes, and needle driving.

5.1 System Design

The system consists of a master-slave teleoperation system, a tactile skin deformation device, and an operating platform with attached force sensor. The master-slave teleoperation system consists of the master tool manipulator and the patient side manipulator of the da Vinci Research Kit (dVRK) [33]. We attached the 3-degree-of-freedom skin deformation tactile feedback device to the end-effector of the right

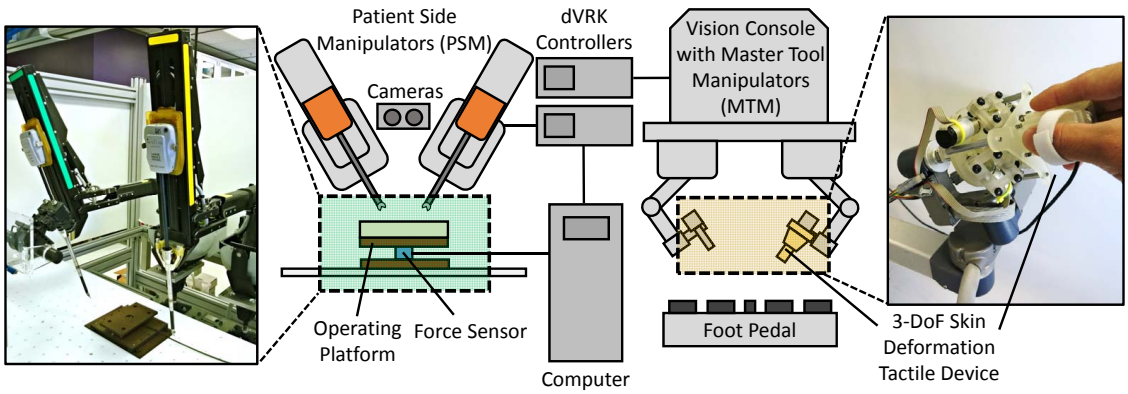

Figure 5.2: System overview of the teleoperation system with tactile skin deformation feedback.

master tool manipulator, shown in Fig. 5.2. The master tool manipulator measures the position and orientation of the user's hand and provides force feedback, while the tactile device provides skin deformation feedback by translating the skin deformation tactors relative to the user's fingerpads.

We used two Flea-3 cameras (Point Grey, Richmond, BC) with 16 mm f1.8 compact instrumentation lenses (Edmund Optics, Barrington, NJ) to capture the visual environment at the patient side manipulators. The visual information is then presented to the users through a stereo vision display with a refresh rate of 60 Hz and resolution of 640×480.

5.1.1 Teleoperation Controller

We used a position-force teleoperation controller [27] to control the motion between the master tool manipulator and the patient side manipulator, and to provide haptic feedback to the user. Using this controller, the position and orientation of the master tool manipulator is used as the desired position and orientation of the patient side manipulator. A local Cartesian proportional-derivative (PD) controller calculates the forces that is send to the patient side manipulator

$$\vec{F}_{\text{controller}} = K_{\text{d,tele}}(S\dot{\vec{x}}_{\text{m}} - \dot{\vec{x}}_{\text{s}}) + K_{\text{p,tele}}(S\vec{x}_{\text{m}} - \vec{x}_{\text{s}}), \tag{5.1}$$

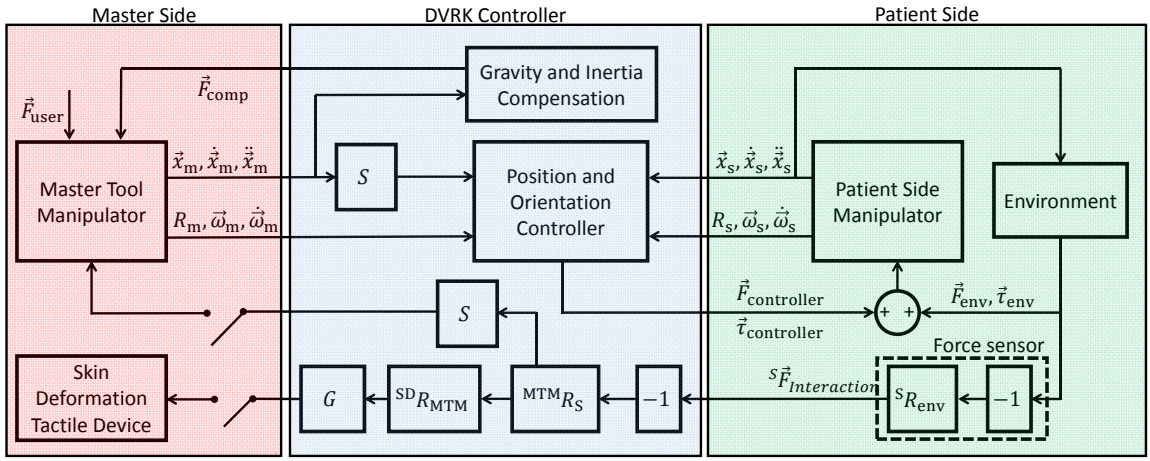

Figure 5.3: Block diagram illustration of the position-force controller used in the teleoperation setup. The position of the master tool manipulator is used as the desired position for the patient side manipulator. The forces that the patient side manipulator exert on the environment is measured by a force sensor on the operating platform, which is then transformed back to the frame of the master side manipulator and the skin deformation tactile device for force or skin deformation feedback.

where $K_{\text{d,tele}}$ is the derivative gain of the teleoperation controller, $K_{\text{p,tele}}$ is the proportional gain of the teleoperation controller, x_m and x_s are the position of the master tool manipulator and the patient side manipulator, S is the scaling factor that scales the motion of the master manipulator, and $\vec{F}_{\text{controller}}$ is the force to the patient side manipulator. For the orientation control, we employed the quaternion orientation control scheme described in [94]. An ATI-Nano 17 force sensor, mounted externally on the operating platform, is used to measure the interaction forces during performance of the task. The measured force ${}^{\text{S}}\vec{F}_{\text{interaction}}$ is transformed from the sensor frame to the right master tool manipulator frame according to the equation

$$ {}^{\text{MTM}}\vec{F}_{\text{interaction}} = {}^{\text{MTM}}R_{\text{S}}\,{}^{\text{S}}\vec{F}_{\text{interaction}}, \tag{5.2} $$

where ${}^{\text{MTM}}R_{\text{Sensor}}$ is the rotational transformation from the sensor frame to right master tool manipulator frame. The kinesthetic force feedback to the user via the

right master tool manipulator is calculated as:

$$\vec{F}_{\mathrm{MTM}} = S \times {}^{\mathrm{MTM}}\vec{F}_{\mathrm{interaction}}, \tag{5.3}$$

where S is the same scaling factor used for the scaling of the master tool manipulator motion, and $\vec{F}_{\mathrm{MTM}}$ is the force to the right master tool manipulator.

To provide skin deformation feedback to the user, ${}^{\mathrm{MTM}}\vec{F}_{\mathrm{interaction}}$ is further transformed from the right master tool manipulator frame to the tactile device frame according to

$${}^{\mathrm{sd}}\vec{F}_{\mathrm{interaction}} = {}^{\mathrm{sd}}R_{\mathrm{MTM}}{}^{\mathrm{MTM}}\vec{F}_{\mathrm{interaction}}. \tag{5.4}$$

The translation skin deformation cue, used to convey force information to the user, is

$$\vec{x}_{\mathrm{sd,d}} = G \times {}^{\mathrm{sd}}\vec{F}_{\mathrm{interaction}}, \tag{5.5}$$

where $\vec{x}_{\mathrm{sd,d}}$ is the desired position of the end-effector of the skin deformation device and G is the skin deformation-to-force ratio.

We performed gravity and inertial compensation control to compensate for the weight and inertia of the tactile device. The gravity compensation was performed by modeling the tactile device (which weighs 260 g) as a point mass on the end-effector of the master tool manipulator. For inertial compensation, we low-pass filtered the linear and angular velocity to obtain the linear and angular acceleration of the master tool manipulator end-effector. The acceleration signals are multiplied by the mass and inertial of the tactile device and added together with the gravity compensation forces/torques. The combined compensation forces/torques $\vec{F}_{\mathrm{comp}}$ was feedforward to the master tool manipulator controller. A schematic representation of the entire system control is shown in Fig. 5.3.

5.1.2 Tactile Device Controller

The joint angles for each of the joints in the skin deformation tactile device was measured by joint encoders within the motors of the tactile device. The end-effector

position of the skin deformation tactile device is calculated through the forward kinematics of the Delta mechanism. A Cartesian position-derivative (PD) controller is used to control the end-effector position of the skin deformation device:

$$\vec{F}_{\mathrm{sd}} = K_{\mathrm{p,sd}}(\vec{x}_{\mathrm{sd,d}} - \vec{x}_{\mathrm{sd}}) - K_{\mathrm{d,sd}}(\dot{\vec{x}}_{\mathrm{sd}}), \tag{5.6}$$

where $\vec{F}_{\mathrm{sd}}$ is the force sent to the skin deformation tactile device, $K_{\mathrm{d,sd}}$ and $K_{\mathrm{p,sd}}$ are the proportional and derivative gain term for the control of the tactile device, and $\vec{x}_{\mathrm{sd}}$ is the position of the end-effector of the tactile device.

5.1.3 Grip Angle Control

The gripping degree of freedom of the da Vinci research kit is originally controlled through magnetic encoders located at the last joint of the master tool manipulator. With the addition of the skin deformation tactile device, however, this method of controlling the gripping degree of freedom is not feasible. To overcome this issue, we utilizes the grip force sensor present in the skin deformation tactile device. By adding a spring between the level and the force sensor, users are able to change the gripper angle at the patient side manipulator by exerting different amount of force on the lever mechanism. The gripping angle θ_{grip} at the patient side manipulator is

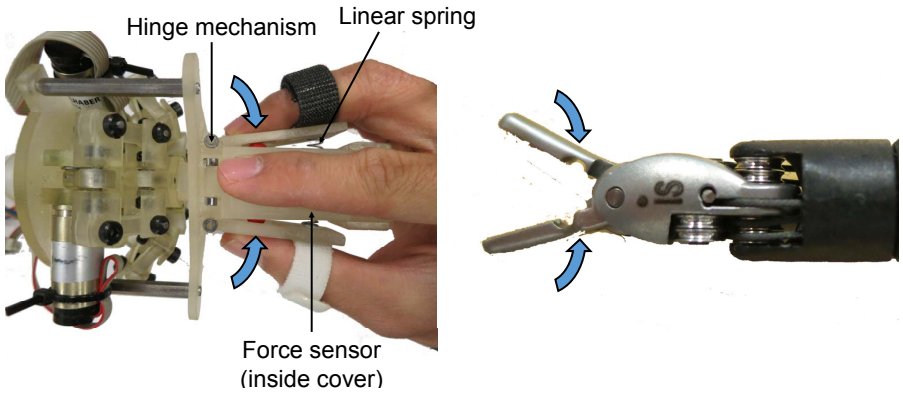

Figure 5.4: Control of the gripper on the patient side manipulator using the hinge mechanism, linear springs, and force sensor in the aperture housing of the skin deformation tactile device.

calculated from the gripping force as

$$\theta_{\text{grip}} = \theta_{\text{open}} - k_{\text{grip}}(||\vec{F}_{\text{gripforce}}||_2 - F_{\text{deadband}}), \tag{5.7}$$

where θ_{open} is the default grip angle in the open configuration, k is the grip force to grip angle ratio, $||\vec{F}_{\text{gripforce}}||_2$ is the magnitude of the grip force measured by the grip force sensor, and F_{deadband} is the minimum amount of grip force that the user has to exert before the gripper starts closing. This minimum amount of grip force is necessary so that users will not close the gripper unintentionally during movement of the master manipulator. An illustration of the grip control is shown if Fig. 5.4.

5.2 User Study Design

5.2.1 Experimental Tasks

We performed a study using within-subject experimental design in which subjects performed tasks using each of the four different feedback conditions:

- ***Visual feedback only***. Participants performed the task using only the 3D stereoscopic video feed through the da Vinci vision console.
- ***Visual with force feedback***. Participants performed the task using the 3D stereoscopic video feed through the da Vinci vision console, and force feedback provided through the da Vinci master tool manipulator
- ***Visual with skin deformation feedback***. Participants performed the task using the 3D stereoscopic video feed through the da Vinci vision console, and skin deformation feedback provided through the tactile device.
- ***Visual with force and skin deformation feedback***. Participants performed the task using the 3D stereoscopic video feed through the da Vinci vision console, force feedback provided through the da Vinci master tool manipulator, and skin deformation feedback provided through the tactile device.

Using each of the four different feedback conditions, participants performed the following three manipulation tasks described below:

- ***Peg transfer***. The pegboard, shown in Fig. 5.5(a), consists of three poles. Participants had to move a circular wooden peg from the left pole, to the middle pole, to the right pole, and back to the left pole. During the execution of

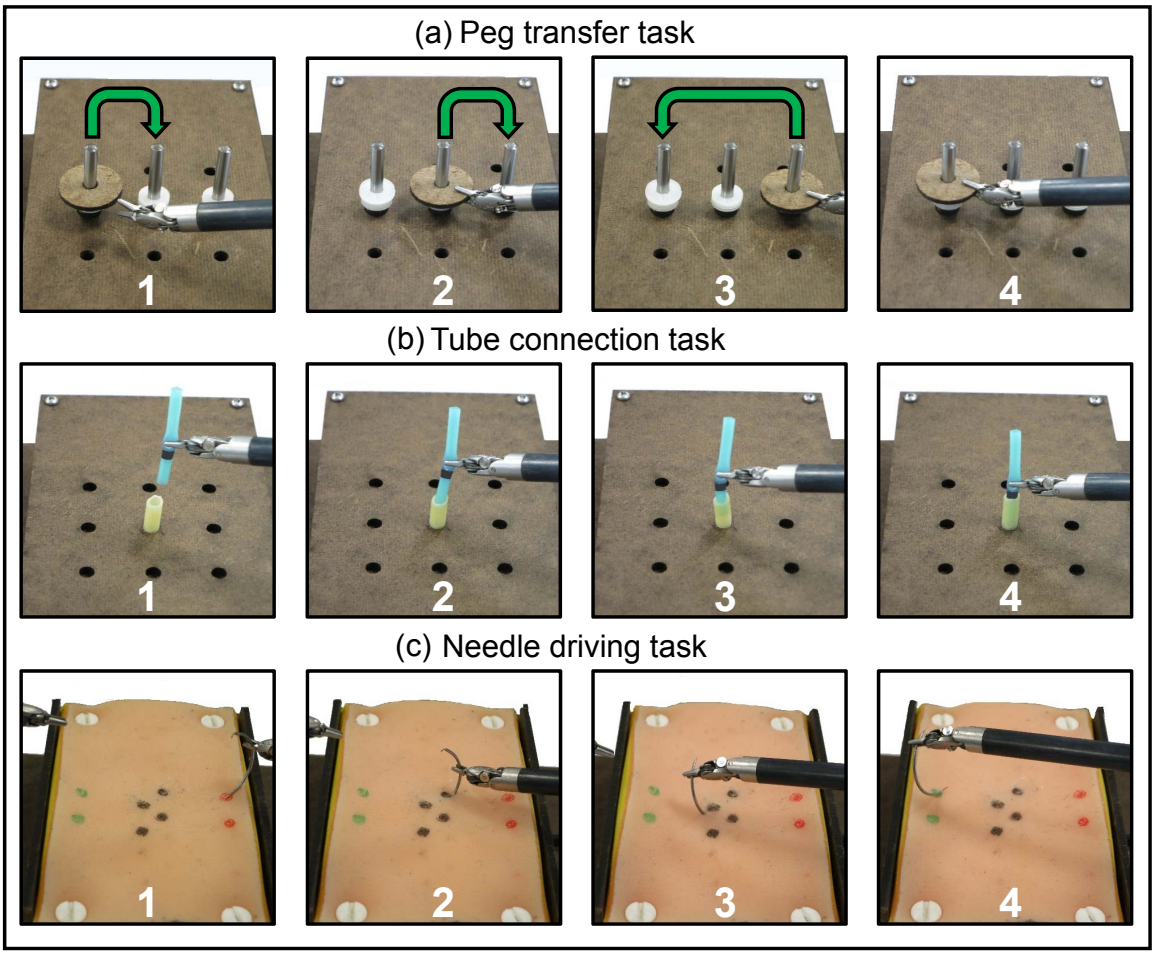

Figure 5.5: Step-by-step illustrations of the three manipulation tasks that participants performed for the study. In the peg transfer task (a), participants shift the circular disk from the left pole, to the middle pole, to the right pole, and back to the left pole. In the tube connection task (b), participants connect the green tube to the yellow tube until the black marking on the green tube touches the tip of the yellow tube. In the needle driving task (c), participants drive and retract the needle through the artificial tissue.

this task, they will be maintaining the grip on the wooden peg. This task is motivated by the Fundamental of Laparoscopic Surgery manual skills test.

- ***Tube connection***. In this task, shown in Fig. 5.5(b), participants have to connect two soft flexible plastic tube together. The tube with the larger diameter is fixed onto the operating platform, while participants manipulate the tube with the smaller diameter and insert it into the larger tube. Participants have to insert the smaller tube until a specific point marked on the tube. This task is motivated by a similar task performed by Wagner et al.[82].

- ***Needle driving***. In this task, shown in Fig. 5.5(c), participants have to drive the needle through specific marked targets on a skin pad (Limbs & Things: Professional Skin Pad Mk 2), and retract the needle out. The needle driving task is selected because of its clinical relevance.

In all of the above tasks, participants performed the manipulation task using only the right master tool manipulator. This is to ensure that any interaction force measured by the force sensor and fed back to the user is due to interaction through the right master tool manipulator. The left master tool manipulator, together with the left patient side manipulator, are stow aside for the peg transfer and the tube connection experiment. For the needle driving experiment, participants uses the left master and patient side manipulator for the initial positioning of the needle. An 8 mm diameter large needle driver were used as the tool on the patient side manipulator.

5.2.2 Experimental Procedure

Participants are first asked to sign a form for their approval to participate in the experiment. They then sit in front of the master console, in which they were briefed by the experimenter on the general experimental procedure, and how to control the da Vinci robots using the master tool manipulators. Participants then performed the experimental task of either the peg transfer task, the cannulus insertion task, or the needle driving task. At the start of each task, the experimenter gives an illustration on how to perform the task. They were instructed to perform the task

Table 5.1: Survey questions presented to the participants at the end of the experiment

	Question	Rating Continuum
1	How would you rate your situational awareness under the different types of feedback?	Not aware - Very aware
2	How consistent is the different types of feedback with your everyday experience?	Not consistent - Very consistent
3	How well do you think you can concentrate under the different types of feedback?	Not well - Very well
4	How well do you think you had performed under the different types of feedback?	Not well - Very well

with minimal interaction force and trial time, but they were to place priority in lowering the interaction force. Participants were given a practice session of three to five minutes, and were permitted to practice longer if requested. After the practice session, participants performed the actual experiment.

In the actual experiment, participants performed a total of 20 trials (5 trials for each of the four feedback types). The feedback types were presented to the participants in a pseudo-random order. Participants are not aware of the feedback type prior to the start of each trial. Throughout the experiment, participants were allowed to rest at the start of each trial. The entire experiment (for each of the three tasks) took around 0.5 hours to complete.

5.2.3 Performance Metrics

Participant's interaction information was recorded at 1 kHz. We used the following metrics to evaluate participants' performance for each of the manipulation tasks:

- ***Mean force magnitude*** that participants exert during the performance of the task

$$F_{\text{mean}} = \frac{1}{N}\sum_{n=1}^{N} |\vec{F}[n]|_2, \tag{5.8}$$

where N is the number of data points recorded for the path, $\vec{F}[n]$ is the interaction force at sample n, and $|.|_2$ is the l^2-norm.

- ***Peak force magnitude*** that participants exert during the performance of the task

$$F_{\text{peak}} = \max_n |\vec{F}[n]|_2, \tag{5.9}$$

- ***Task completion time*** was calculated as the time to complete the task

Besides objective performance metric, we also performed a subjective post-experiment survey in which participants rate the different feedback conditions. The perceived benefit of the different feedback conditions was measured on a 7-degree Likert scale as the answer to the question presented in Table. 5.1.

5.2.4 Data Analysis

We performed a one-way ANOVA with repeated measures using the above performance metrics as dependent variables and feedback types as independent variables. Whenever the feedback effect was significant, we performed post-hoc comparisons between the different combinations of feedback types. Statistical analysis was performed using the MATLAB `fitrm` and `ranovan` functions. For the post-experiment survey results, we used the Wilcoxon signed-rank test to compare between the different combinations of feedback types. This test is performed using the MATLAB `signrank` function. Statistical significance was determined at the 0.05 level, with the appropriate Bonferroni correction for multiple comparisons.

5.2.5 Participants

A total of 10 participants (6 males and 4 females) aged between 22 and 32 performed the peg transfer task, 10 participants (8 males and 2 females) aged between 22 and 33 performed the tube connection task, while 3 surgeon participants (2 males and 1 female) age between 35 and 54, with 7 and above years of experience with the clinical da Vinci system, performed the needle driving task. Surgeons only participated in

the needle driving task, as the task turned out to be too challenging for novice users to perform. All participants gave informed consent. The experimental protocol was approved by the Stanford University Institutional Review Board.

5.3 Results

5.3.1 Peg transfer task

Fig. 5.6 shows the results for the peg transfer task. There is a reduction in the mean applied force, peak applied force, and sum of squared force when force feedback, skin deformation feedback, or the combined feedback are added, as shown in Fig. 5.6a, b, and c. The combined feedback case also performs better in the mean applied force, peak applied force, and sum of squared force then either the force feedback or the skin deformation feedback case. There is no difference in the trial time performance for the

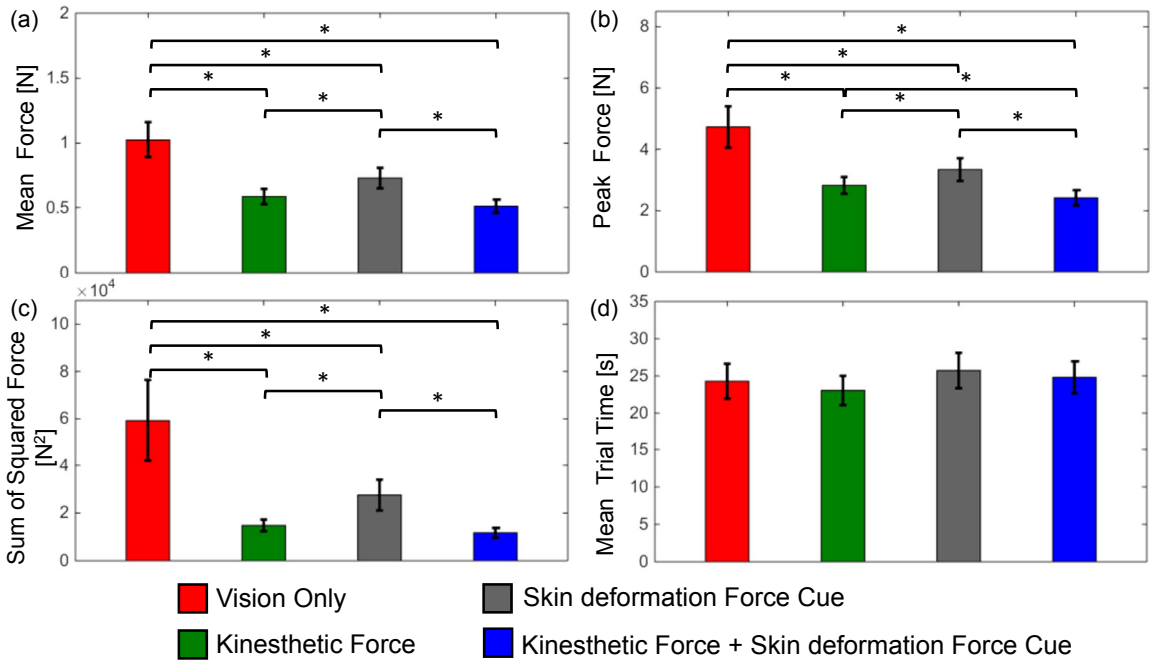

Figure 5.6: Mean and 95% confidence interval for the (a) mean force, (b) peak force, (c) sum of square force, and (d) trial time for the peg transfer experiment. The asterisk (*) indicate statistical significance at the 0.05 level.

different feedback types. ANOVA analysis on mean applied force shows a statistically significant effect of force feedback ($F_{1,9} = 36.2, p < 0.001$), skin deformation feedback ($F_{1,9} = 35.0, p < 0.001$), and the combined feedback ($F_{1,9} = 6.1, p = 0.036$). ANOVA analysis on peak applied force shows a statistically significant effect of force feedback ($F_{1,9} = 19.4, p = 0.002$), skin deformation feedback ($F_{1,9} = 26.8, p < 0.001$), and the combined feedback ($F_{1,9} = 5.7, p = 0.041$), and ANOVA analysis on sum of squared force shows a statistically significant effect of force feedback ($F_{1,9} = 36.8, p < 0.001$), skin deformation feedback ($F_{1,9} = 29.0, p < 0.001$), and the combined feedback ($F_{1,9} = 8.1, p = 0.019$).

Fig. 5.7a, b, c, and d shows the result to the post-experiment survey for the peg transfer task. The presence of force, skin deformation, and combined feedback increases participants' situational awareness of the environment. Participants felt that the addition of force or skin deformation feedback is more consistent with

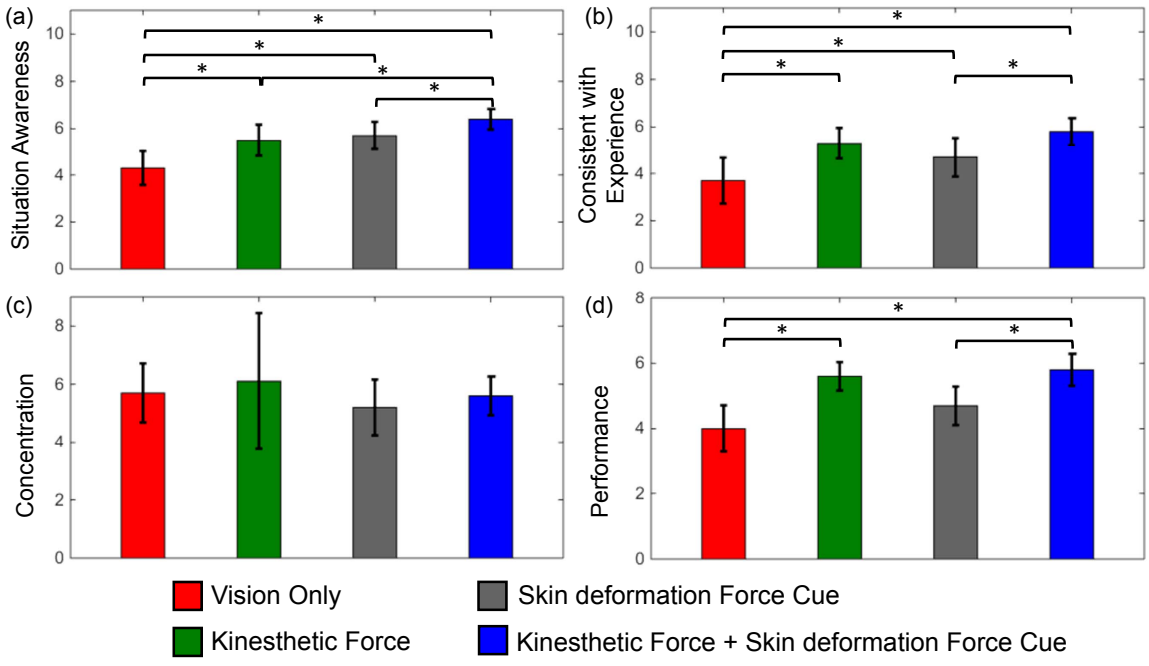

Figure 5.7: Mean and 95% confidence interval for the post-experiment survey (a) situational awareness, (b) consistency with experience, (c) concentration, and (d) performance for the peg transfer experiment. The asterisk (*) indicate statistical significance at the 0.05 level.

their interaction experience, while the combined force and skin deformation feedback did not improve the consistency any further. In terms of performance perception, participants felt that only force feedback improves task performance. The presence of skin deformation feedback, or the addition of skin deformation feedback to force feedback did not affect the perception of task performance by the participants. Participants also answered that the addition of force and/or skin deformation feedback did not affect their concentration on the task. ANOVA analysis on the situational awareness ranking shows a statistically significant effect of force feedback ($F_{1,9} = 30.0, p < 0.001$), skin deformation feedback ($F_{1,9} = 30.0, p < 0.001$), and the combined feedback ($F_{1,9} = 7.36, p = 0.024$). ANOVA analysis on the consistency ranking shows a statistically significant effect of force feedback ($F_{1,9} = 18.8, p = 0.002$) and skin deformation feedback ($F_{1,9} = 6.0, p = 0.037$), while ANOVA analysis on performance perception ranking shows a statistically significant effect of force feedback ($F_{1,9} = 46.5, p < 0.001$).

5.3.2 Tube connection task

Fig. 5.8 shows the performance results for the tube connection task. There is a reduction in the mean applied force, peak applied force, and sum of squared force when force feedback is provided. When skin deformation feedback is provided, there is no statistical difference in the mean applied force, peak applied force, and sum of squared force. The combination of force and skin deformation feedback causes a decrease in the mean applied force, while there is no statistical difference in the peak applied force and sum of squared force. ANOVA analysis on mean applied force shows a statistically significant effect of force feedback ($F_{1,9} = 16.4, p = 0.003$), and the combined feedback ($F_{1,9} = 8.67, p = 0.016$). ANOVA analysis on peak applied force shows a statistically significant effect of force feedback ($F_{1,9} = 11.2, p = 0.009$), and ANOVA analysis on sum of square force shows a statistically significant effect of force feedback ($F_{1,9} = 10.0, p = 0.011$).

Fig. 5.9a, b, c, and d shows the result to the post-experiment survey for the tube

connection task. Similar to the peg-trasnfer task, the presence of force, skin deformation, and combined feedback increases participants' situational awareness of the environment, and they answered that the teleoperation experience with the presence of the different feedback type is more consistent with the their everyday interaction experience. The presence of the different feedback also did not affect their concentration on the task. ANOVA analysis on the situational awareness ranking shows a statistically significant effect of force feedback ($F_{1,9} = 5.5, p = 0.043$), skin deformation feedback ($F_{1,9} = 28.1, p < 0.001$), and the combined feedback ($F_{1,9} = 6.7, p = 0.029$). ANOVA analysis on the consistency ranking shows a statistically significant effect of force feedback ($F_{1,9} = 5.71, p = 0.041$) and skin deformation feedback ($F_{1,9} = 20.5, p = 0.001$), while ANOVA analysis on performance perception ranking shows a statistically significant effect of skin deformation feedback ($F_{1,9} = 19.0, p = 0.002$).

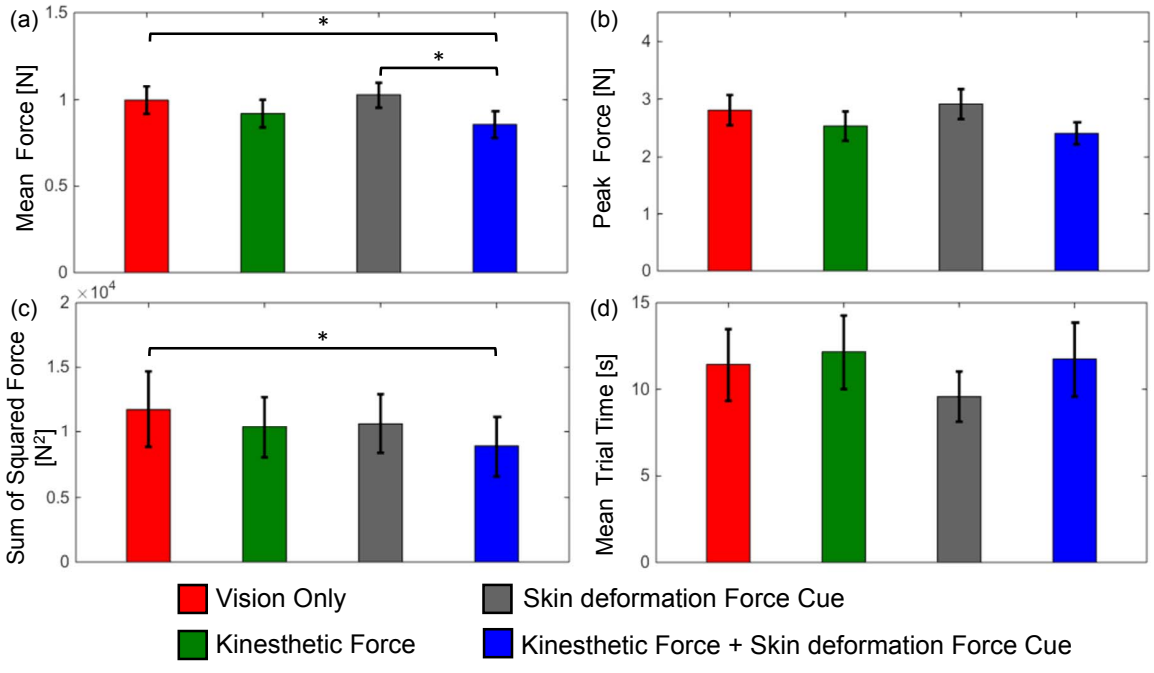

Figure 5.8: Mean and 95% confidence interval for the (a) mean force, (b) peak force, (c) sum of square force, and (d) trial time for the tube connection experiment.

5.3.3 Needle driving task

Fig. 5.10 shows the performance results for the needle driving task, for each of the surgeon participants and the overall mean. There is a reduction in the mean applied force, peak applied force, and sum of squared force when force feedback is provided. There is no change in performance when skin deformation feedback is added. We did not perform a statistical analysis on the performance for the needle driving task due to the small amount of surgeon participants.

Fig. 5.11a, b, c, and d shows the result to the post-experiment survey for the needle driving task, for each of the surgeon participants and the overall mean. The first participant agreed that the feedback increases his/her awareness of what he/she is doing to the tissue, but feels that the feedback is not convincing, distracting, and affected his/her task performance. The second participant feels neutral to the different

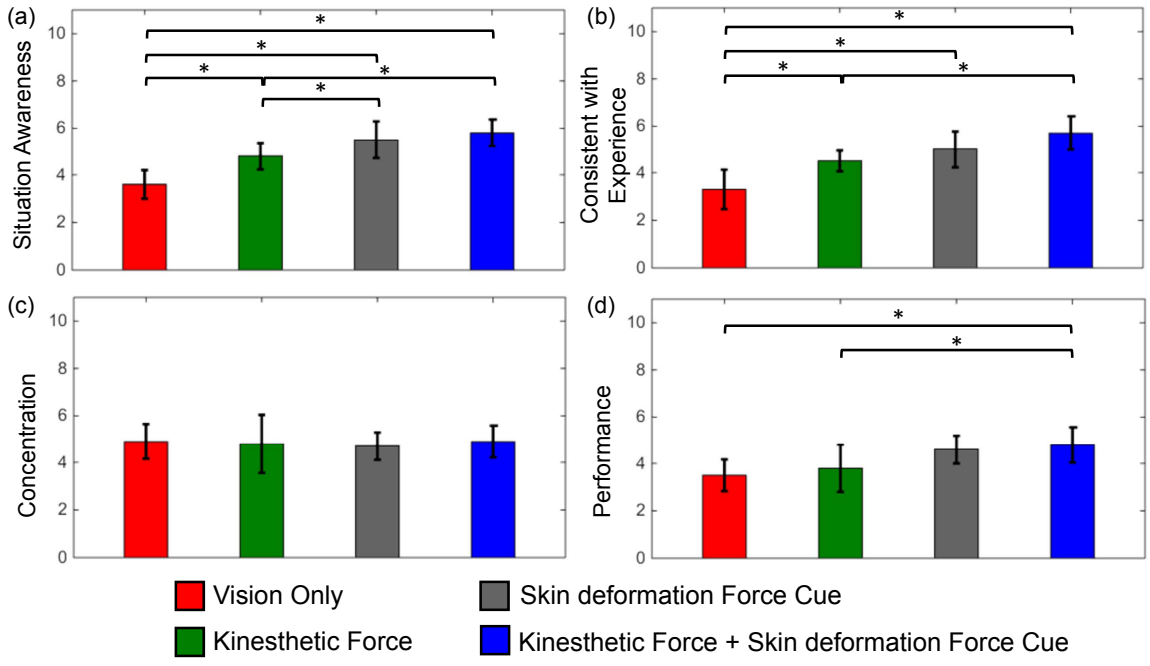

Figure 5.9: Mean and 95% confidence interval for the post-experiment survey (a) situational awareness, (b) consistency with experience, (c) concentration, and (d) performance for the tube connection experiment. The asterisk (*) indicate statistical significance at the 0.05 level.

mode of feedback. The third participant feel that he/she feels equally awareness of the environment, and that the feedback does not affect his/her concentration or performance. However, he/she feels that the feedback felt more consistent with daily interaction experience.

5.4 Discussion

5.4.1 Task dependent performance improvement for skin deformation feedback

From the experiment results, we saw that force feedback improves the mean force, peak force, and sum of squared force performance metric across the three tasks,

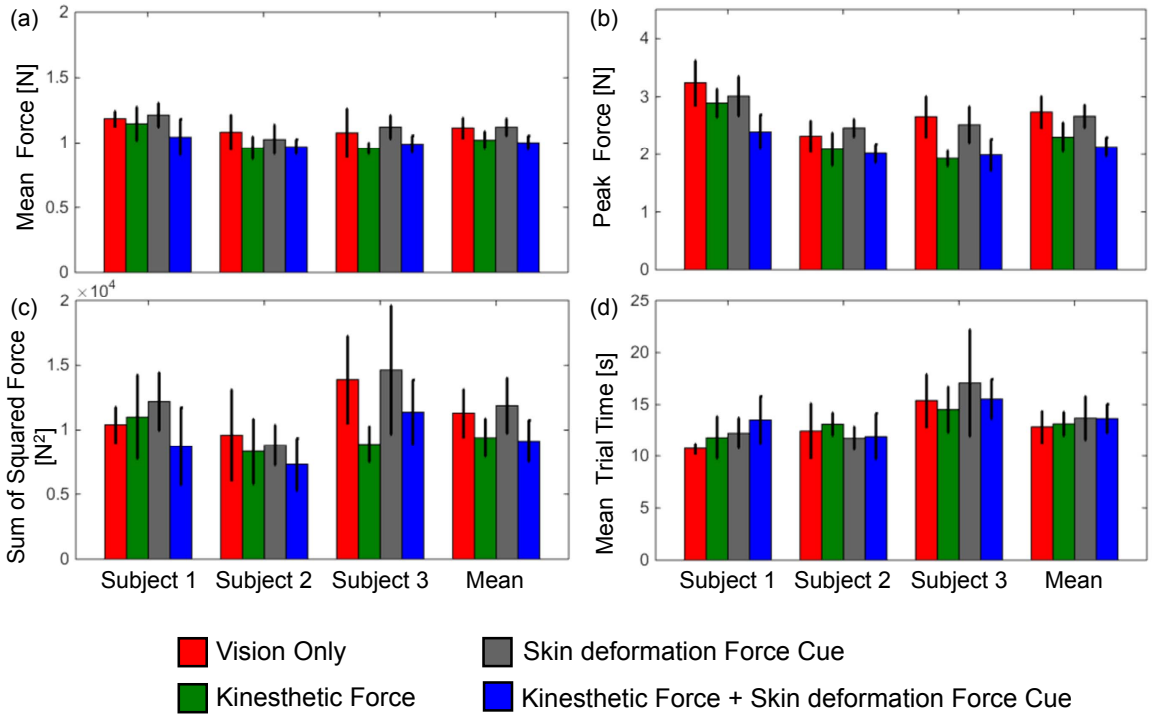

Figure 5.10: Mean and 95% confidence interval for the (a) mean force, (b) peak force, (c) sum of square force, and (d) trial time for the needle driving experiment, for subjects 1,2,3 and the overall mean.

while skin deformation feedback improves performance for the peg transfer task and maintains performance for the tube connection and needle driving tasks. The reason for this difference can be attributed to the nature of the feedback, and the nature of the task. The nature of the feedback is that force feedback provides interaction force information and physical constraint, while skin deformation feedback only provides information about the interaction force. For both the tube connection and needle driving task, a minimum amount of interaction forces are needed to overcome the friction between the tubes during insertion, and to drive the needle through the artificial tissue. Participants are unable to use the force information provided by either force feedback or skin deformation feedback to adjust their motion to improve task performance, but the physical constraint provided by force feedback passively prevents the participants from exerting large interaction forces.

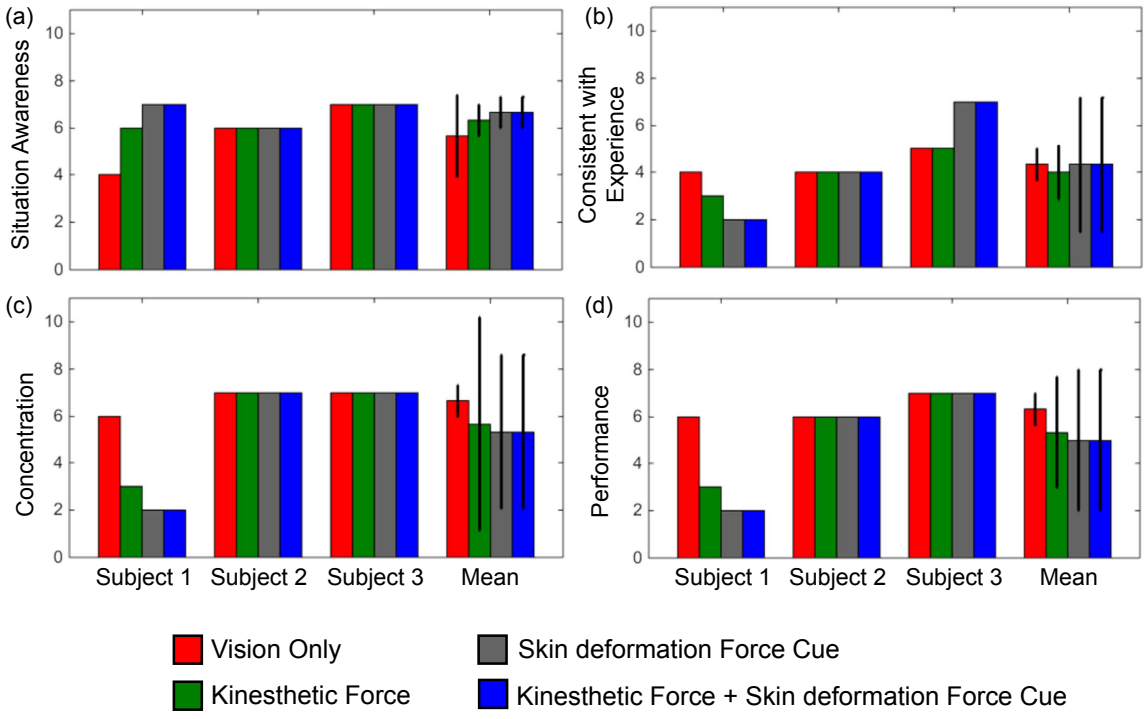

Figure 5.11: Mean and 95% confidence interval for the post-experiment survey (a) situational awareness, (b) consistency with experience, (c) concentration, and (d) performance for the needle driving experiment, for subjects 1,2,3 and the overall mean.

For the peg transfer task, however, participants do not have to exert a minimum amount of interaction forces to complete the task. When properly executed, participants should exert zero interaction forces. For this task, participants are able to use the force information provided by force feedback or skin deformation feedback to actively adjust their motion to reduce interaction forces, while the physical constraint provided by force feedback further prevent the participants from exerting large forces.

The above explanation is further strengthened by the observation that the improvement in task performance by force feedback is higher for the peg transfer task than for the tube connection and needle driving task.

5.4.2 Skin deformation feedback improves situational awareness

Our experiment results showed that force feedback provides better situational awareness for the peg transfer task than for the needle driving task. This observation can be explained by the environment impedance for each task. The peg transfer task involves interaction between rigid bodies, while the tube connection and needle driving task involves interaction between soft, deformable bodies. The impedance of the environment is therefore larger for the peg transfer task compared to the tube connection and needle driving task. Therefore, with force feedback, contact with the environment for the peg transfer task will induce larger forces that is more perceptible than that for the tube connection and needle driving task.

For skin deformation feedback, however, we do not observe this difference. This can be attributed to the reason that skin deformation cues, even with small displacement and at slow speed [20], is perceptible to the participants.

The issue of situational awareness provided by force or skin deformation feedback will be of more importance when the motion and force scaling between the master and patient side manipulator decreases. With a smaller scale factor, the forces sensed at the patient side robot are scaled down further to maintain stability of the teleoperation system before it is displayed on the master manipulator. Forces displayed

at the master manipulator will be less perceptible, decreasing the situational awareness that the feedback provides. For skin deformation feedback, since the feedback does not affect the stability of the system, the skin deformation-to-force ratio can be increased to maintain the perceptibility of the cue and maintain the situational awareness benefits provided by the feedback.

5.4.3 Benefits of combined feedback

Our experiment results showed that with the combined force and skin deformation feedback, participants achieved task performance that is better than or equal to the performance with individual feedback alone. In addition, the combined feedback also obtained equal or better participants rating (situational awareness, consistency with experience, and performance perception) than either force or skin deformation feedback. With combined feedback, force feedback provides the physical constraint and force information, while skin deformation feedback provides additional information to augment the information provided by force feedback. Augmenting force feedback with skin deformation feedback is therefore a good way to improve the transparency while maintaining the stability of the teleoperation system.

5.4.4 Divided opinions among expert and novice users

Our results showed that there are divided opinions among expert and novice users about the different feedback types. Particularly, we saw that two of the surgeon participants were neutral about how the feedback improves their situational awareness, concentration, and performance. On the other hand, many of the novice users felt increased situational awareness and think that the feedback improves their performance. We think that these differences can be attributed to the reason that the surgeons had been trained to operate the da Vinci console and perform surgery tasks using visual only feedback. During the post-experiment questioning with the surgeons, all three of the surgeons replied that they were only concentrating on the vision system and did not pay attention to the force or tactile feedback provided.

5.5 Conclusions

We integrated a 3-DoF skin deformation tactile device with a surgical teleoperation system and performed a study in which participants performed surgically related tasks with visual, force, skin deformation, and combined force and skin deformation feedback. Results showed that participants are able to utilize the feedback for improved task performance, although the benefit of the feedback depends on the nature of the task. Participants also feel that the additional feedback made them more aware of what they are doing to their environment, that the feedback make the interaction feels more natural, and that the feedback improve their task performance. The combined force and skin deformation feedback also achieved better performance and higher participants' rating compared to the individual force or skin deformation feedback. We also found that novice users of the system generally preferred the feedback, either in the form of force feedback, skin deformation, or combined force and skin deformation feedback, whereas expert users did not.

Chapter 6

Conclusions and Future Work

This dissertation presents the design, implementation, and experimental human-user validation of a class of tactile haptic devices that provides skin deformation to the user's fingerpad skin. This chapter summarizes the results obtained from Chapters 2, 3, 4, and 5, reviews the contributions made in this dissertation, and provides suggestions for extension and improvement to this work.

6.1 Summary of Results

The most significant results from this research are that tactile skin deformation are linked to the human perception of force/stiffness, and that tactile skin deformation feedback can be used for effective sensory substitution and augmentation of force feedback. We showed that skin deformation can be used in conjunction with force feedback to improve the perception of stiffness of surfaces. In addition, when skin deformation feedback is used to substitute force feedback to perform manipulation tasks in both virtual and teleoperated scenarios, there is no degradation in performance, and in some of the tasks, there is an improvement in performance compared to the case when no feedback is provided. We also observed a similar performance improvement when skin deformation feedback was used to augment force feedback in these manipulation tasks. Many of the participants had little to no experience with skin deformation feedback prior to the experiments. Altogether, these results showed

that skin deformation feedback is an intuitive form of tactile feedback which can be used for sensory substitution and augmentation of kinesthetic force and/or torque feedback.

6.2 Review of Contributions

The major contributions of this thesis are:

- Investigation and modeling of the effect of skin stretch feedback on the perception of stiffness. In Chapter 2, human participants performed psychophysical experiments to better understand the effect of augmenting force feedback with tangential skin stretch feedback on the perception of stiffness of virtual surfaces. Experiments showed that participants felt an increase in perceived stiffness of the virtual surface when tangential skin stretch feedback is added in the direction of force feedback. However, there is no consistent effect of augmentation when the tangential skin stretch is added opposite to the direction of force feedback. A model was proposed to explain the effect of tangential skin stretch on the perception of stiffness. The model, which showed that there is a linear effect of skin stretch gain on stiffness perception, was verified through psychophysical experiments.

- Design and evaluation of a 3-Degree-of-Freedom (DoF) fingerpad skin deformation tactile device for sensory substitution and augmentation of force feedback. In Chapter 3, we designed and built a tactile device that is able to provide 3-DoF tangential skin stretch and normal skin deformation tactile feedback to the user's fingerpad. An experiment involving human participants showed that participants are able to use the 3-DoF force information provided by the tactile feedback to improve task performance when used as a sensory substitute for force feedback, or when paired with force feedback for augmentation of force feedback.

- Design and evaluation of a 6-Degree-of-Freedom (DoF) fingerpad skin deformation tactile device for sensory substitution and augmentation of force and torque feedback. In Chapter 4, we designed and built a tactile device that is able to provide 6-DoF tangential skin stretch and normal skin deformation tactile feedback for sensory substitution and augmentation of force and/or torque feedback. Human participants experiment showed that participants can interpret the skin deformation force or torque cues when each is rendered separately. When both force and torque cues are rendered together, participants experienced confusion over the cues, due partially to an increase in the rate of saturation of the tactile device, resulting in a decrease in cue interpretability and hence a degradation in task performance. When we augment force and torque information with skin deformation feedback, participants are able to combine the kinesthetic force and skin deformation force cues for improved force-related task performance. No such effect was observed for torque and torque related task performance.

- Integration of skin deformation tactile device with a teleoperation system. In Chapter 5, we integrated the 3-DoF skin deformation tactile feedback device with a teleoperation system. We performed human subjects experiment to investigate the usefulness of the skin deformation tactile feedback for teleoperation of surgically related tasks. Results showed that participants are able to utilize the tactile feedback to maintain or improve task performance. The improvement in task performance depended on the nature of the task. The tactile feedback also increases the situation awareness, and feels more natural than manipulation with only visual feedback. Results also showed that with the combined force and tactile feedback , participants are able to achieve the best task performance. Participants also preferred the combined feedback over either force or skin deformation feedback alone.

6.3 Future Work

6.3.1 Improvements in Device Design

The benefits of tactile devices lie in their ability to be compact, lightweight, and wearable. These devices can be used together with a 3D virtual reality headset, or the da Vinci master console, to create an immersive virtual reality or telepresence experience for the user. However, the current tactile devices developed and used in this thesis are add-on to existing kinesthetic force-feedback devices such as the Force Dimension Omega-3 and the master manipulator of the da Vinci research kit. These tactile devices are currently too heavy, and they lack the sensors to be used as an independent wearable tactile haptic device. As most of the weight of the devices lies in the actuators, future improvement to reduce the weight of the device can look into replacing the RC-servos or DC-motors with piezoelectric motors. These motors are lightweight, have small motion scale and are able to exert large forces/torques. These motors are therefore ideal candidates for use in our skin deformation tactile device, which requires small end-effector motion and requires large forces to deform the users' fingerpad skin.

In the design and evaluation of the 6-DoF skin deformation tactile device, we found that participants experienced confusion when both force and torque skin deformation tactile cues are rendered together. This confusion is due to the coupling of the skin deformation force and torque cues, resulting in increased device saturation and decreased interpret-ability of the cues. To solve this issue, Guinan et al. [23] had designed a tangential skin stretch device which stretches the user's palm to provide realistic rotational inertia sensation in gaming applications. Future iteration of the skin deformation tactile device can therefore decouple the rendering of force and torque cues, by rendering forces and torque cues on separate location of the hand, such as the user's fingerpad and palm.

6.3.2 Comparing with Other Sensory Substitution Methods

In this thesis, we explored how people are able to make use of the skin deformation tactile cues to improve their task performance in virtual or teleoperated tasks. An important question of whether skin deformation is better than other sensory substitution method such as visual, audio, or vibrotactile feedback remains. Schorr et al. [70] performed a preliminary comparison between the different sensory substitution methods including skin stretch. Their task, however, involves only palpation of tissue, which is a subset of the spectrum of possible tasks that can be done in teleoperation. Future work can look into the comparison of the different sensory substitution method for a wide range of tasks. It will also be interesting to look into the learning curve behind each of the different sensory substitution methods, i.e., the amount of time that users took to achieve a certain competency in using the different sensory substitution methods.

6.3.3 Expanding the Use of Skin Deformation Tactile Feedback

The usefulness of skin deformation tactile feedback lies in its ability to provide information to the user via the cutaneous haptic channel, independent of kinesthetic force and/or torque feedback. While we primary utilizes the skin deformation tactile feedback for sensory substitution and augmentation of force and/or torque feedback in this thesis, skin deformation tactile feedback can be used to provide other types of information to the user. An interesting use of skin deformation tactile feedback is to provide guidance information to the user in telemanipulation task, as shown in a preliminary work done in a virtual environment by Schorr et al. [69]. The coupling of environmental forces and guidance forces in a teleoperation system can caused confusion among users of the teleoperation system. The ability for skin deformation tactile feedback to provide both direction and magnitude information makes it an ideal candidate to provide guidance information, while retaining the ability for users to interact and experience environmental forces through kinesthetic force feedback.

The feedback types can also be switched around, in which environment force information are feedback to the user through tactile skin deformation, while guidance are provided using kinesthetic force/torque feedback.

Appendix A

Kinematics Calculation of Mechanisms

The 3-Degree-of-Freedom and 6-Degree-of-Freedom skin deformation tactile device presented in Chapter 3 and Chapter 4 were designed based upon the Delta and the Hunt-Type 6-Rotational-Universal-Spherical parallel mechanism. In this appendix, the forward kinematics, inverse kinematics, and the jacobian calculation for the two mechanisms are derived.

A.1 Kinematics of Delta Parallel Kinematic Mechanism

A.1.1 Forward Kinematics

As illustrated in the Fig. A.1, let l_{base} be the distance from the center of the base to each of the connection point F_i, $i = 1, 2, 3$. Then, the vectors OF_1, OF_2, and OF_3

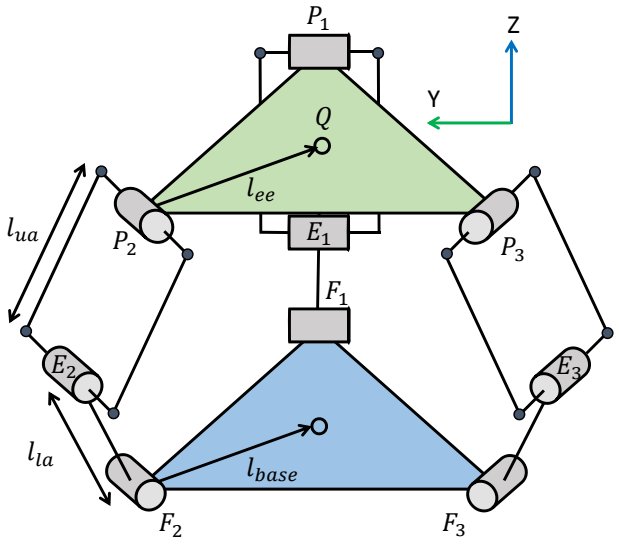

Figure A.1: Kinematic diagram for the Delta mechanism.

are given by

$$\vec{OF}_1 = \begin{bmatrix} l_{base} \\ 0 \\ 0 \end{bmatrix}, \quad \vec{OF}_2 = R_z\left(\frac{2\pi}{3}\right)\begin{bmatrix} l_{base} \\ 0 \\ 0 \end{bmatrix}, \quad \vec{OF}_3 = R_z\left(\frac{4\pi}{3}\right)\begin{bmatrix} l_{base} \\ 0 \\ 0 \end{bmatrix}, \quad \text{(A.1)}$$

where $R_z(\theta)$ is the rotation matrix generated by a rotation about the z axis by an angle of θ radian.

Let θ_1, θ_2, and θ_3 be the joint angles at the base, and let l_la be the length of the lower arm of the delta mechanism. Then, the vector F_i, E_i, $i = 1, 2, 3$, where E_i are the i^{th} elbow locations, are given by

$$\vec{F_1E_1} = \begin{bmatrix} l_{la}cos(\theta_1) \\ 0 \\ l_{la}sin(\theta_1) \end{bmatrix}, \quad \vec{F_2E_2} = R_z\left(\frac{2\pi}{3}\right)\begin{bmatrix} l_{la}cos(\theta_2) \\ 0 \\ l_{la}sin(\theta_2) \end{bmatrix}, \quad \vec{F_3E_3} = R_z\left(\frac{4\pi}{3}\right)\begin{bmatrix} l_{la}cos(\theta_3) \\ 0 \\ l_{la}sin(\theta_3) \end{bmatrix}, \quad \text{(A.2)}$$

Therefore, the vectors $\vec{OE_i}$, $i = 1, 2, 3$ are given by

$$\vec{OE_1} = \begin{bmatrix} l_{base} + l_{la}cos(\theta_1) \\ 0 \\ l_{la}sin(\theta_1) \end{bmatrix}, \tag{A.3}$$

$$\vec{OE_2} = R_z\left(\frac{2\pi}{3}\right) \begin{bmatrix} l_{base} + l_{la}cos(\theta_2) \\ 0 \\ l_{la}sin(\theta_2) \end{bmatrix}, \tag{A.4}$$

$$\vec{OE_3} = R_z\left(\frac{4\pi}{3}\right) \begin{bmatrix} l_{base} + l_{la}cos(\theta_3) \\ 0 \\ l_{la}sin(\theta_3) \end{bmatrix}, \tag{A.5}$$

Due to the joint mechanism, the locus of the end effector connection point P_i forms a sphere around the elbow point $E_i, i = 1, 2, 3$. In order to the determine the position of the end effector center point Q, we translate E_i to E_i', by the amount equal to the translation from P_i to Q. The connection point at the end effector P_i will also be shifted to the point P_i'. The intersection of the three locus will be the end effector center point Q.

Let l_{ee} be the distance from the center of the end effector point Q to the various connection point $P_i, i = 1, 2, 3$. Then,

$$\vec{P_1Q} = \begin{bmatrix} -l_{ee} \\ 0 \\ 0 \end{bmatrix}, \ \vec{P_2Q} = R_z\left(\frac{2\pi}{3}\right) \begin{bmatrix} -l_{ee} \\ 0 \\ 0 \end{bmatrix}, \ \vec{P_3Q} = R_z\left(\frac{4\pi}{3}\right) \begin{bmatrix} -l_{ee} \\ 0 \\ 0 \end{bmatrix}, \tag{A.6}$$

Therefore,

$$\vec{E_1E_1'} = \vec{P_1Q} = \begin{bmatrix} -l_{ee} \\ 0 \\ 0 \end{bmatrix}, \tag{A.7}$$

$$\vec{E_2E_2'} = \vec{P_2Q} = R_z\left(\frac{2\pi}{3}\right) \begin{bmatrix} -l_{ee} \\ 0 \\ 0 \end{bmatrix}, \tag{A.8}$$

$$\vec{E_3E_3'} = \vec{P_3Q} = R_z\left(\frac{4\pi}{3}\right) \begin{bmatrix} -l_{ee} \\ 0 \\ 0 \end{bmatrix}, \tag{A.9}$$

Therefore

$$\vec{OE_1'} = \begin{bmatrix} l_{base} + l_{la}cos(\theta_1) - l_{ee} \\ 0 \\ l_{la}sin(\theta_1) \end{bmatrix}, \tag{A.10}$$

$$\vec{OE_2'} = R_z\left(\frac{2\pi}{3}\right) \begin{bmatrix} l_{base} + l_{la}cos(\theta_1) - l_{ee} \\ 0 \\ l_{la}sin(\theta_2) \end{bmatrix}, \tag{A.11}$$

$$\vec{OE_3'} = R_z\left(\frac{4\pi}{3}\right) \begin{bmatrix} l_{base} + l_{la}cos(\theta_1) - l_{ee} \\ 0 \\ l_{la}sin(\theta_3) \end{bmatrix}, \tag{A.12}$$

Let l_ua be the length of the upper arm of the delta mechanism. Then, in order to determine the center of the end effector Q, the following systems of equations need

to be solved:

$$(x_Q - x_1)^2 + (y_Q - y_1)^2 + (z_Q - z_1)^2 = (l_{ua})^2, \tag{A.13}$$
$$(x_Q - x_2)^2 + (y_Q - y_2)^2 + (z_Q - z_2)^2 = (l_{ua})^2, \tag{A.14}$$
$$(x_Q - x_3)^2 + (y_Q - y_3)^2 + (z_Q - z_3)^2 = (l_{ua})^2, \tag{A.15}$$

Expanding, we get

$$x_Q^2 + y_Q^2 + z_Q^2 - 2x_1x_Q - 2y_1y_Q - 2z_1z_Q + x_1^2 + y_1^2 + z_1^2 = l_{ua}^2, \tag{A.16}$$
$$x_Q^2 + y_Q^2 + z_Q^2 - 2x_2x_Q - 2y_2y_Q - 2z_2z_Q + x_2^2 + y_2^2 + z_2^2 = l_{ua}^2, \tag{A.17}$$
$$x_Q^2 + y_Q^2 + z_Q^2 - 2x_3x_Q - 2y_3y_Q - 2z_3z_Q + x_3^2 + y_3^2 + z_3^2 = l_{ua}^2, \tag{A.18}$$

From A.16 - A.17:

$$2x_Q(x_2 - x_1) + 2y_Q(y_2 - y_1) + 2z_Q(z_2 - z_1) = (x_2^2 + y_2^2 + z_2^2 - x_1^2 - y_1^2 - z_1^2), \tag{A.19}$$

From A.17 - A.18:

$$2x_Q(x_3 - x_2) + 2y_Q(y_3 - y_2) + 2z_Q(z_3 - z_2) = (x_3^2 + y_3^2 + z_3^2 - x_2^2 - y_2^2 - z_2^2), \tag{A.20}$$

From A.18 - A.16:

$$2x_Q(x_1 - x_3) + 2y_Q(y_1 - y_3) + 2z_Q(z_1 - z_3) = (x_1^2 + y_1^2 + z_1^2 - x_3^2 - y_3^2 - z_3^2), \tag{A.21}$$

Let

$$w_1 = x_1^2 + y_1^2 + z_1^2, \tag{A.22}$$
$$w_2 = x_2^2 + y_2^2 + z_2^2, \tag{A.23}$$
$$w_3 = x_3^2 + y_3^2 + z_3^2, \tag{A.24}$$

Then,

$$2x_Q(x_2 - x_1) + 2y_Q(x_2 - x_1) + 2z_Q(x_2 - x_1) = w_2 - w_1, \tag{A.25}$$
$$2x_Q(x_3 - x_2) + 2y_Q(x_3 - x_2) + 2z_Q(x_3 - x_2) = w_3 - w_2, \tag{A.26}$$
$$2x_Q(x_1 - x_3) + 2y_Q(x_1 - x_3) + 2z_Q(x_1 - x_3) = w_1 - w_3, \tag{A.27}$$

From A.28 and A.29, we get that

$$2x_Q(x_2 - x_1)(y_1 - y_3) + 2y_Q(y_2 - y_1)(y_1 - y_3) + 2z_Q(z_2 - z_1)(y_1 - y_3) = (w_2 - w_1)(y_1 - y_3), \tag{A.28}$$
$$2x_Q(x_1 - x_3)(y_2 - y_1) + 2y_Q(y_1 - y_3)(y_2 - y_1) + 2z_Q(z_1 - z_3)(y_2 - y_1) = (w_1 - w_3)(y_2 - y_1), \tag{A.29}$$

And

$$x_Q(2(x_2 - x_1)(y_1 - y_3) - 2(x_1 - x_3)(y_2 - y_1)) + z_Q(2(z_2 - z_1)(y_1 - y_3) - 2(z_1 - z_3)(y_2 - y_1)) = (w_2 - w_1)(y_1 - y_3) - (w_1 - w_3)(y_2 - y_1), \tag{A.30}$$

in which we can obtain x_Q in terms of z_Q.

Similarly, from A.28 and A.27, we get that

$$2x_Q(x_2 - x_1)(x_1 - x_3) + 2y_Q(y_2 - y_1)(x_1 - x_3) + 2z_Q(z_2 - z_1)(x_1 - x_3) = (w_2 - w_1)(x_1 - x_3), \tag{A.31}$$
$$2x_Q(x_1 - x_3)(x_2 - x_1) + 2y_Q(y_1 - y_3)(x_2 - x_1) + 2z_Q(z_1 - z_3)(x_2 - x_1) = (w_1 - w_3)(x_2 - x_1), \tag{A.32}$$

And

$$y_Q(2(y_2 - y_1)(x_1 - x_3) - 2(y_1 - y_3)(x_2 - x_1)) + z_Q(2(z_2 - z_1)(x_1 - x_3) - 2(z_1 - z_3)(x_2 - x_1)) = (w_2 - w_1)(x_1 - x_3) - (w_1 - w_3)(x_2 - x_1), \tag{A.33}$$

in which we obtained y_Q in terms of z_Q.

Using the above two relations, together with A.16, a quadratic equation in z_Q is obtained, which can be solved to obtained z_Q. From, z_Q, x_Q, and y_Q can be subsequently obtained from the above two relations.

A.1.2 Inverse Kinematics

For the inverse kinematics, we want to find the position of the elbow points $E_i, i = 1, 2, 3$, given the end-effector point Q. Let the end-effector point Q be

$$O\vec{Q}' = \begin{bmatrix} x_Q \\ y_Q \\ z_Q \end{bmatrix}, \tag{A.34}$$

and the location of the 3 elbow points be

$$O\vec{E}_1 = \begin{bmatrix} x_{E_1} \\ y_{E_1} \\ z_{E_1} \end{bmatrix}, \quad O\vec{E}_2 = \begin{bmatrix} x_{E_2} \\ y_{E_2} \\ z_{E_2} \end{bmatrix}, \quad O\vec{E}_3 = \begin{bmatrix} x_{E_3} \\ y_{E_3} \\ z_{E_3} \end{bmatrix}, \tag{A.35}$$

Let l_{ee} be the distance from the center of the end-effector point Q to the various connection point $P_i, i = 1, 2, 3$. Then,

$$P_1\vec{Q} = \begin{bmatrix} -l_{ee} \\ 0 \\ 0 \end{bmatrix}, \quad P_2\vec{Q} = R_z\left(\frac{2\pi}{3}\right)\begin{bmatrix} -l_{ee} \\ 0 \\ 0 \end{bmatrix}, \quad P_3\vec{Q} = R_z\left(\frac{4\pi}{3}\right)\begin{bmatrix} -l_{ee} \\ 0 \\ 0 \end{bmatrix}, \tag{A.36}$$

From the end-effector point Q, we can calculate that

$$\vec{OP_1} = \begin{bmatrix} x_Q \\ y_Q \\ z_Q \end{bmatrix} + \begin{bmatrix} l_{ee} \\ 0 \\ 0 \end{bmatrix} = \begin{bmatrix} x_{P_1} \\ y_{P_1} \\ z_{P_1} \end{bmatrix}, \tag{A.37}$$

$$\vec{OP_2} = \begin{bmatrix} x_Q \\ y_Q \\ z_Q \end{bmatrix} + R_z\left(\frac{2\pi}{3}\right) \begin{bmatrix} l_{ee} \\ 0 \\ 0 \end{bmatrix} = \begin{bmatrix} x_{P_2} \\ y_{P_2} \\ z_{P_2} \end{bmatrix}, \tag{A.38}$$

$$\vec{OP_3} = \begin{bmatrix} x_Q \\ y_Q \\ z_Q \end{bmatrix} + R_z\left(\frac{2\pi}{3}\right) \begin{bmatrix} l_{ee} \\ 0 \\ 0 \end{bmatrix} + R_z\left(\frac{2\pi}{3}\right) \begin{bmatrix} l_{ee} \\ 0 \\ 0 \end{bmatrix} = \begin{bmatrix} x_{P_3} \\ y_{P_3} \\ z_{P_3} \end{bmatrix}, \tag{A.39}$$

Let l_{base} be the distance from the center of the base to each of the connection point $F_i, i = 1, 2, 3$. Then, the vectors $\vec{OF_1}$,$\vec{OF_2}$, and $\vec{OF_3}$ are given by

$$\vec{OF_1} = \begin{bmatrix} l_{base} \\ 0 \\ 0 \end{bmatrix} = \begin{bmatrix} x_{F_1} \\ y_{F_1} \\ z_{F_1} \end{bmatrix}, \tag{A.40}$$

$$\vec{OF_2} = R_z\left(\frac{2\pi}{3}\right) \begin{bmatrix} l_{base} \\ 0 \\ 0 \end{bmatrix} = \begin{bmatrix} x_{F_2} \\ y_{F_2} \\ z_{F_2} \end{bmatrix}, \tag{A.41}$$

$$\vec{OF_3} = R_z\left(\frac{4\pi}{3}\right) \begin{bmatrix} l_{base} \\ 0 \\ 0 \end{bmatrix} = \begin{bmatrix} x_{F_3} \\ y_{F_3} \\ z_{F_3} \end{bmatrix}, \tag{A.42}$$

Then, for each $i, i = 1, 2, 3$, we have

$$(x_{P_i} - x_{E_i})^2 + (y_{P_i} - y_{E_i})^2 + (z_{P_i} - z_{E_i})^2 - l_{ua}^2 = 0, \tag{A.43}$$

$$(x_{E_i} - x_{F_i})^2 + (y_{E_i} - y_{F_i})^2 + (z_{E_i} - z_{F_i})^2 - l_{la}^2 = 0, \tag{A.44}$$

$$G_{0,i} + G_{1,i}x_{P_i} + G_{2,i}y_{P_i} + G_{3,i}z_{P_i} = 0, \tag{A.45}$$

Equation A.43 states that the locus of the elbow point E_i is a sphere of radius l_{ua} around the point P_i, while the equation A.44 states the locus of the elbow point E_i is a sphere of radius l_{ua} around the point F_i. Equation A.45 states that the point E_i lies in a plane containing the base point O and the connection point F_i, and that the plane is perpendicular to the joint axis i. Solving the three equations, we can obtained x_{E_i}, y_{E_i}, and z_{E_i}. The angle of joint i can then be calculated based on the position of OF_i and the elbow point OE_i.

A.1.3 Jacobian Calculation

We have the relation that

$$|E_iP_i|^2 - l_{ua}^2 = 0, i = 1, 2, 3, \tag{A.46}$$

Let s_i denote the vector E_iP_i. Then,

$$s_i^T s_i - l_{ua}^2 = 0, \tag{A.47}$$

The vector s_i is

$$s_i = OP_i - OE_i = R_z\Big(\phi_i\Big) \begin{bmatrix} x_Q \\ y_Q \\ z_Q \end{bmatrix} + \begin{bmatrix} l_{ee} - l_{base} - l_{la}cos(\theta_i) \\ 0 \\ l_{la}sin(\theta_3) \end{bmatrix},$$

where

$$\phi_1 = 0, \;\; \phi_2 = \frac{2\pi}{3}, \;\; \phi_3 = \frac{4\pi}{3}, \tag{A.48}$$

Differentiating A.47, we obtain

$$s_i^T \dot{s}_i = 0, \tag{A.49}$$

The first derivative of s_i is

$$\begin{aligned} \dot{s}_i &= \begin{bmatrix} \dot{x_Q} \\ \dot{y_Q} \\ \dot{z_Q} \end{bmatrix} + R_z\Big(\phi_i\Big) \begin{bmatrix} l_{la} sin(\theta_i) \\ 0 \\ -l_{la} cos(\theta_i) \end{bmatrix} \dot{\theta} \\ &= \dot{\vec{x}} + b_i \dot{\theta}, \end{aligned} \tag{A.50}$$

For one robot arm, we get

$$s_i^T \dot{\vec{x}} + s_i^T (b_i \dot{\theta}_i) = 0, \tag{A.51}$$

For the three robot arms, we get

$$\begin{bmatrix} s_1^T \\ s_2^T \\ s_3^T \end{bmatrix} \dot{\vec{x}} + \begin{bmatrix} -s_1^T b_1 & 0 & 0 \\ 0 & -s_2^T b_2 & 0 \\ 0 & 0 & -s_3^T b_3 \end{bmatrix} \begin{bmatrix} \dot{\theta}_1 \\ \dot{\theta}_2 \\ \dot{\theta}_3 \end{bmatrix} = \begin{bmatrix} 0 \\ 0 \\ 0 \end{bmatrix}, \tag{A.52}$$

Let

$$J_x = \begin{bmatrix} s_1^T \\ s_2^T \\ s_3^T \end{bmatrix}, \quad J_\theta = \begin{bmatrix} -s_1^T b_1 & 0 & 0 \\ 0 & -s_2^T b_2 & 0 \\ 0 & 0 & -s_3^T b_3 \end{bmatrix}, \tag{A.53}$$

Equation A.52 can then be written as

$$J_x \dot{\vec{x}} = J_\theta \dot{\theta} \tag{A.54}$$

A.2 Kinematics of Hunt-Type 6-Rotational-Universal-Spherical Parallel Kinematic Mechanism

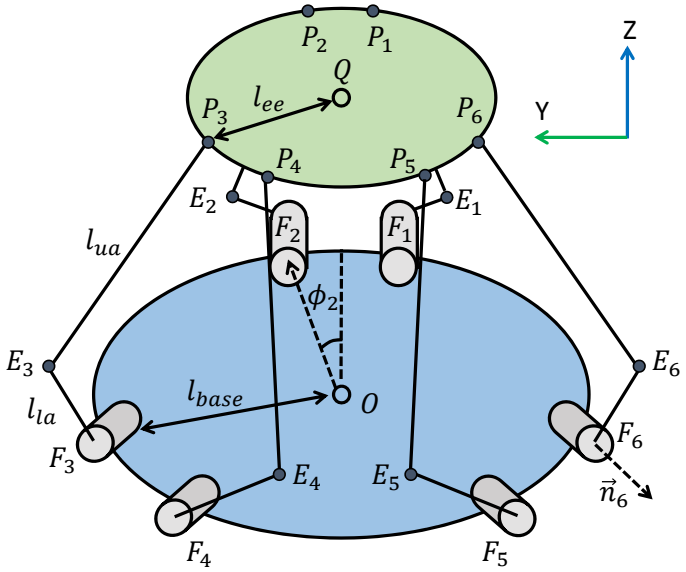

Figure A.2: Kinematic diagram for the Hunt-type 6-RUS mechanism.

A.2.1 Forward Kinematics

As illustrated in the Fig. A.2, let l_{base} be the distance from the center of the base to each of the connection point F_i, $i = 1, 2, 3$. The vectors OF_i, for $i = 1, ..., 6$, are calculated as

$$\vec{OF}_i = R_z\Big(\phi_i\Big) \begin{bmatrix} l_{base} \\ 0 \\ 0 \end{bmatrix}, \tag{A.55}$$

where $R_z(\phi)$ is the rotation matrix generated by a rotation about the z axis by an angle of ϕ radian.

Let θ_i be the joint angle of the ith joint, and let $\vec{n}_i = (n_{i,x}, n_{i,y}, n_{i,z})$ be the actuator axis of joint i. The point OE_i can be calculated as the solution to the simultaneous

equation

$$(x_{E_i} - x_{F_i})^2 + (y_{E_i} - y_{F_i})^2 + (z_{E_i} - z_{F_i})^2 - l_{la}^2 = 0, \tag{A.56}$$

$$\vec{n}_i.\vec{OE}_i - \vec{n}_i.\vec{OF}_i = 0, \tag{A.57}$$

Equation A.56 constraint the point E_i such that the distance FE_i is equal to the lower arm length l_{la}, while Equation A.57 constraints the point E_i such that the direction $\vec{FE}_i$ is normal to the actuator axis $\vec{n}_i$.

Let $\vec{OQ} = (x_Q, y_Q, z_Q)$ be the position of the point Q, and R_{ee} be the rotation matrix describing the orientation of the end-effector. To solve for the position and orientation of the end-effector, we have

$$(x_{P_i} - x_{E_i})^2 + (y_{P_i} - y_{E_i})^2 + (z_{P_i} - z_{E_i})^2 - l_{ua}^2 = 0, \tag{A.58}$$

These 6 equations in Equation A.58 enforces the constraint that the distance EP_i is equal to the upper arm legnth l_{ua}. From the position and orientation of the end-effector, we can determine the position of the points P_i as

$$OP_i = OQ + R_{\text{ee}} \times ({}^{\text{ee}}QP_i), \tag{A.59}$$

Equation A.59 provides 6 equations that specify the position of the point OP_i using the position OQ and the orientation R_{ee}. By combining equation A.59 with equation A.58, and enforcing the condition that the rotation matrix is orthonormal, we can obtain 12 equations with 12 unknowns (3 unknowns for position Q and 9 unknowns for orientation R_{ee}). The position OQ and the orientation R_{ee} can be obtained numerically.

A.2.2 Inverse Kinematics

For the inverse kinematics, we want to find the position of the elbow points $E_i, i = 1, 2, 3, 4, 5, 6$, given the end-effector position OQ and orientation R_{ee}. From the specified end-effector position and orientation, the position of the points OP_i can be

calculated using equation A.59. We then follow the method discussed in the section A.1.0.2 to find the elbow point OE_i, of which the joint angles θ_i can be obtained.

A.2.3 Jacobian Calculation

There is no analytical form of the Jacobian matrix for the Hunt-Type 6-DoF parallel mechanism. The Jacobian matrix at a particular point $O\vec{Q}_1$ of the end-effector can be obtained by numerically running through the inverse kinematic at the point $O\vec{Q}_1$, and its neighboring points perturbed in the translational Cartesian x, y, z direction, and rotational Cartesian x, y, and z axis, to obtain the correspond joint angles. The inverse of the Jacobian matrix, J^{-1}, can be formulated by dividing the change in joint angles by the amount of perturbation in the translational x, y, z axis, and rotation x, y, and z axis respectively:

$$\delta\theta = J^{-1}\delta x. \tag{A.60}$$

The Jacobian matrix can then be obtained by taking the inverse of J^{-1}.

Bibliography

[1] J.J. Abbott and A.M. Okamura. Stable forbidden-region virtual fixtures for bilateral telemanipulation. *Journal of Dynamic Systems, Measurement, and Control*, 128:53–64, 2008.

[2] K. Bark, J. Wheeler, P. Shull, J. Savall, and M.R. Cutkosky. Rotational skin stretch feedback: A wearable haptic display for motion. *IEEE Transactions on Haptics*, 3(3):166–176, 2010.

[3] S. J. Bensmaïa, Y. Y. Leung, S. S. Hsiao, and K. O. Johnson. Vibratory adaptation of cutaneous mechanoreceptive afferents. *Journal of Neurophysiology*, 94(5):3023–3036, 2005.

[4] W.M. Bergmann Tiest and A.M.L. Kappers. Cues for haptic perception of compliance. *IEEE Transactions on Haptics*, 2(4):189–199, 2009.

[5] WouterM. Bergmann Tiest, Connie Lyklema, and AstridM.L. Kappers. Investigating the effect of area of stimulation on cutaneous and proprioceptive weight perception. In Poika Isokoski and Jukka Springare, editors, *Haptics: Perception, Devices, Mobility, and Communication*, volume 7283 of *Lecture Notes in Computer Science*, pages 7–12. Springer Berlin Heidelberg, 2012.

[6] J. Biggs and M.A. Srinivasan. Tangential versus normal displacements of skin: relative effectiveness for producing tactile sensations. In *10th Symposium on Haptic Interfaces for Virtual Environment and Teleoperator Systems.*, pages 121–128, 2002.

[7] E. Burdet, R. Osu, D.W. Franklin, T.E. Milner, and M. Kawato. The central nervous system stabilizes unstable dynamics by learning optimal impedance. *Nature*, 414:446–449, 2001.

[8] Seungmoon Choi, Laron Walker, Hong Z. Tan, Scott Crittenden, and Ron Reifenberger. Force constancy and its effect on haptic perception of virtual surfaces. *ACM Transaction of Applied Perception*, 2(2):89–105, 2005.

[9] E.C. Chubb, J.E. Colgate, and M.A. Peshkin. Shiverpad: A glass haptic surface that produces shear force on a bare finger. *IEEE Transactions on Haptics*, 3(3):189–198, 2010.

[10] D. Constantinescu, S. E. Salcudean, and E. A. Croft. Haptic rendering of rigid contacts using impulsive and penalty forces. *IEEE Transactions on Robotics*, 21(3):309 – 323, 2005.

[11] Francois Conti, Federico Barbagli, Dan Morris, and Christopher Sewell. CHAI3D: An open source library for the rapid development of haptic scenes. In *IEEE World Haptics Conference*, 2005.

[12] Thomas Debus, Theresia Becker, Pierre Dupont, Tae-Jeong Jang, and Robert Howe. Multichannel vibrotactile display for sensory substitution during teleoperation. In *SPIE International Symposium of Intelligent Systems and Advanced Manufacturing*, volume 2, pages 390–397, 2004.

[13] Thomas Debus, Tae-Jeong Jang, Pierre Dupont, and Robert Howe. Multichannel vibrotactile display for teleoperated assembly. *International Journal of Control, Automation, and Systems*, 2(3):390–397, 2004.

[14] N. Diolaiti, G. Niemeyer, F. Barbagli, and J.K. Salisbury. Stability of haptic rendering: Discretization, quantization, time delay, and coulomb effects. *IEEE Transactions on Robotics*, 22(2):256–268, 2006.

[15] Knut Drewing, Michael Fritschi, Regine Zopf, Marc O. Ernst, and Martin Buss. First evaluation of a novel tactile display exerting shear force via lateral displacement. *ACM Transactions on Applied Perception*, 2(2):118–131, 2005.

[16] Marc O. Ernst and Martin S. Banks. Humans integrate visual and haptic information in a statistically optimal fashion. *Nature*, 415(6870):429–433, 2002.

[17] J.J. Gil, I. Zabalza, J. Ros, J.M. Pintor, and J.M. Jimenez. Kinematics and dynamics of a 6-RUS hunt-type parallel manipulator by using natural coordinates. In J. Lenarcic and C. Galletti, editors, *On Advances in Robot Kinematics*, pages 329–335. Springer Netherlands, 2004.

[18] Stanton A. Glantz and Bryan K. Slinker. *Primer of Applied Regression and Analysis of Variance*. McGraw-Hill, 1990.

[19] B.T. Gleeson, S.K. Horschel, and W.R. Provancher. Design of a fingertip-mounted tactile display with tangential skin displacement feedback. *IEEE Transactions on Haptics*, 3(4):297–301, 2010.

[20] B.T. Gleeson, S.K. Horschel, and W.R. Provancher. Perception of direction for applied tangential skin displacement: Effects of speed, displacement, and repetition. *IEEE Transactions on Haptics*, 3(3):177–188, 2010.

[21] B.T. Gleeson, C.A. Stewart, and W.R. Provancher. Improved tactile shear feedback: Tactor design and an aperture-based restraint. *IEEE Transactions on Haptics*, 4(4):253–262, 2011.

[22] A. L Guinan, N. C Hornbaker, M. N Montandon, A. J Doxon, and William R. Provancher. Back-to-back skin stretch feedback for communicating five degree-of-freedom direction cues. *IEEE World Haptics Conference*, pages 13–18, 2013.

[23] A.L. Guinan, M.N. Montandon, A.J. Doxon, and W.R. Provancher. Discrimination thresholds for communicating rotational inertia and torque using differential skin stretch feedback in virtual environments. In *IEEE Haptics Symposium*, pages 277–282, 2014.

[24] J.C. Gwilliam, M. Mahvash, B. Vagvolgyi, A. Vacharat, D. D. Yuh, and A.M. Okamura. Effects of haptic and graphical force feedback on teleoperated palpation. In *IEEE International Conference on Robotics and Automation*, pages 677–682, 2009.

[25] Landon T. Gwilliam, Andrew J. Doxon, and William R. Provancher. Haptic matching of directional force and skin stretch feedback cues. In *IEEE World Haptics Conference*, pages 19–24, 2013.

[26] B. Hannaford, L. Wood, D.A McAffee, and H. Zak. Performance evaluation of a six-axis generalized force-reflecting teleoperator. *IEEE Transactions on Systems, Man and Cybernetics*, 21(3):620–633, 1991.

[27] Keyvan Hashtrudi-Zaad and S.E. Salcudean. Analysis of control architectures for teleoperation systems with impedance/admittance master and slave manipulators. *International Journal of Robotics Research*, 20(6):419–445, 2001.

[28] Vincent Hayward and Juan Manuel Cruz-Hernndez. Tactile display device using distributed lateral skin stretch. In *Proceedings, 8th Haptic Symposium*, pages 1309–1314, 2000.

[29] J. M. Hillis, M. O. Ernst, M. S. Banks, and M. S. Landy. Combining sensory information: Mandatory fusion within, but not between, senses. *Science*, 298(5598):1627–1630, 2002.

[30] R.S. Johansson and A.B. Vallbo. Tactile sensory coding in the glabrous skin of the human hand. *Trends in Neurosciences*, 6:27–32, 1983.

[31] L.A. Jones and E. Piateski. Contribution of tactile feedback from the hand to the perception of force. *Experimental Brain Research*, 168(1-2):298–302, 2006.

[32] H. Kajimoto. Electrotactile display with real-time impedance feedback using pulse width modulation. *IEEE Transactions on Haptics*, 5(2):184–188, 2012.

[33] P. Kazanzides, Z. Chen, A. Deguet, G. Fischer, R. Taylor, and S. Dimaio. An open-source research kit for the da vinci surgical system. In *IEEE International Conference on Robotics and Automation*, pages 21–29, 2014.

[34] F. Kimura, A. Yamamoto, and T. Higuchi. Development of a 2-dof softness feeling display for tactile tele-presentation of deformable surfaces. In *IEEE International Conference on Robotics and Automation*, pages 1822–1827, 2010.

[35] C.H. King, M.O. Culjat, M.L. Franco, C.E. Lewis, E.P. Dutson, W.S. Grundfest, and J.W. Bisley. Tactile feedback induces reduced grasping force in robot-assisted surgery. *IEEE Transactions on Haptics*, 2(2):103–110, 2009.

[36] M. Kitagawa, D. Dokko, A.M. Okamura, and D.D. Yuh. Effect of sensory substitution on suture-manipulation forces for robotic surgical systems. *The Journal of Thoracic and Cardiovascular Surgery*, 129(1):151–158, 2005.

[37] Dimitrios A. Kontarinis and Robert D. Howe. Tactile display of vibratory information in teleoperation and virtual environments. *Presence*, 4:387–402, 1996.

[38] Katherine J. Kuchenbecker, June Gyu Park, and Günter Niemeyer. Characterizing the human wrist for improved haptic interaction. In *72nd ASME International Mechanical Engineering Congress and Exposition*, pages 591–598, 2003.

[39] K.J. Kuchenbecker, J. Fiene, and G. Niemeyer. Improving contact realism through event-based haptic feedback. *IEEE Transactions on Visualization and Computer Graphics*, 12(2):219–230, 2006.

[40] M. Kuschel, M. Di Luca, M. Buss, and R.L. Klatzky. Combination and integration in the perception of visual-haptic compliance information. *IEEE Transactions on Haptics*, 3(4):234–244, 2010.

[41] D A. Lawrence, L Y. Pao, A M. Dougherty, M A. Salada, and Y. Pavlou. Rate-hardness: a new performance metric for haptic interfaces. *IEEE Transactions on Robotics and Automation*, 16(4):357–371, 2000.

[42] D.A. Lawrence. Stability and transparency in bilateral teleoperation. *IEEE Transactions on Robotics and Automation*, 9(5):624–637, 1993.

[43] Susan J. Lederman and Roberta L. Klatzky. Sensing and displaying spatially distributed fingertip forces in haptic interfaces for teleoperator and virtual environment systems. *Presence: Teleoperator and Virtual Environment*, 8(1):86–103, 1999.

[44] U. Lindblom. Touch perception threshold in human glabrous skin in terms of displacement amplitude on stimulation with single mechanical pulses. *Brain Research*, 82(2):205–210, 1974.

[45] D.Z. Loesch and N.G. Martin. Finger ridge patterns and tactile sensitivity. *Annals of Human Biology*, 11(2):113–124, 1984.

[46] M. Lopez, E. Castillo, G. Garcia, and A. Bashir. Delta robot: Inverse, direct, and intermediate jacobians. *Journal of Mechanical Engineering Science*, 220:103–109, 2006.

[47] M. Mahvash and A.M. Okamura. Friction compensation for enhancing transparency of a teleoperator with compliant transmission. *IEEE Transactions on Robotics*, 23(6):1240–1246, 2007.

[48] K. Matsui, S. Okamoto, and Y. Yamada. Relative contribution ratios of skin and proprioceptive sensations in perception of force applied to fingertip. *IEEE Transactions on Haptics*, 7(1):78–85, 2014.

[49] Scott E. Maxwell and Harold D. Delaney. *Designing Experiments and Analyzing Data: A Model Comparison Perspective*. Routledge Academic, 2nd edition, 2003.

[50] B.J. McCarragher and H. Asada. Qualitative template matching using dynamic process models for state transition recognition of robotic assembly. *ASME Journal of Dynamics Systems, Measurement, and Control*, 115(2A):261–269, 1993.

[51] W. McMahan, J. Gewirtz, D. Standish, P. Martin, J.A. Kunkel, M. Lilavois, A. Wedmid, D. I. Lee, and K. J. Kuchenbecker. Tool contact acceleration feedback for telerobotic surgery. *IEEE Transactions on Haptics*, 4(3):210–220, 2011.

[52] K. Minamizawa, D. Prattichizzo, and S. Tachi. Simplified design of haptic display by extending one-point kinesthetic feedback to multipoint tactile feedback. In *IEEE Haptics Symposium*, pages 257–260, 2010.

[53] M.N. Montandon and W.R. Provancher. A smart phone peripheral with bimanual skin stretch haptic feedback and user input. In *IEEE International Conference on Consumer Electronics*, pages 45–46, 2013.

[54] S. Okamoto, M. Konyo, and S. Tadokoro. Vibrotactile stimuli applied to finger pads as biases for perceived inertial and viscous loads. *IEEE Transactions on Haptics*, 4(4):307–315, 2011.

[55] Allison M. Okamura, Mark R. Cutkosky, and J T. Dennerlein. Reality-based models for vibration feedback in virtual environments. *IEEE/ASME Transactions on Mechatronics*, 6(3):245–252, 2001.

[56] A.M. Okamura. Haptic feedback in robot-assisted minimally invasive surgery. *Current opinion in Urology*, 19(1):102–107, 2009.

[57] M.K. O'Malley and M. Goldfarb. The effect of virtual surface stiffness on the haptic perception of detail. *IEEE/ASME Transactions on Mechatronics*, 9(2):448–454, 2004.

[58] C. Pacchierotti, A. Tirmizi, and D. Prattichizzo. Improving transparency in teleoperation by means of cutaneous tactile force feedback. *ACM Transactions on Applied Perception*, In press, 2014.

[59] Jaeyoung Park, A.J. Doxon, W.R. Provancher, D.E. Johnson, and H.Z. Tan. Haptic edge sharpness perception with a contact location display. *IEEE Transactions on Haptics*, 5(4):323–331, 2012.

[60] Emmanuel Vander Poorten and Yasuyoshi Yokokohji. Rendering a rigid virtual world through an impulsive haptic interface. In *IEEE/RSJ International Conference on Intelligent Robots and Systems*, pages 1547–1552, 2006.

[61] Domenico Prattichizzo, Claudio Pacchierotti, and Giulio Rosati. Cutaneous force feedback as a sensory subtraction technique in haptics. *IEEE Transactions on Haptics*, 5(4):289–300, 2012.

[62] William R. Provancher and Nicholas D. Sylvester. Fingerpad skin stretch increases the perception of virtual friction. *IEEE Transactions on Haptics*, 2(4):212–223, 2009.

[63] W.R. Provancher, M.R. Cutkosky, K.J. Kuchenbecker, and G. Niemeyer. Contact location display for haptic perception of curvature and object motion. *International Journal of Robotics Research*, 24(9):691–702, 2005.

[64] Z.F. Quek, S.B. Schorr, I Nisky, AM. Okamura, and W.R. Provancher. Augmentation of stiffness perception with a 1-degree-of-freedom skin stretch device. *IEEE Transactions on Human-Machine Systems*, 44(6):731–742, 2014.

[65] Z.F. Quek, S.B. Schorr, I. Nisky, W.R. Provancher, and A.M. Okamura. Sensory substitution using 3-degree-of-freedom tangential and normal skin deformation feedback. *IEEE Haptics Symposium*, pages 27–33, 2014.

[66] C.E. Reiley, T. Akinbiyi, D. Burschka, D.C. Chang, A.M. Okamura, and D.D. Yuh. Effects of visual force feedback on robot-assisted surgical task performance. *The Journal of Thoracic and Cardiovascular Surgery*, 135(1):196–202, 2008.

[67] S. E. Salcudean and T. D. Vlaar. On the emulation of stiff walls and static friction with a magnetically levitated input/output device. *Journal of Dynamic Systems, Measurement, and Control*, 119(1):127–132, 1997.

[68] R.E. Schoonmaker and C.G.L. Cao. Vibrotactile force feedback system for minimally invasive surgical procedures. In *IEEE International Conference on Systems, Man and Cybernetics*, volume 3, pages 2464–2469, 2006.

[69] S. B. Schorr, Z. F. Quek, I. Nisky, W.R. Provancher, and A. M. Okamura. Tactile skin deformation feedback for conveying environment forces in teleoperation. In *Proceedings of the Tenth Annual ACM/IEEE International Conference on Human-Robot Interaction Extended Abstracts*, pages 195–196, 2015.

[70] S. B. Schorr, Z. F. Quek, I. Nisky, W.R. Provancher, and A. M. Okamura. Tactor-induced skin stretch as a sensory substitution method in teleoperated palpation. In *IEEE Transactions on Haptics*, 2015. Epub ahead of print.

[71] A. Serio, M. Bianchi, and A. Bicchi. A device for mimicking the contact force/contact area relationship of different materials with applications to softness rendering. In *IEEE/RSJ International Conference on Intelligent Robots and Systems*, pages 4484–4490, 2013.

[72] Reza Shadmehr and O A. Mussa-ivaldi. Adaptive representation of dynamics during learning of a motor task. *Journal of Neuroscience*, 14:3208–3224, 1994.

[73] T.B. Sheridan. Space teleoperation through time delay: review and prognosis. *IEEE Transactions on Robotics and Automation*, 9(5):592–606, 1993.

[74] M. A. Srinivasan and R. H. LaMotte. Tactual discrimination of softness. *Journal of Neurophysiology*, 73(1):88–101, 1995.

[75] R.H. JR Sturges. A three-dimensional assembly task quantification with application to machine dexterity. *The International Journal of Robotics Research*, 7(4):34–78, 1988.

[76] A. Talasaz, A.L. Trejos, and R.V. Patel. Effect of force feedback on performance of robotics-assisted suturing. In *IEEE International Conference on Biomedical Robotics and Biomechatronics*, pages 823–828, 2012.

[77] H.W. Tappeiner, R.L. Klatzky, B. Unger, and R. Hollis. Good vibrations: Asymmetric vibrations for directional haptic cues. In *IEEE World Haptics Conference*, pages 285–289, 2009.

[78] M. Tavakoli, R.V. Patel, and M. Moallem. Haptic feedback and sensory substitution during telemanipulated suturing. In *IEEE World Haptics Conference*, pages 543–544, 2005.

[79] G. Tholey, J.P. Desai, and A.E. Castellanos. Force feedback plays a significant role in minimally invasive surgery: Results and analysis. *Annals of Surgery*, 241(1):102–109, 2005.

[80] A. Tirmizi, C. Pacchierottie, and D. Prattichizzo. On the role of cutaneous force in teleoperation: subtracting kinesthesia from complete haptic feedback. *IEEE World Haptics Conference*, pages 371–376, 2013.

[81] F. van Beek, W. Bergmann Tiest, and A. Kappers. Anisotropy in the haptic perception of force direction and magnitude. In *IEEE Transactions on Haptics*, 2013. Epub ahead of print, doi 10.1109/TOH.2013.37.

[82] Christopher R. Wagner, Nicholas Stylopoulos, Patrick G. Jackson, and Robert D. Howe. The benefit of force feedback in surgery: Examination of blunt dissection. *Presence: Teleoperators and Virtual Environment*, 16(3):252–262, 2007.

[83] C.R. Wagner and R.D. Howe. Mechanisms of performance enhancement with force feedback. In *IEEE World Haptics Conference*, pages 21–29, 2005.

[84] J.M. Walker, A.A. Blank, P.A. Shewokis, and M.K. O'Malley. Tactile feedback of object slip improves performance in a grasp and hold task. In *IEEE Haptics Symposium*, pages 461–466, 2014.

[85] Qi Wang and Vincent Hayward. In vivo biomechanics of the fingerpad skin under local tangential traction. *Journal of Biomechanics*, 40:851–860, 2007.

[86] B. Weber, S. Schatzle, T. Hulin, C. Preusche, and B. Deml. Evaluation of a vibrotactile feedback device for spatial guidance. In *IEEE World Haptics Conference*, pages 349–354, 2011.

[87] Robert J. Webster, III, Todd E. Murphy, Lawton N. Verner, and Allison M. Okamura. A novel two-dimensional tactile slip display: Design, kinematics and perceptual experiments. *ACM Transactions on Applied Perception*, 2(2):150–165, 2005.

[88] D. W. Weir and J. E. Colgate. Stability of haptic displays. In *Haptic Rendering: Foundations, Algorithms, and Applications*. M. C. Lin and M. Otaduy, Eds., AK Peters, 2008.

[89] Felix A. Wichmann and N. Jeremy Hill. The psychometric function: I. Fitting, sampling, and goodness of fit. *Perception & Psychophysics*, 63(8):1293–313, November 2001.

[90] Felix A. Wichmann and N. Jeremy Hill. The psychometric function: II. Bootstrap-based confidence intervals and sampling. *Perception & Psychophysics*, 63(8):1314–29, November 2001.

[91] J. Wildenbeest, D. Abbink, C. Heemskerk, F. Van der Helm, and H. Boessenkool. The impact of haptic feedback quality on the performance of teleoperated assembly tasks. *IEEE Transactions on Haptics*, 6(2):242–252, 2013.

[92] L. Winfield, J. Glassmire, J.E. Colgate, and M. Peshkin. T-pad: Tactile pattern display through variable friction reduction. In *IEEE World Haptics Conference*, pages 421–426, 2007.

[93] S. Yazdian, A.J. Doxon, D.E. Johnson, H.Z. Tan, and W.R. Provancher. Compliance display using a tilting-plate tactile feedback device. In *IEEE Haptics Symposium*, pages 13–18, 2014.

[94] J.S. Yuan. Closed-loop manipulator control using quaternion feedback. *IEEE Journal of Robotics and Automation*, 4(4):434–440, 1988.

[95] C. B. Zilles and J.K. Salisbury. A constraint-based god-object method for haptic display. In *IEEE/RSJ International Conference on Intelligent Robots and Systems*, pages 146–151, 1995.